High Pressure Synthesis and Superconducting Properties of New Series of High-T_c Oxide Superconductors

Tetsuya KAWASHIMA

A dissertation submitted to the Doctoral Program
in Geoscience, the University of Tsukuba
in partial fulfillment of the requirements for the
degree of Doctor of Philosophy (Science)

January, 1999

Contents

Abstract

Since the discovery of the first high-temperature oxide superconductor in 1986, superconductivity science and technology have made rapid progress. Studies of this research field are deeply related to various disciplines such as solid-state physics, solid-state chemistry, energy-related technology, information, communications, electronics, etc. and superconductivity is expected to be key technology in 21'st century. The most important property of superconductors for practical applications is, no doubt, superconducting transition temperature (T_C). Since 1986, many new oxide superconductors have been discovered thanks to tremendous efforts of scientists all over the world and the record of T_C reached up to 135 K. However, after 1992, the reports of new superconductors prepared at ambient pressure decrease seriously in number. We have to say that the synthetic study of new superconductors by the conventional ambient-pressure reaction faces large difficulty.

Instead of solid-state reaction under ambient pressure, high pressure synthesis has been recognized in these several years as a very effective method to explore new high-T_C oxide superconductors. Indeed, number of oxide superconductors prepared under high pressure reached to over 30. This fact suggests that high pressure condition is favorable for layered structures of Cu-based oxide superconductors. The crystal structures of the cuprate superconductors consist of conduction layers including the CuO_2 planes and blocking layers which separates the conduction layers. Under high pressure, we can vary widely the number of the CuO_2 planes in a conduction layer, and moreover, a variety of elements can be introduced into cation sites of the blocking layer. In this treatise, we summarize our phase-search experiments under high-pressure

and discuss superconducting and structural properties of various series of high-T_c oxide superconductors discovered newly.

Followed by introduction in Chap. 1, we describe in Chap. 2 detailed high-pressure generation technique which we used throughout the present study. Chapter 3 is devoted to new series of oxycarbonate superconductors. We satisfactorily prepared at 5 GPa, 1200~1250 °C oxycarbonate family, $(Cu_{0.5}C_{0.5})_mBa_{m+1}Ca_{n-1}Cu_nO_{2(m+n)+1}$ ((Cu,C)-m(m+1)(n-1)n). Five members of the family have been isolated as almost single phases and all of them show superconductivity. In particular, the m=1 and n=4 member of this series, (Cu,C)-1234, has T_c as high as 117 K. This value is the highest record of T_c among the oxycarbonate superconductors known thus far.

In Chapter 4, we discuss new oxyborate superconducting family, $BSr_2Ca_{n-1}Cu_nO_{2n+3}$ (B-12(n-1)n; n=3~5), which were prepared at 6 GPa and 1200~1300 °C. In this series, one of the smallest cation B^{3+} occupies the cation site of blocking layer and such a series can never be prepared without using high-pressure technique.

Chapter 5 is devoted to two high-pressure stable series of superconductors, $Sr_2Ca_{n-1}Cu_nO_y$ (02(n-1)n; n=1~4) and $Sr_2Ca_{n-1}Cu_nO_{2n+\delta}F_{2\pm y}$ (02(n-1)n-F; n=2,3). Although, various results were reported for the former series, T_c of each member was not specified because of the difficulty in getting high quality samples. We reinvestigated this series and succeeded to determine T_c of each phase by comparing superconducting properties of various samples. The latter is a series of superconductors including fluorine prepared for the first time. We discuss influence of fluorine substitution for superconducting properties based on experimental results for these two series.

1. Introduction

1.1. Significance of searching for new substances in the study of oxide superconductors

Superconductivity is a physical phenomenon wherein a substance reaches an electric resistance of zero when cooled to low temperatures. It was discovered by the Dutch physicist Onnes in 1911. Superconductivity is realized in a variety of materials such as single elements, alloys, oxides, intermetallic compounds, sulfides and organic substances. Of them, oxide superconductors have been researched the most, starting after the 1986 discovery of the first high-temperature superconductor. Today, studies of the sort are observed in numerous areas, such as natural science, synthetic chemistry, thin films and device applications. Meanwhile, many new oxide superconductors were found and we now know of a substance having a superconducting transition temperature (T_C) topping 130K, a value unthinkable before the advent of high-temperature superconductors.

The problem in using superconductors is that realizing a superconducting state requires liquid helium as a refrigerant, which requires large-scale cooling equipment, thus limiting practical application owing to cost and technological factors. The discovery of high-temperature superconductors enabled the use of liquid nitrogen as a refrigerant, allowing a much wider range of practical superconductivity use. The find also had a profound impact on the field of theoretical solid-state physics, as the conventional BCS-theory of superconductivity had put the top limit of T_C at about 30K. Nevertheless a material with a far higher T_C in fact emerged. Research on this advanced rapidly to explain how superconductivity is generated, and as the precipitate we have begun to understand the electric and magnetic properties of transition metal oxides.

Various fields of materials science such as synthesis, structure analysis, single crystal growth, thin-film formation, processing, etc. are involved in superconductivity research and they provide information needed in basic theoretical study. Among them, the exploration of new superconducting materials is deserving special mention. Starting with the discovery of a La-based oxide superconductor in 1986, scientists found a series of new oxide superconductors in quick succession, and clearly these discoveries have furnished the momentum for all spheres of superconducting research. When seeking new substances in the study of oxide superconductors, the key lies in synthesis and evaluation, thereby providing knowledge to build theories for how superconductivity is generated and assisting research on the practical use of such substances. In this, the obvious goal is to find a superconducting material having the highest T_C ever.

1.2. Background of the study of copper oxide superconductors

Since 1986 scientists have discovered dozens of copper oxide high-temperature superconductors (Table. 1.1), which merits a brief review of the history of studies of copper oxide superconductors.

Bednorz and Müller of the IBM Zurich Institute in 1986 found that La-Ba-Cu-O oxides show superconductivity at about 30K [1]. A follow-up experiment by Uchida et al. of the University of Tokyo proved $(La,Ba)_2CuO_4$ with a K_2NiF_4-type structure to be responsible for superconductivity [2], and the results marked the start of studies of copper oxide superconductors. Kishio et al. of the same university substituted Sr for Ba and synthesized $(La,Sr)_2CuO_4$ having T_C of about 40K, thus updating the T_C record [3]. Early the next year, Chu et al. of Houston University synthesized oxide superconductor $YBa_2Cu_3O_{7-\delta}$ having T_C above liquid nitrogen temperature (77K) for the first time [4]. With that

as the turning point, researchers in physics and chemistry throughout the world launched research on synthesis to find superconductors having even higher T_c levels, thus causing "superconductivity fever". Earlier, Chu et al. found that T_c of $(La,Ba)_2CuO_4$ rises under high pressure and looked to obtain high-T_c substances by inducing chemical pressures in the crystal by replacing La^{3+} with Y^{3+} or a lanthanide ion having a smaller ionic radius, and their work resulted in finding $YBa_2Cu_3O_{7-\delta}$, whose crystal structure was elucidated by Siegrist et al. [5] and Izumi et al. [6] using neutron rietveld analysis. These experiments showed that the $YBa_2Cu_3O_{7-\delta}$ crystal structure was not of K_2NiF_4 type, as advocated by The University of Tokyo group, but based on an oxygen-deficient perovskite structure wherein both CuO_4 chains and CuO_2 planes exist.

In 1988 Maeda et al. of the National Research Institute for Metals discovered $Bi_2Sr_2Ca_{n-1}Cu_nO_{2n+4}$ (n=1-3; $T_c \leq 110K$) [7], and Sheng et al. and Parkin et al. discovered $Tl_2Ba_2Ca_{n-1}Cu_nO_{2n+4}$ (n=1-3; $T_c \leq 127K$) and $TlBa_2Ca_{n-1}Cu_nO_{2n+1}$ (n=1-4; $T_c \leq 122K$), respectively [8, 9]. These series were found by introducing a new trivalent element, Bi or Tl. When it was seen that these Bi-based and Tl-based compounds are so structured that n oxygen-deficient perovskite-type layers lie between rock-salt-type layers, it became clear that the layered structures based on the CuO_2 plane are mandatory for superconductivity and the CuO_4 chain seen in the $YBa_2Cu_3O_7$ structure does not play an important role for realizing superconductivity.

The 1989 discovery of $(Nd,Ce)_2CuO_4$ (T_c of about 23K) [10] greatly helped to elucidate how superconductivity is generated and became the first copper oxide superconductor with electrons as carriers. It is considered that the CuO_2 conductive plane is supplied with holes through the apical oxygen immediately above Cu in the plane. In Nd_2CuO_4, the CuO_2 plane is sandwiched by fluorite-type blocks of

Nd_2O_2, and the hole introduction into the CuO_2 plane is inhibited owing to the lack of apical oxygen. However, replacing Nd^{3+} with Ce^{4+} and removing a small amount of oxygen from the CuO_2 plane by reduction results in electron introduction into the CuO_2 plane, inducing the n-type superconductivity. Next came the synthesis of $(Nd,Ce,Sr)_2CuO_4$, wherein $(La,Sr)_2CuO_4$ and $(Nd,Ce)_2CuO_4$ blocks are stacked alternately along the c-axis [11].

After the discovery of Tl-based oxide superconductors, the search for new substances continued, which resulted in finding Pb [12] and CO_3 [13] based superconductors. Moreover, in 1993, Putilin et al. discovered an oxide superconductor containing Hg [14]. Later, in the synthesis of the Hg-based series, $HgBa_2Ca_2Cu_3O_{8+\delta}$ recorded T_c of 135K, the highest T_c at present [15].

1.3. Principles for designing new superconductors

As evident from the above research, all high-T_c oxide superconductors contain copper. The crystal structures of many oxide superconductors have been determined by X-ray and neutron analysis. Tokura et al. [16] were the first to attempt conceptual structural classification of cuprate superconductors. According to their concept, an oxide superconductor structure consists of a conduction layer and a blocking layer, and carriers are supplied from the latter layer to the former (Fig. 1.1). A CuO_2 plane or a group of CuO_2 planes separated by a Ca, Y or lanthanide plane constitutes a conduction layer. Various types of blocking layers have been known thus far. For instance, $YBa_2Cu_3O_{7-\delta}$ and $Bi_2Sr_2Ca_{n-1}Cu_nO_{2n+4}$ contain BaO-CuO-BaO triple planes and SrO-BiO-BiO-SrO composite planes as the blocking layer, respectively. As shown in Fig. 1.2, a crystal structure of a high-T_c superconductor is built up by stacking blocking layers and conduction

layers alternately. Number of the CuO_2 planes in a conduction layer is usually less than three. However, a conduction layer with higher number of the CuO_2 planes is often realized by thin film formation and high pressure synthesis.

1.4. Effectiveness of high pressure synthesis

Principles for material design obviously are important in searching for oxide superconductors. The challenge becoming even keener these days is how to synthesize a specimen as designed. A close look at recent trends indicates a shift in synthesis method from the simple solid-state reaction process to the thin-film formation, high pressure synthesis and other processes using more complex equipment. Among them, the high pressure synthesis process is regarded as one of the most effective for seeking new materials.

In the search for superconducting substances using high pressure, Okai et al. of the National Institute for Research in Inorganic Materials and Takano et al. of Kyoto University played a pioneering role. In 1990 Okai synthesized $YSr_2Cu_3O_7$ (T_c = 60 K) at a pressure of 7 GPa as part of his research for $Y(Ba_{1-x}Sr_x)_2Cu_3O_7$ [17]. Using the high pressure process, the Takano's group in 1992 synthesized a p-type infinite-layer oxide superconductor $(Sr,Ca)_{0.9}CuO_2$ (T_c=110 K) [18]. Smith et al. reported that n-type infinite layer oxide superconductors can be obtained by replacing part of the (Sr,Ca) site with Nd [19] under high pressure. The infinite-layer structure is very simple consisting of only the CuO_2 plane and an alkaline earth plane stacked alternately (Fig. 1.3). The infinite-layer compound is considered as the common mother oxide for all high-T_c superconductors.

These studies can be called valuable in that they showed ahead of others the effectiveness of searching for materials under high pressure.

The advent of high pressure synthesis has made possible the realization of a designed structure. However, to explain why high pressure works in synthesizing oxide superconductors is not easy. One possible answer is that the basic structure of an oxide superconductor is of high pressure stable perovskite type. However, it is not clear if that in fact is the case. The structures of cuprate superconductors are not exactly of perovskite type but have more complicated features and no ground exists for asserting that all oxide superconductors are high pressure stable.

In reality, high pressure products easily formed are infinite-layer or perovskite compounds, frequently resulting in the lack of a superconducting phase. This seems to happen when the reaction temperature is too high in which condition Cu and other B-site metals (see Fig. 1.2) or Sr(Ba) and Ca tend to be mixed randomly, resulting in a simple perovskite or infinite-layer structure. To synthesize a superconducting phase, it is vital to find effective ways to set temperatures, oxygen contents, pressure and other parameters.

1.5. Purpose of this study

This study seeks new copper oxide superconductors by high pressure synthesis. Target substances in the quest for new materials included oxide superconductors centered on the perovskite-related structure containing copper based on earlier findings and changing the types of metal atoms in the blocking layer and the number of the CuO_2 planes. Accordingly, we successfully synthesized new superconductors as described in Chapter 3 and thereafter.

Table 1.1. The history of the discovery of new oxide superconductors.

year	materials	
1986	$(La_{1-x}Ba_x)_2CuO_4$	(T_c~30 K)
	$(La_{1-x}Sr_x)_2CuO_4$	(T-structure、T_c~40 K)
1987	$YBa_2Cu_3O_{7-\delta}$	(T_c~30 K)
1988	$Bi_2Sr_2Ca_{n-1}Cu_nO_{2n+4}$	(n=1~3、$T_c \leq 110$ K)
	$Tl_2Ba_2Ca_{n-1}Cu_nO_{2n+4}$	(n=1~3、$T_c \leq 127$ K)
	$TlBa_2Ca_{n-1}Cu_nO_{2n+3}$	(n=1~4、$T_c \leq 122$ K)
	$TlSr_2Ca_{n-1}Cu_nO_{2n+3}$	
1989	$(Nd_{1-x}Ce_x)_2CuO_4$	(T'-structure)
	$(Nd,Ce,Sr)_2CuO_4$	(T*-structure)
	$YBa_2Cu_4O_8$	
	$Y_2Ba_4Cu_7O_{15}$	
	$(La_{1-x}Sr_x)_2CaCu_2O_6$	
	$PbBaSrYCu_3O_y$	
1990	$YSr_2Cu_3O_7$	(HP-synthesis)
1991	$(Sr,Nd)CuO_2$	(Infinite layer)
1992	$(Sr_{0.7}Ca_{0.3})_{0.9}CuO_2$	(Infinite layer、HP-synthesis)
	$(Ba_{1-x}Sr_x)_2Cu_{1+y}O_{2+2y+z}(CO_3)_{1-y}$	
	$HgBa_2Ca_{n-1}Cu_nO_{2n+\delta}$	(n=1~3、$T_c \leq 135$ K)
1993	$Sr_{n+1}Cu_nO_{2n+1+\delta}$	(HP-synthesis)
	$Sr_2Ca_{n-1}Cu_nO_y$	(HP-synthesis)
	$CuBa_2Ca_{n-1}Cu_nO_{2n+3}$	(HP-synthesis)
	$(Cu,Ag)Ba_2Ca_{n-1}Cu_nO_{2n+3}$	(HP-synthesis)
	$(Cu_{0.5}C_{0.5})Ba_2Ca_{n-1}Cu_nO_{2n+3}$	(n=3,4、HP-synthesis)
1994	$(Cu_{0.5}C_{0.5})_2Ba_3Ca_{n-1}Cu_nO_{2n+5}$	(n=3~5、HP-synthesis)
	$GaSr_2Ca_{n-1}Cu_nO_{2n+3}$	(n=3,4、HP-synthesis)
	$AlSr_2Ca_{n-1}Cu_nO_{2n+3}$	(n=4,5、HP-synthesis)
	$Sr_2CuO_2F_{2+\delta}$	
	$(Ca,Na)_2CuO_2Cl_2$	(HP-synthesis)
1995	$BSr_2Ca_{n-1}Cu_nO_{2n+3}$	(n=3~5、HP-synthesis)
	$(Cu_{0.5}S_{0.5})Sr_2Ca_{n-1}Cu_nO_y$	(n=3~7、HP-synthesis)
1996	$Sr_2Ca_{n-1}Cu_nO_{2n+\delta}F_{2\pm y}$	(n=2,3、HP-synthesis)
	$(Cu_{0.5}P_{0.5})Sr_2Ca_{n-1}Cu_nO_y$	(n=3~6、HP-synthesis)
	$(Cu,Ge)Sr_2Ca_2Cu_3O_y$	(HP-synthesis)

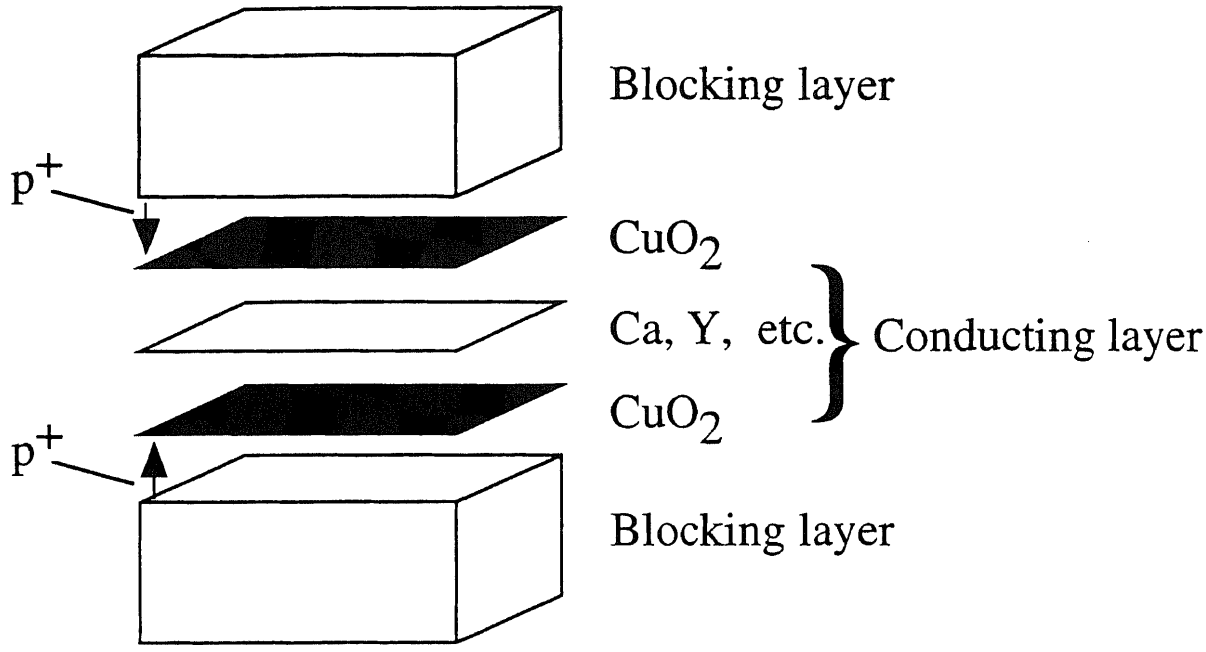

Fig. 1.1. General crystal structure of oxide superconductors.

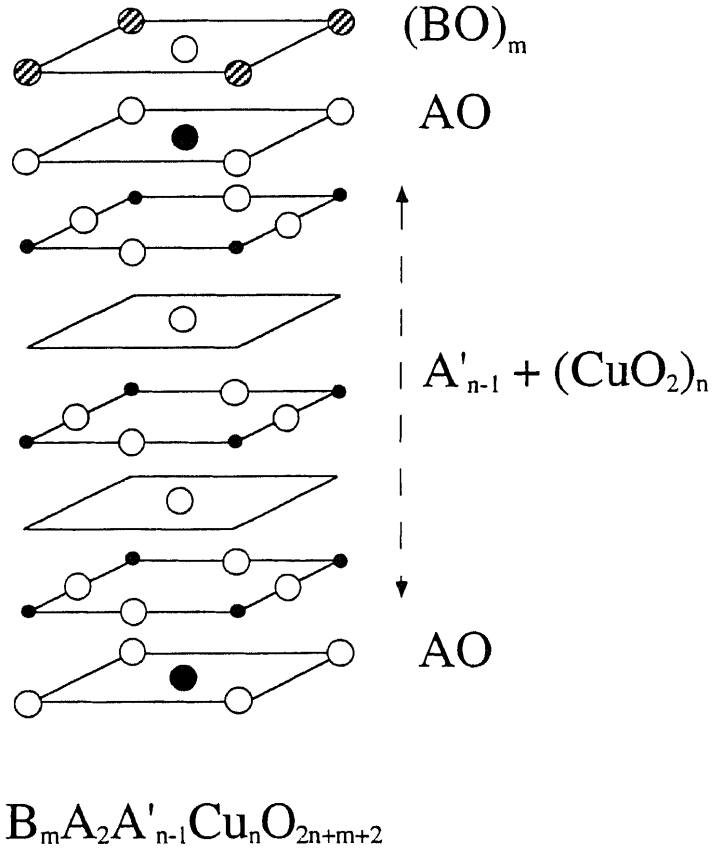

Fig. 1.2. An example of the crystal structure based on the principles for material designing.

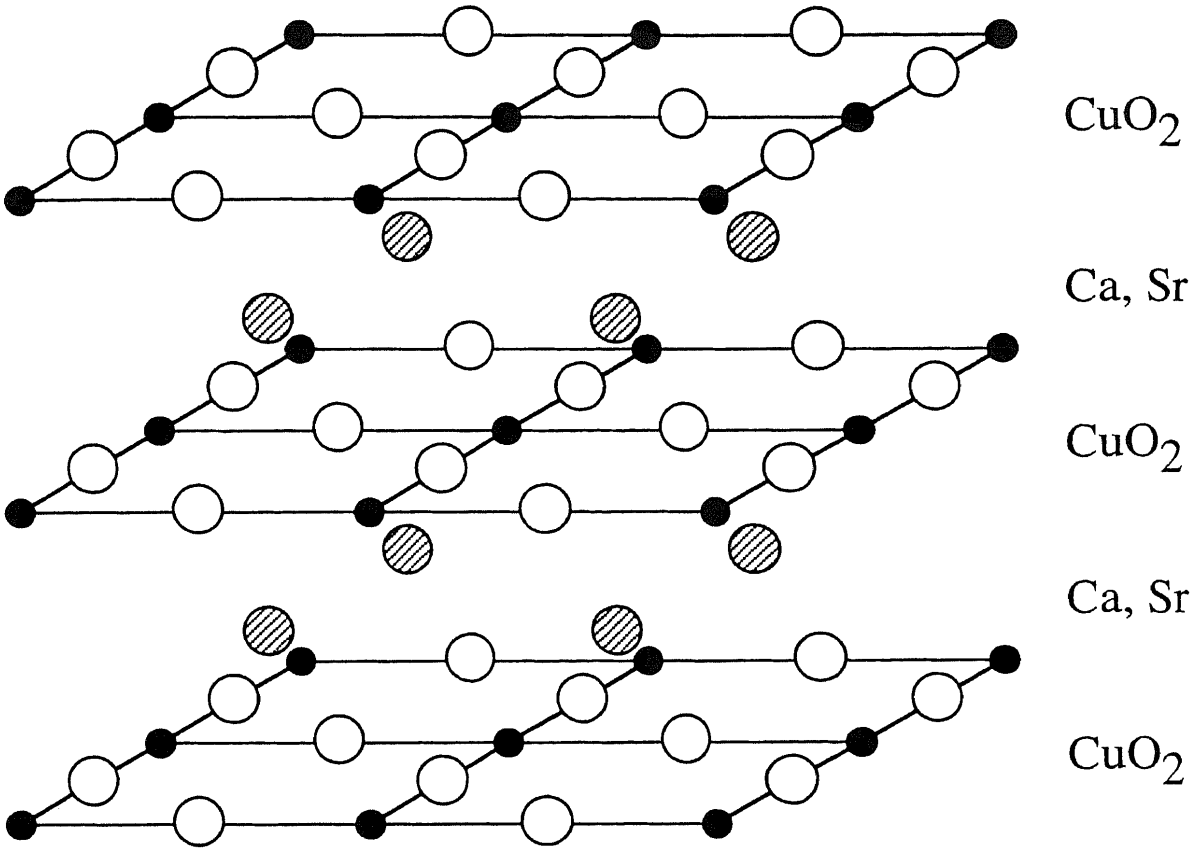

Fig. 1.3. Crystal structure of the infinite layer compound, (Sr,Ca)CuO_2.

2. High pressure synthesis method

This chapter will discuss matters related to high pressure apparatus and synthesis.

2.1. Belt-type high pressure apparatus

Belt-type high pressure apparatus, developed by General Electric (USA) in the 1950s to synthesize diamond, is so structured that a cylinder having a near-conical cross section is put between two conform anvils, one at the top, the other at the bottom, (Fig. 2.1) generates pressure by applying uniaxial force from the directions of the upper and lower anvils. Space between the anvils and the cylinder is filled with compressible gasket, which serves to lock pressure in the sample area and produce compression therein.

A salient feature of this apparatus is its relatively larger sample space, which is most desirable in experiments intended to synthesize material. In high pressure experimentation, the question generally is whether the experiments can be reproduced. The belt-type apparatus has larger sample space, enabling the use a large heater that is highly precise in terms of dimensions. Thus the belt-type apparatus permits thoroughly reproducible experiments.

Since forming its High pressure Research Station in 1977, National Institute for Research in Inorganic Materials (NIRIM) has worked to expand the sample space, increase experimental pressure and broaden temperature conditions in developing belt-type high pressure apparatus. At present four types -- FB-25H, FB-30H, FB-40H and FB-60H -- are operating under various pressure ranges up to 10 GPa.

In this study FB-30H was mainly used. The following paragraphs refer to this type only.

2.2. High pressure experiments: the preparation stage

2.2.1. Synthesis of starting material powder

When Cu-based oxide superconductor is synthesized, oxide powder comprising various substances is needed for starting material. In most cases chemical reagents with a purity of over 99.9% can be bought from manufacturers, but various kinds of oxide powder, not commercially available, must be synthesized in the lab. This section described a method for synthesizing starting materials.

($SrCuO_2$)

$SrCO_3$ powder (99.9%) and CuO powder (99.9%) were weighed so that the ratio of $SrCO_3$ to CuO in mol equaled 1:1 and were mixed using agate mortar to assure uniform quality. This mixture was then allowed to react in an aluminum crucible by firing it in an electric furnace at 1,000 °C for about three days, during which it was taken out several times for grinding and mixing. After firing, the synthesized powder underwent powder X-ray diffraction analysis and was confirmed to be single phase. Carbon analysis detected 0.04 % of carbon by weight.

($BaCuO_2$)

$BaCO_3$ powder (99.9%) and CuO powder (99.9%) were weighed so that the ratio of $BaCO_3$ to CuO in mol concentration equaled 1:1 and mixed using agate mortar to ensure uniform quality. Next the mixture was synthesized in an aluminum crucible and fired in an electric furnace at 900 °C for about a week, during which it was taken out several times for grinding and mixing. Pursuant to firing, the synthesized powder was subjected to powder X-ray diffraction analysis and verified to be single phase. Carbon analysis identified 0.95 % of carbon by weight.

(Ca_2CuO_3)

$CaCO_3$ powder (99.9%) and CuO powder (99.9%) were weighed so that the ratio of $CaCO_3$ to CuO in mol equaled 2:1 and were mixed using agate mortar to produce uniform quality. The mixture was then synthesized in an aluminum crucible and fired in an electric furnace at 1,000 °C for about three days, during which it was taken out several times for grinding and mixing. After firing, the synthesized powder underwent powder X-ray diffraction analysis and it was confirmed to be single phase. Carbon analysis detected very little carbon.

(SrO_2)

$SrCl_2$ powder (99.9%) was dissolved in distilled water. Proper amounts of reagent grade H_2O_2 and NH_3 were added to the solution, SrO_2 powder was settled in it, and the precipitate was separated through suction and filtration and cleaned with distilled water and ethanol. The separated powder was dried in an oxygen flow at 150 °C. The synthesized powder was subjected to powder X-ray diffraction analysis and was confirmed to be single phase. Carbon analysis detected 0.37 % of carbon by weight. It seems that these carbon were included in the H_2O_2 and NH_3 liquid.

(BaO_2)

Reagent grade $Ba(NO_3)_2$ powder was dissolved in distilled water, proper amounts or reagent grade H_2O_2 and NH_3 were added to the solution, and BaO_2 powder was settled in it. The precipitate was then separated through suction and filtration while sprayed with nitrogen gas and cleaned with distilled water and ethanol. The separated powder was dried in an oxygen flow at 200 °C. The synthesized powder underwent powder X-ray diffraction analysis and was verified to be single phase.

Carbon analysis detected 0.23 % of carbon by weight. It seems that these carbon were included in the H_2O_2 and NH_3 liquid.

2.2.2. Making gold capsules to contain sample powder and enclosing the powder in them

Experiments for Cu-based oxide superconductor high pressure synthesis generally call for the use of gold capsules to prevent NaCl, a pressure medium, from mixing with the sample powder and to keep oxygen content unchanging. This section describes how to make gold capsules and enclose the sample powder in them.

2.2.2.1. Gold capsules: the recipe

An order for gold pipes (outer diameter 6.8 mm, 0.2 mm thick, 8.0 mm long) and gold disks (outer diameter 6.2 mm, 0.2 mm thick) was placed with a manufacturer. One pipe and two disks were used to make one capsule.

A 6.9 ϕ die and punch of tungsten-carbide and a 6.3 ϕ rod made of the same material were prepared. The rod was passed through a gold pipe so that the end of the rod remained about 2 mm inside one end of the pipe. Then a gold disk was put inside the rim of the pipe (Fig. 2.2 (a)) and the protruding rim of the pipe was bent symmetrically inside using tweezers (Fig. 2.2 (b)). This piece was set in the die and punch and a load of two tons/cm^2 was applied with a hand press (Fig. 2.2 (c)), thereby producing a gold capsule (Fig. 2.2 (d)).

2.2.2.2. Enclosing the powder sample

About 250 to 300 mg of sample powder was enclosed in the completed gold capsule. Slight pressure was applied to the powder using the 6.3 mm diameter rod to flatten the surface of the powder (Fig. 2.3

(a)). Next a gold disk was placed on the powder surface (Fig. 2.3 (b)) and the rim of the capsule was bent inside with tweezers (Fig. 2.3 (c)).

It was then set in the 6.9 ϕ die and punch and applied with two tons/cm^2 pressure using a hand press (Fig. 2.3 (d)), which compressed the gold between the die and punch, and sealed the powder in the capsule (Fig. 2.3 (e)).

2.2.3. Making components for high pressure experiments

High pressure experiments need high pressure cells, gaskets and other parts. This section treats the making of components required for high pressure experiments.

2.2.3.1. High pressure cell

A high pressure cell consists of five components:

[1] Two NaCl-10wt%ZrO_2 compacted rings with a steel ring:

26 mm outer diameter, 12 mm inner diameter, 8 mm high

[2] One graphite sleeve:

12 mm outer diameter, 10 mm inner diameter, 16 mm high

[3] Two graphite disks:

10.05 mm diameter, 1.0 mm thick

[4] Two NaCl-20wt%ZrO_2 disks: 10 mm diameter, 1.5 mm thick

[5] Two NaCl disks including a gold capsule:

10 mm diameter, 5.5 mm in thick

The following describe ways to make these components.

[1] NaCl-10wt%ZrO_2 compacted ring with a steel ring

A 26 ϕ die and punch made of Tungsten-Carbide (specifically, a die, upper and lower punch with a 12 ϕ hole, and a 12 ϕ rod) were prepared.

The die was set on the table of the press for molding a pressure medium and the lower punch of the press was used as a flat base. Then 2.5% of water in weight was added to NaCl-10wt%ZrO_2 powder. Next, the lower punch of the press and the 12 ϕ rod were set in the cylinder, a steel ring (outer diameter 26 mm, inner diameter 18 mm, 4 mm high), and 5.3 g of the powder was put in the cylinder. The powder surface was leveled by lightly applying the upper punch of the press from above. Then an NaCl-10wt%ZrO_2 compacted ring was molded by applying about 3.5 tons/cm^2 pressure to the powder (Fig. 2.4 (a)). After molding the ring, pressure was reduced, the lower punch of the press was changed to a device for drawing out the ring, and the ring was extracted by again applying pressure (Fig. 2.4 (b)). The finished ring was demoisturized in a drier for 24 hours at 150 °C before use.

[2] Graphite sleeve

An order for a graphite sleeve (outer diameter 12 mm, inner diameter 10 mm, height 20 mm, material quality: G-530) was placed with a manufacturer.

[3] Graphite disk

A 10.05 ϕ graphite rod ordered from a maker was sliced into about a 1.2 mm thick disk using a cutter and finished by sanding both sides with emery paper to a thickness of 1.00±0.02 mm.

[4] NaCl-20wt%ZrO_2 disk

A 10 ϕ die and punch made of Tungsten-Carbide (specifically, a die, upper and lower punch, a 30 ϕ metal rod, a 30 ϕ metal rod with a hole) were prepared. Then 2.0% of water in weight was added to NaCl-20wt%ZrO_2 powder. Next, the 30 ϕ metal rod, 10 ϕ die and 10 ϕ lower

punch were set on the lower punch of the electric press, 0.4 g of the powder was put into the hole of the 10 ϕ die, and the powder surface was leveled by applying light pressure using the 10 ϕ lower punch. Then an NaCl-20wt%ZrO_2 disk was molded by applying about four tons/cm^2 to the powder using the press (Fig. 2.5 (a)). After molding the disk, pressure was reduced, the 30 ϕ metal rod was replaced with the 30 ϕ metal rod with a hole, and the disk was drawn out after again applying pressure (Fig. 2.5 (b)). The finished disk was demoisturized in a drier for 24 hours at 150 °C prior to use.

[5] NaCl disk including a gold capsule

A 10 ϕ die and punch made of Tungsten-Carbide (specifically, a die, upper and lower punch, a 30 ϕ metal rod, a 30 ϕ metal rod with a hole) and NaCl powder dried at 150 °C were prepared. The 30 ϕ metal rod was set on the lower punch of the electric press, a steel ring and the 10 ϕ lower punch were placed it, and lastly the 10 ϕ die. Next, 0.55 g of the powder was put into the hole of the 10 ϕ die and the powder surface was leveled by striking the top face of the 10 ϕ die with a wooden mallet. A gold capsule containing sample powder and kept horizontal was pushed into the powder in the 10 ϕ die hole, 0.2 g of the powder was put in the cylinder, and the powder surface was leveled by lightly applying pressure using the 10 ϕ lower punch. Then an NaCl disk was molded by applying a load of about four tons/cm^2 to the powder with the electric press (Fig. 2.6 (a)). After molding the disk, pressure was reduced, the 30 ϕ metal rod was replaced with the 30 ϕ metal rod with a hole, and the completed disk was drawn out after another application of pressure (Fig. 2.6 (b)).

2.2.3.2. Pyrophyllite gasket (Fig. 2.7 and 2.8)

2.2.3.2.1. Making the inner pyrophyllite gasket

An inner pyrophyllite gasket, or inner gasket for short, was fashioned from a pyrophyllite sleeve ordered from a manufacturer (outer diameter 40 mm, inner diameter 26 mm, 40 mm long) using a lathe with a special cutting bite. It is necessary to make an inner gasket that precisely fits the curved interior of the cylinder by adjusting the dimensions of the outer diameter of the gasket's tapering end according to the inner diameter of the cylinder core of the high pressure apparatus being used. Details of processing are omitted here. For reader reference, a photo of the scene of manufacture of inner gasket is presented in Fig. 2.9.

2.2.3.2.2. Making the outer pyrophyllite powder compact gasket

Outer pyrophyllite powder compact gasket, or simply outer gasket, was made by molding pre-arranged pyrophyllite powder using a special press.

A 65 ϕ die and punch made of Tungsten-Carbide (specifically, a die, upper and lower punch with a 40 ϕ hole, a 40 ϕ rod) were prepared. A 65 ϕ die was attached to the table of the press for molding the gasket. The lower punch of the press was used as a flat base and the 65 ϕ lower punch with a 40 ϕ hole and the 40 ϕ rod were inserted in the hole of the 65 ϕ die. Then 45 g of the pyrophyllite powder was put into the hole of the 65 ϕ die, with its surface leveled by lightly applying pressure from above using the 65 ϕ upper punch with a 40 ϕ hole. Then outer gasket was molded by applying about five tons/cm^2 to the powder using the press (Fig. 2.10 (a)). Pursuant to molding the gasket, pressure was reduced, the lower punch of the press was changed into a device for drawing out the gasket, after which it was extracted after applying pressure again (Fig. 2.10 (b)). The finished outer gasket was

demoisturized in a drier for 48 hours at 100 °C and stored in a constant-humidity desiccator for more than 24 hours before use.

2.2.4. Assembling high pressure cells

2.2.4.1. Composing NaCl-ZrO_2 rings and a graphite sleeve

First, two NaCl-10wt%ZrO_2 rings with a steel ring were prepared. The steel-ring side of the rings was sanded, then the other side of the rings was ground so that their height was 8.00±0.02 mm. A graphite sleeve was inserted in the two NaCl-10wt%ZrO_2 rings with a steel ring using a hand press. The portion of graphite sleeve longer than the NaCl-10wt%ZrO_2 rings combined in line was sanded off. Finally, the inside of the graphite sleeve was hollowed and finished using a 10mm hand reamer. The external surface of the finished high pressure cell was ground using sandpaper, with its dimensions adjusted to fit in inner gasket used in the experiment. Fig. 2.11 shows the picture of finished high pressure cell (outer part).

2.2.4.2. Adjustment of cell component dimensions

Among the cell components manufactured in 2.2.3.1, the two NaCl disks with a gold capsule and the two NaCl-20wt%ZrO_2 disks were sanded to adjust their thickness. Standard size for the former is 5.5 mm, for the latter, 1.5 mm. But if the total height of the four components combined in line is 14 mm, any of the four being slightly longer or shorter than the norm will pose no problem.

2.2.4.3. Assembling the high pressure cell

The two adjusted NaCl disks with a gold capsule, two adjusted NaCl-20wt%ZrO_2 disks, and graphite disks were incorporated into the graphite sleeve, the making of which was treated in 2.2.4.1. Fig. 2.12 shows the cross section of the high pressure cell .

2.3. Experimental method

A high pressure experiment was conducted using the FB-30H flat belt-type high pressure apparatus (Fig. 2.13) installed in a 1,500ton press owned by NIRIM.

2.3.1. Setting the high pressure cell and gaskets

The high pressure cell and the gasket were combined and put into the high pressure apparatus. At the same time, to protect the top of the anvil, a stainless steel plate (SUS plate), a steel ring for the flow electric current into the sample area (current ring), and a molybdenum plate to prevent graphic heater deterioration (MO plate) were placed at the top and bottom of the high pressure cell. The current ring was made by forcing a ZrO_2 disk ordered from a manufacturer into a steel ring using an electric press.

Next, to prevent the gasket from overflowing and cooling water from invading the sample area, a 4-mm and a 5-mm thick rubber plate were arranged outside the outer powder compact gasket. Fig. 2.14 shows the overall setting of the high pressure experiment. In actual experiments, these components are set for each of the two (upper and lower) anvils but details of this are omitted here.

2.3.2. High temperature, high pressure experiment

After the high pressure cell, gasket and other components were set, pressure was increased by operating the press until reaching the required force. The relationship between hydraulic press pressure and pressure generated should be found in advance using the measurement formula described in the next section. After pressure grew to the specified strength, it was secured by pressing the control system's HOLD button,

and a hose for cooling water was connected to the upper and lower anvils to introduce the flow. After confirming the flow of coolant, a heating program that served the purpose of experiment was prepared based on the relationship between electric power and temperature that was found using the temperature measurement formula described in the following section, and the program began by switching on the heat power source. With this, the sample area started to grow hotter. Fig 2.15 gives an example of heating program patterns.

2.3.3. End of experiment

When the heating program ended, the electric current to the sample area was cut and the sample was rapidly cooled at 100 °C per second. At the close of the heating program, the coolant was stopped and its hose was replaced with one for compressed air to expel water remaining between the cylinder and anvil. Next, an oil pressure control program was executed to decrease pressure in the sample area. It took about 40 minutes to lower pressure in the sample area. Details of the pressure decreasing procedure are omitted here. The sample was removed following pressure decrease.

2.4. Pressure and temperature calibration

Synthesizing crystal, sinter and other substances at high pressures and temperatures demands the design and development of super-high pressure apparatus, but at the same time it is vitally important to measure and regulate pressure and steadily boost, measure and control temperature under high pressure. This section treats the pressure and temperature calibration methods used in context with belt-type high pressure apparatus.

2.4.1. Pressure calibration

Usually, phase transition of metal at room temperature is utilized to measure pressure in high pressure apparatus. This section describes a means of calibration using bismuth (Bi), thallium (Tl) and barium (Ba) required for high pressure apparatus up to 6 GPa.

2.4.1.1. Preparing components and making high pressure cells for pressure calibration

A pyrophyllite ring (outer diameter 12 mm, inner diameter 10 mm, height 1-2 mm) was tooled using a lathe. A round pyrophyllite rod was fixed to the lathe. First, a 10.0 mm diameter hole was cut in the rod, after which the rod's exterior was gradually shaved until its external diameter was 12.0±0.02 mm (the outer diameter of the pyrophyllite ring must fits the internal diameter of the NaCl-10wt%ZrO_2 ring with a steel ring).

Two NaCl-10wt%ZrO_2 rings with steel ring were readied for use. First, the steel-ring side was sanded, then the other side was ground to a height of 8.00±0.02 mm (combined height of the two rings in within 16.00±0.05 mm).

A graphite sleeve was prepared and forced into the two connected rings using a hand press. At both ends, the portion of the graphite sleeve exceeding the length of the rings was sanded off.

The graphite sleeve was pushed from one end using the upper and lower punches until the end of its sleeve protruded by 1 mm, with the protrusion sanded off. The pyrophyllite ring was then pushed into a gap created at the other end of the graphite sleeve, with the portion of the ring that protruded sanded off.

The interior of the graphite sleeve was hollowed out and finished using a 10-mm hand reamer. The outer surface of the high pressure cell was sanded so that it fit inside inner gasket used in the experiment. The 10.05 ϕ graphite disk was removed from the dryer and ground and finished to a height of 1.00±0.02 mm.

The NaCl-10wt%ZrO_2 powder (dried at 150 °C) was readied for use and two disks with a diameter of 10 mm (height 7.3 mm and 8.3 mm, respectively) were fashioned using a 10 ϕ die and punch made of Tungsten-Carbide. At this time, pressure applied using a press was four tons/cm^2. Both sides of the completed disks were sanded and finished to heights of 7.00±0.02 mm and 8.05±0.02 mm, respectively. It is advisable that the total height of the 10 mm diameter graphite disk and the two disks combined exceed that of the high pressure cells for pressure calibration by about 0.05 mm..

The side of the NaCl-10wt%ZrO_2 disks were rubbed using wet tissue and their size was adjusted to the extent that the disks passed inside the graphite sleeve smoothly.

Finally, using a hand press the graphite disk, kept horizontal, was pushed inside the graphite sleeve from the other side of the pyrophyllite ring. Fig. 2.16 (a) shows the cross section of the completed high pressure cells for pressure calibration.

2.4.1.2. Cells for pressure calibration

A hole was cut in the two NaCl-10wt%ZrO_2 disks using a drill with a 0.09 mm diameter bit, the hole made as close as possible to the edge of the disk (Fig. 2.16 (b)).

Gold leaf with a thickness of 0.02 mm was cut into fine pieces (thin enough to pass through a 0.09 mmϕ hole) and two gold lead lines were prepared. If the lines were slack, they were flattened using a steel rod.

2.4.1.3. Preparation of metal wire for pressure calibration

The two gold lines were threaded through the hole of the two disks, then cut so that both ends protruded from the disks by around 5.0 mm. For the 8 mm high disk, the protruding portions of the gold line were secured to the surface of the disk with a adhesive agent (bond), taking care not to let the adhesive stick to the upper side of the gold line. On the 7 mm high disk, the protruding portion of the gold line on one side was stuck to its surface with Cemedine (the protruding portion of the line on the other side, where bismuth piece were to be placed, left loose). Bismuth (Bi) attached like a thin film to the surface of a glass plate was prepared and cut into fine pieces using a razor blade so that one piece was about 0.1 to 0.2 mm thick Masses of thallium (Tl) and barium (Ba) were stretched into a thin leaf using a hand press before use. First, a piece of appropriate size was cut from these metals and put between the upper and lower punches and a drop of liquid paraffin added to them to forestall oxidation. The upper and lower punches were placed on a hand press and force of about three tons/cm^2 was applied to them. Pressure was reduced and the punches were taken out. These metals rolled as shown in Fig. 2.16 (c : left). The rolled metals were cut into pieces of appropriate size using a razor as shown in Fig. 2.16 (c : right) and further pressed under three

tons/cm^2 using a hand press. The metal pieces became sufficiently thin after two applications of pressure.

A drop of liquid paraffin was applied to the rolled metal pieces and they were further cut using a new razor blade. At this time, the Tl piece was about as thin as a human hair, with that of the Ba piece around three times as much. The three metal pieces were set on the 7mm disk as shown in Fig. 2.16 (d). First, the Bi piece was placed under the gold line and both ends of the line were stuck to the disk with Cemedine to link the gold line and the Bi piece. Next, the Tl and Ba pieces were set on the disk with one end of the Tl piece placed on the Bi piece and one end of the Ba piece placed on the Tl piece, taking care not to let the end of these metal pieces reach the edge of the disk, since if their end touched the edge of the disk, they would short-circuit the graphite heater, making it impossible to confirm the phase transition point of these metals.

After the three metal pieces were set on the disk, the 7mm disk was carefully inserted in the pressure calibration cell, with the side having the metal pieces facing up. Next, the 8mm disk was inserted in the cell so that it was on the 7mm disk. The two disks were inserted with their locations coordinated so that the gold line on the upper disk touched the Ba piece on the lower disk.

The completed pressure calibration cell was put between two sheets of stainless and resistance was measured using a tester. A resistance of 2-3 Ω is satisfactory. If there is no continuity or resistance is unusually low, it would be better to prepare a new set.

2.4.1.4. Setting peripheral equipment to pressure calibration

Firstly, a booth bar on the temperature control system of the high pressure apparatus was insulated. Usually, there are two booth bars but only one is insulated. Four screws for fixing the booth bar were loosened

and a sheet of thick paper like cardboard was put between the two metal plates. Then various pieces of peripheral equipment were set (Fig. 2.16 (e)).

2.4.1.5. How to read signals

A minimum of two persons were required to conduct pressure calibration experiments. One person record data on strokes occurring when oil pressure increases by 10 kg/cm^2, the other observe changes in voltage, shown on the recorder, which accompanied the phase transition of the metals and recorded oil pressure values when such change started and ended. Fig. 2.16 (f) shows voltage fluctuations, shown on the recorder, which accompanied the phase transition of the metals. Care was taken not to mistakenly set voltmeter range since it varies depending on types of metals. Phase transition pressure for each metal at room temperature is:

$Bi_{I\text{-}II}$	2.55 GPa
$Bi_{II\text{-}III}$	2.71 GPa
Tl	3.67 GPa
Ba	5.5 GPa

Values of phase transition pressure for each metal obtained in the experiments were converted to pressure values using the above data and the relationships between oil pressure and transition pressure were expressed in the form of a graph.

2.4.1.6. Handling samples after calibration

Following the completion of measurement and pressure was completely lowered, the high pressure cell was taken out, with the disks in

the graphite sleeve removed with extreme care. Usually, the disks are disfigured as shown in Fig. 2.16 (g). Disk diameter at their top and bottom edges and at the center as well as disk height were measured using slide calipers and recorded in a notebook. The diameter of the disk at the center was compared with previous data to confirm any significant difference between them.

2.4.2. Temperature calibration

Various ways to calibrate the temperature of the belt-type and other types of high pressure apparatus in which solids are used as a pressure medium have been proposed. But under the present circumstances the most appropriate method in terms of reliability and convenience is one that calibrates temperature using various thermocouples.

It is not impossible to insert a thermocouple in the high pressure cell when synthesis experiments are conducted but it is inconvenient because it takes too long to make a high pressure cell, the sample space is limited by the presence of a thermocouple, hydrostatic pressure drops and moisture (from the cement used to fix the thermocouple) is mixed with the cell. Compared with multi-anvil high pressure and other types of high pressure apparatus, belt-type high pressure apparatus makes possible the use of a fairly large graphite heater precise in dimensions, enabling highly reproducible resistance heating thanks to electric power control.

For the reasons described above, our research group is calibrating temperature at reasonable intervals (say, once every three to six months) by inserting a thermocouple in the sample area in advance, thus seeking data on the relationship between temperature and electric power at fixed pressure values. Based on these data, electric power suitable for experimental conditions is estimated and in routine synthesis experiments, temperature is regulated through electric power control.

The thermal electromotive force of thermocouples varies according to pressure, or so it has been reported, but our research group did not consider the pressure effects of such force.

2.4.2.1. Types of thermocouples

When calibrating temperature, NIRIM generally uses three types of thermocouples:

[1] Alumel (Ni: 94%; Al: 2%; Si: 1%; Mn: 2.5%)-Chromel (Ni: 80%; Cr: 20%)

Range of temperature measured: Up to 1,360 °C

[2] Platinum-Rhodium

Range of temperature measured:

Up to 1,600 °C for Pt/Pt13%Rh

Up to 1,700 °C for Pt6%Rh/Pt30%Rh

Up to 1,800 °C for Pt20%Rh/Pt40%Rh

[3] Tungsten-Rhenium

Range of temperature measured:

Up to 2,300 °C for W5%Re/W26%Re

In our experiments a gold capsule was used as described above, thus ruling out tests at temperatures exceeding the melting point of gold (e.g., 1,380 °C under pressure of 6 GPa). Therefore, a 0.5 mmϕ alumel-chromel thermocouple was used for temperature measurement.

2.4.2.2. Preparation of the high pressure cell for temperature calibration

2.4.2.2.1. Assembly of a thermocouple and a protective tube

Both lines of a thermocouple were each twisted three to five times and threaded through a two-hole alumina insulation tube (outer diameter 2.5 mm, about 9.0 mm in length; with two 0.7 mm diameter holes). The twisted lines of the thermocouple were cut so that their points protruded by around 3 mm from the edge and were fixed with cement.

2.4.2.2.2. Making a high pressure cell for temperature calibration

Unlike regular cells for synthesis experiments, a high pressure cell for temperature calibration must have space for the insertion of a thermocouple (hBN-20wt%ZrO_2). Other parts may have components similar to those of cells for synthesis experiments. Fig. 2.17 shows the cross section of a high pressure cell for temperature calibration.

2.4.2.2.3. Fixing the thermocouple to high pressure cell

To insert the thermocouple fixed to the alumina protective tube in the heater, a 2.6 mm diameter hole was drilled in the center of the hBN-20wt%ZrO_2 disk (Fig. 2.18 (a)). The hole was painstakingly bored so that the edge of the alumina protective tube went about 0.5 mm deep in the outer surface of the high pressure cell. The alumina protective tube with the inserted thermocouple was put into this hole and fixed with cement. By hardening the cement in a oven at more than 100 °C, the alumina protective tube with its thermocouple was secured to the high pressure cell (Fig. 2.18 (b)).

2.4.2.2.4. Fixing the thermocouple's inner pyrophyllite gasket

A groove about 3 mm wide and 1.5 mm deep was dug in the inner pyrophyllite gasket to secure the thermocouple, taking care to make the bottom of the groove flat. Tools such as a chisel, saw blade or file can be used to cut the groove. Usually, four grooves are dug to accommodate two pairs of thermocouples.

After making the four grooves (Fig. 2.19 (a)), the inner gasket was combined so that the surface of its tapering end came to the center of the high pressure cell to which the alumina protective tube with its thermocouple was fixed. The lines of the two pairs of thermocouples were bent so that they fit the groove in the inner gasket. At this time, the lines of the thermocouples were wound to reduce the risk of being cut during the experiment. After the lines of the thermocouples were wound, the inner gasket and high pressure cell were fixed with cement and heated in a oven.

When the inner gasket with high pressure cell were dry, it was placed on the core of a well-used anvil, and the lines of the thermocouple were put in the groove of the gasket and fixed to the anvil core with adhesive tape (Fig. 2.19 (b)). Next, cement was applied to the groove so that the thermocouple lines were covered, after which the cement was allowed to dry naturally and slowly. When the cement solidified, it was heated in a oven for more than 30 minutes.

After this drying process, a pyrophyllite plate 3 mm wide and 1.5 to 2 mm thick was processed into pieces of appropriate length, with the pieces then fixed to the groove with cement. The cement was dried as described above. After drying, the processed pyrophyllite plate was shaved and finished using a diamond file so that its surface matched the curved surface of the inner gasket.

2.4.2.3. Attaching the high pressure cell for temperature calibration

The 5mm-thick outer gasket and rubber plate were placed on the cylinder (Fig. 2.20) by combining them with the high pressure cell for temperature calibration; next the molybdenum plate, current ring and stainless plate were attached to the cell. The lines of the thermocouples were then taken out while winding them, and connected with vinyl-covered copper lines prepared in advance and which were led outside the high pressure vessel. At this time, the copper and thermocouple line connections were wrapped with vinyl tape to ensure their insulation from the cylinder and the anvil. After completing these procedures, the 4mm-thick outer gasket and rubber plate were set to cover the thermocouples. Following completion of arrangements on top of the cylinder, the inner and outer gasket, stainless plate, current ring and molybdenum plate were placed on the lower anvil as in regular experiments.

2.4.2.4. Increased pressure and calibration of temperature under high pressure

Based on the previously examined pressure-hydraulic pressure relationship (2.4.1), pressure was raised to the level at which our research team wanted to find the relationship between electric power and temperature. As pressure increased, electrical thermocouple resistance was measured to confirm that they were not cut. If both of the two pairs of thermocouples are cut during the pressure increase, farther apply of the pressure should be stopped, with the sample removed after pressure lowers in order to clarify the place of thermocouples cut and its reason.

When pressure rose to the desired level without cutting of the thermocouples, the heating power source program was set and values of electric current, voltage and thermal electromotive force, as well as

strokes, were read and recorded at a specific electric power level. These data were collected at various electric power levels.

Data on thermal electromotive force thus obtained were converted to temperature data to express in the form of a graph the relationship between electric power and heat.

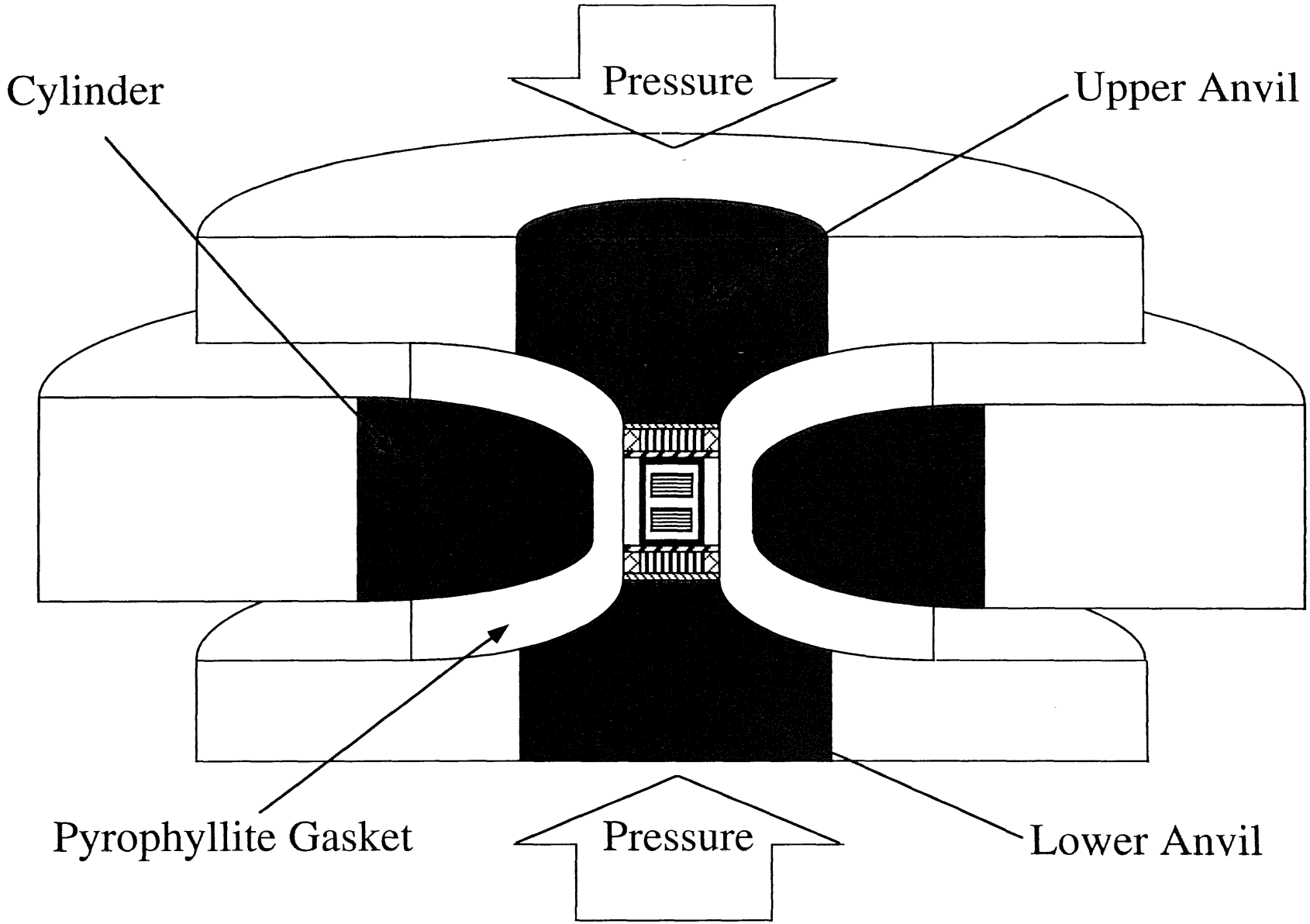

Fig. 2.1. The cross section of the flat-belt-type high pressure apparatus

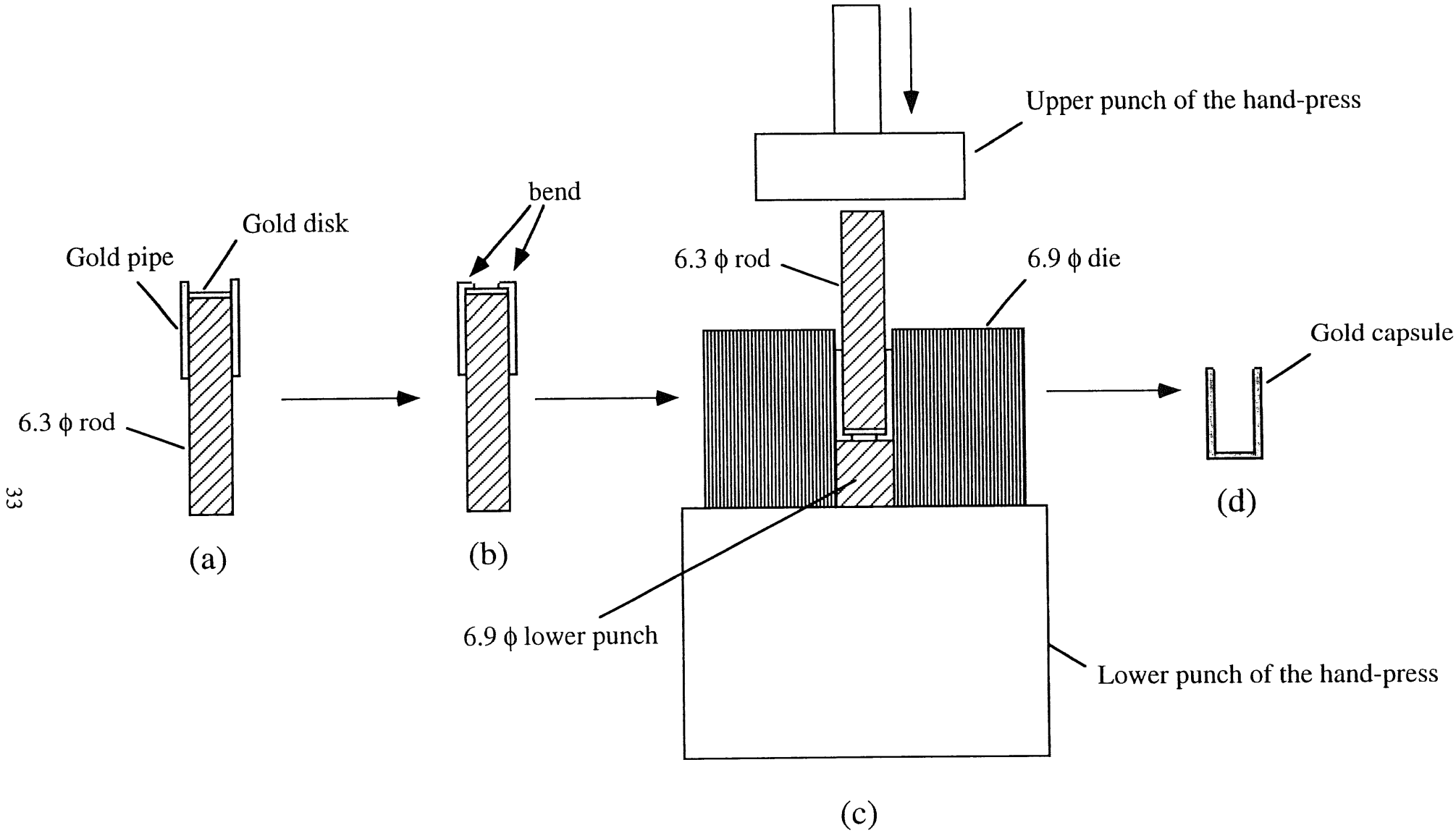

Fig.2.2. The way of manufacture of gold capsule (Cross section)

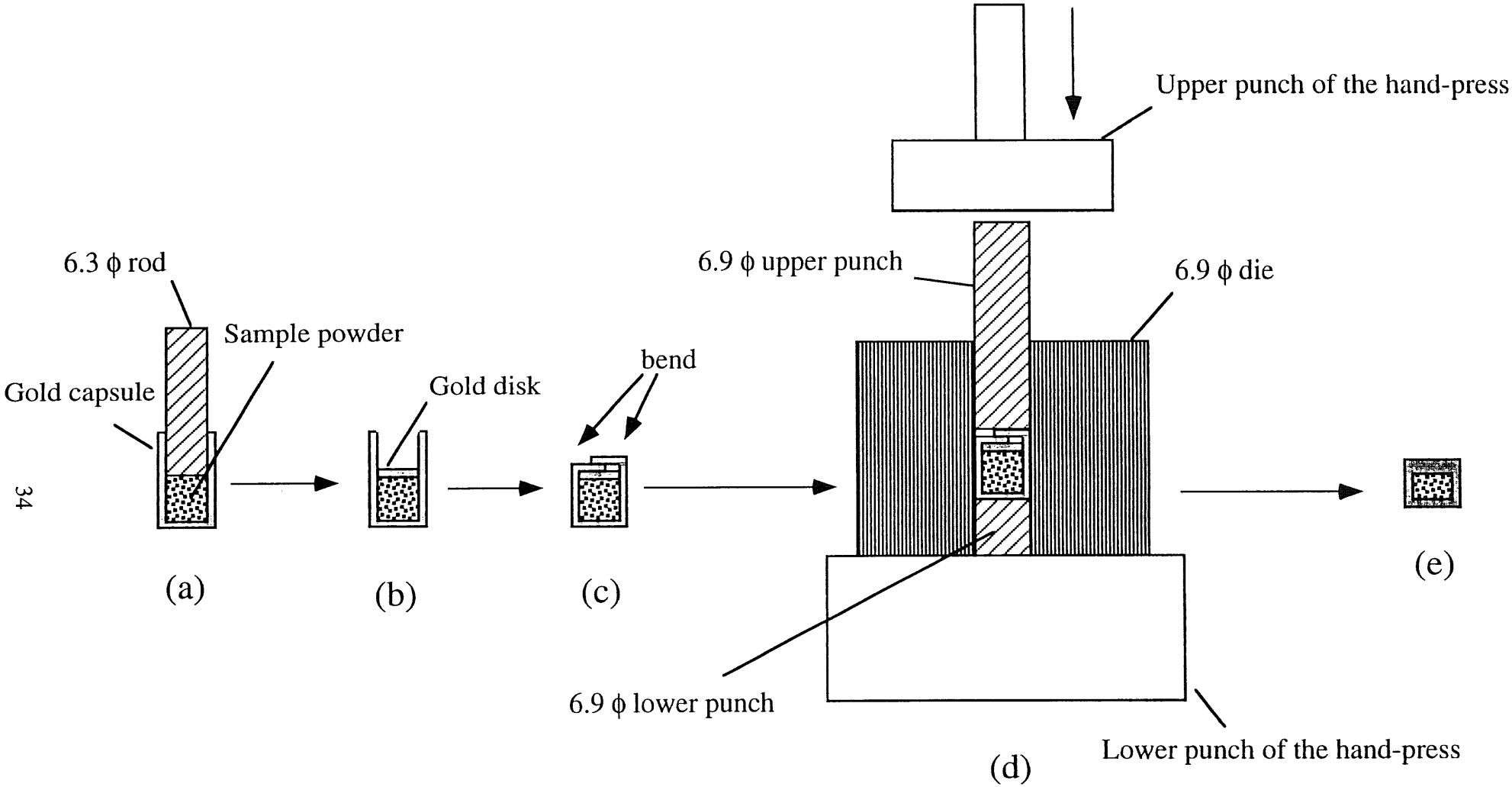

Fig.2.3. The way of enclosing the powder sample in gold capsule (Cross section)

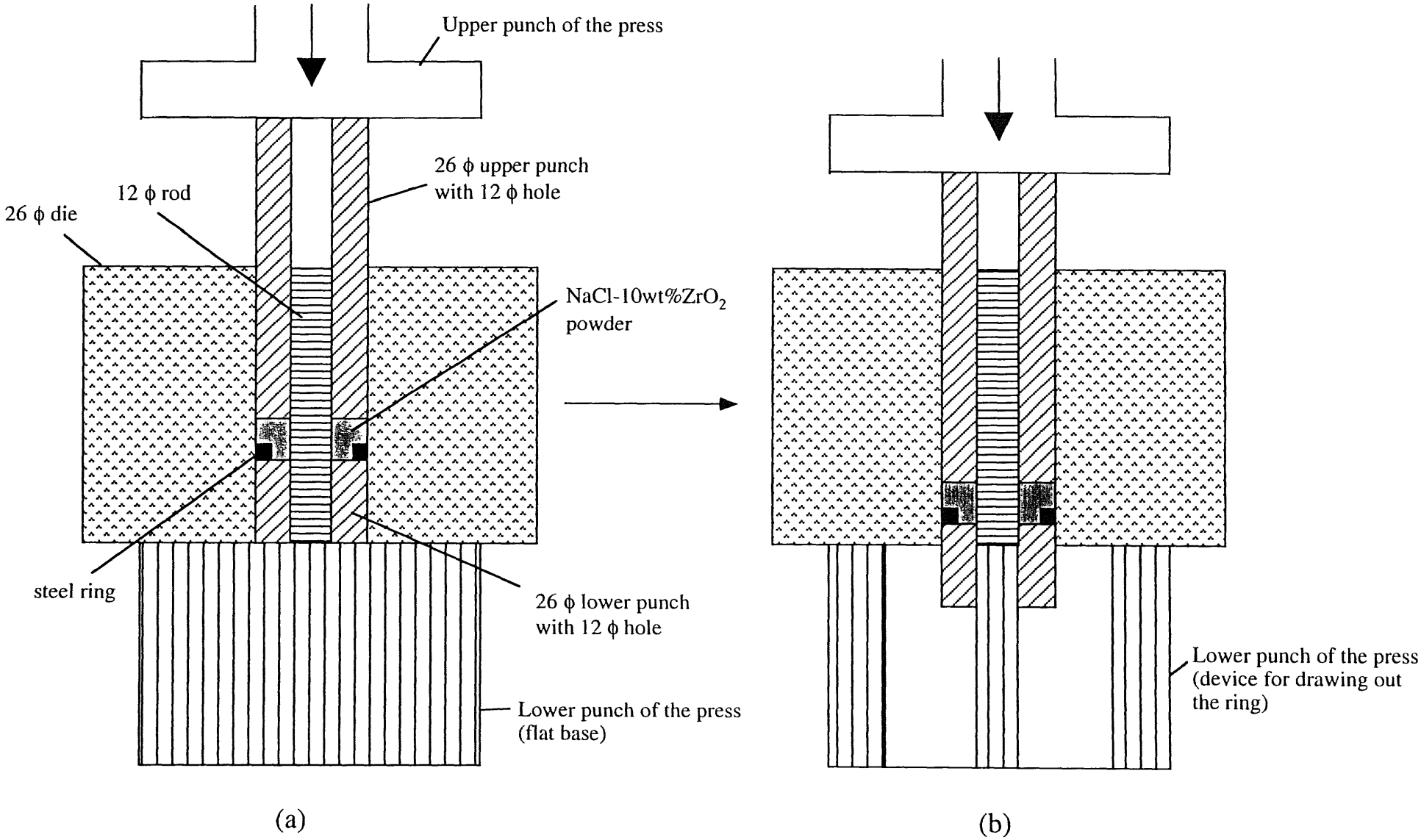

Fig. 2.4. The way of manufacture of NaCl-10wt%ZrO_2 compacted ring with a steel ring.

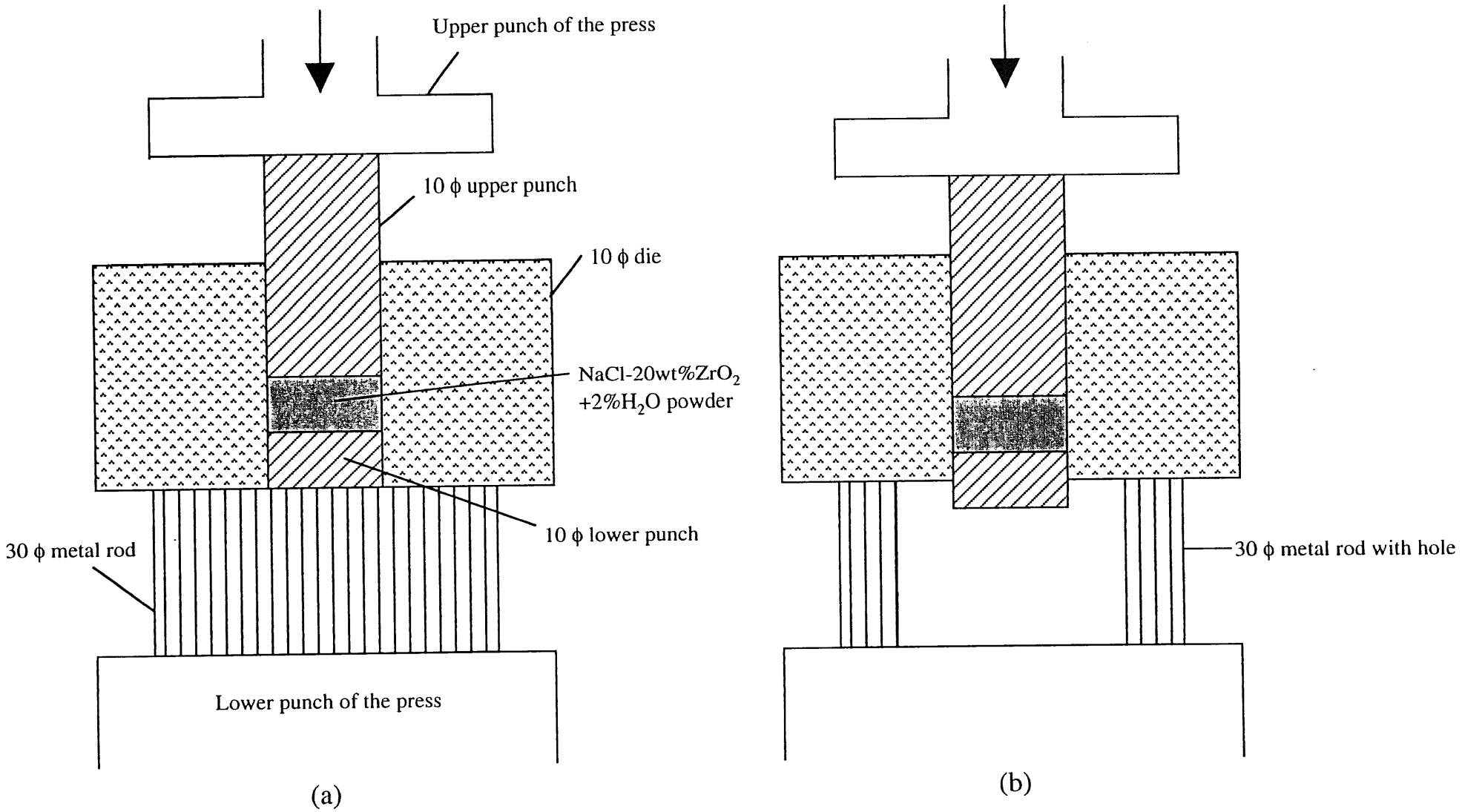

Fig. 2.5. The way of manufacture of NaCl-20wt%ZrO_2 disk.

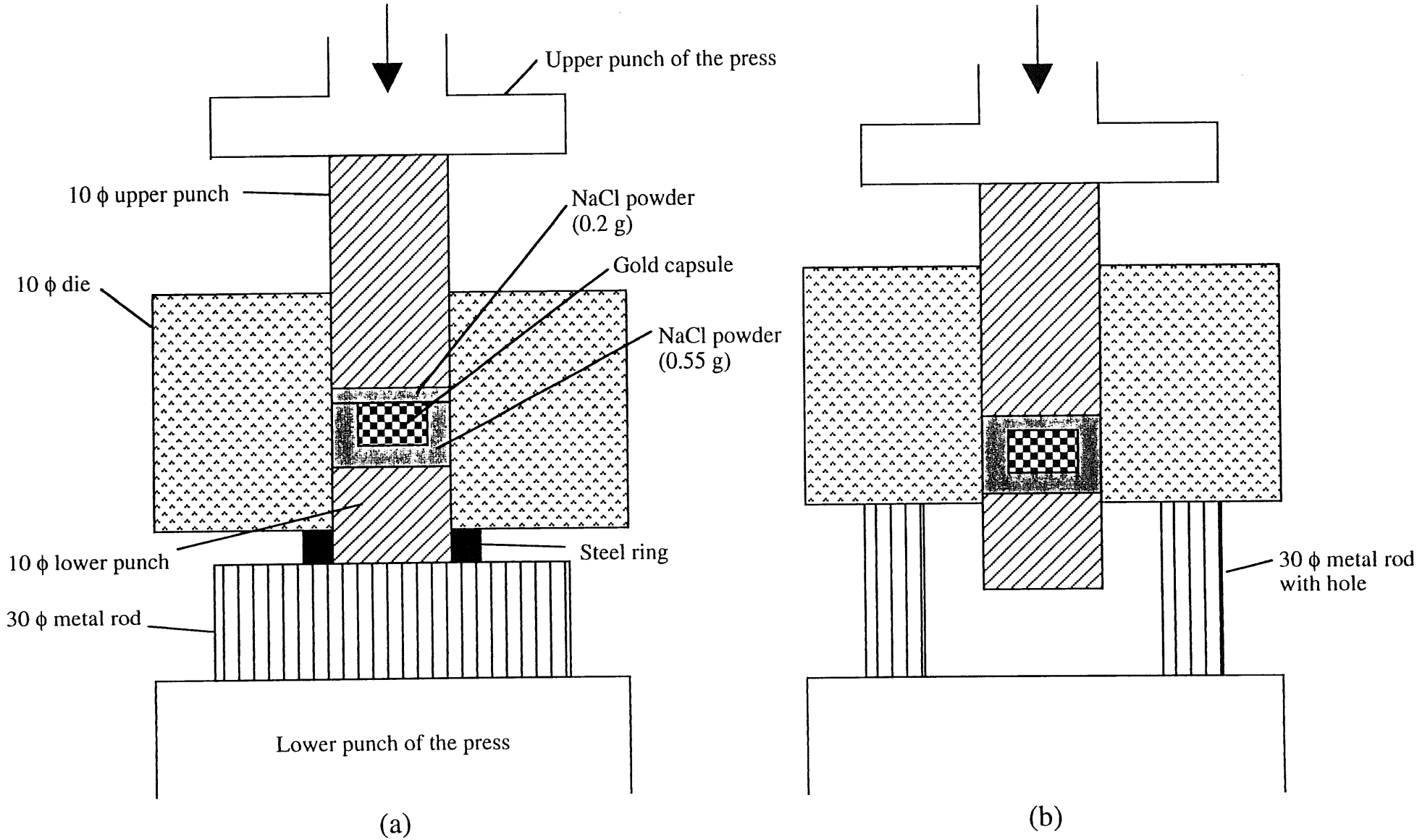

Fig. 2.6. The way of manufacture of NaCl disk including a gold capsule.

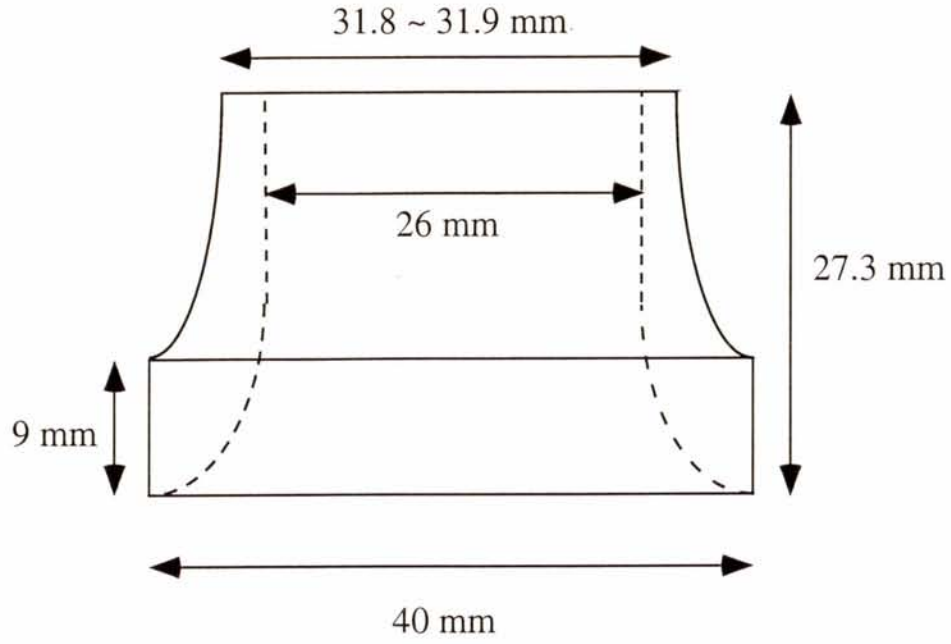

(a)

(b)

Fig. 2.7. Inner pyrophyllite gasket, the side view (a) and picture (b).

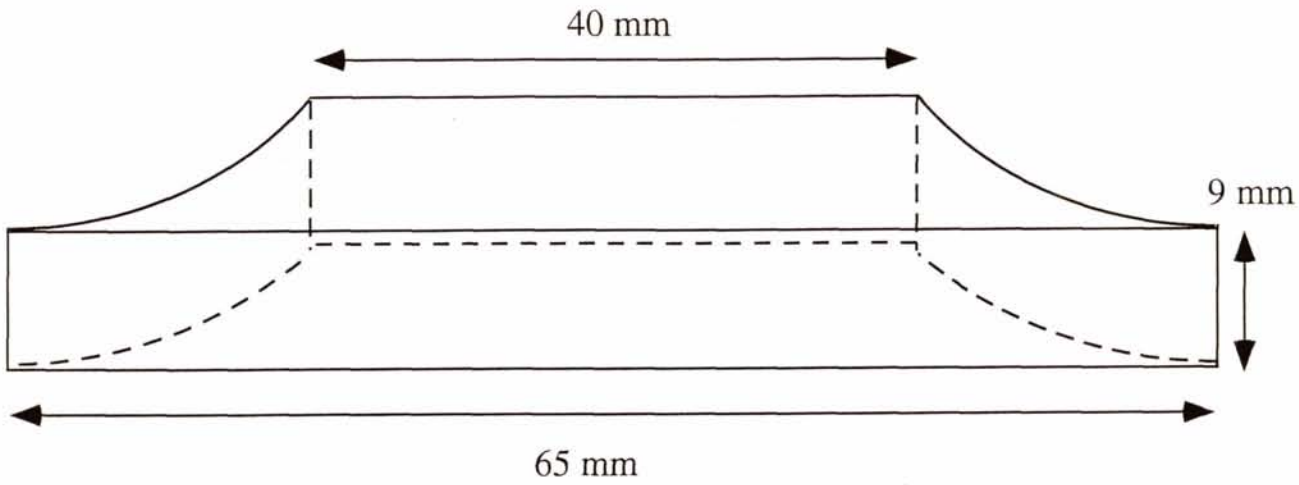

(a)

(b)

Fig. 2.8. Outer pyrophyllite powder compact gasket, the side view (a) and picture (b).

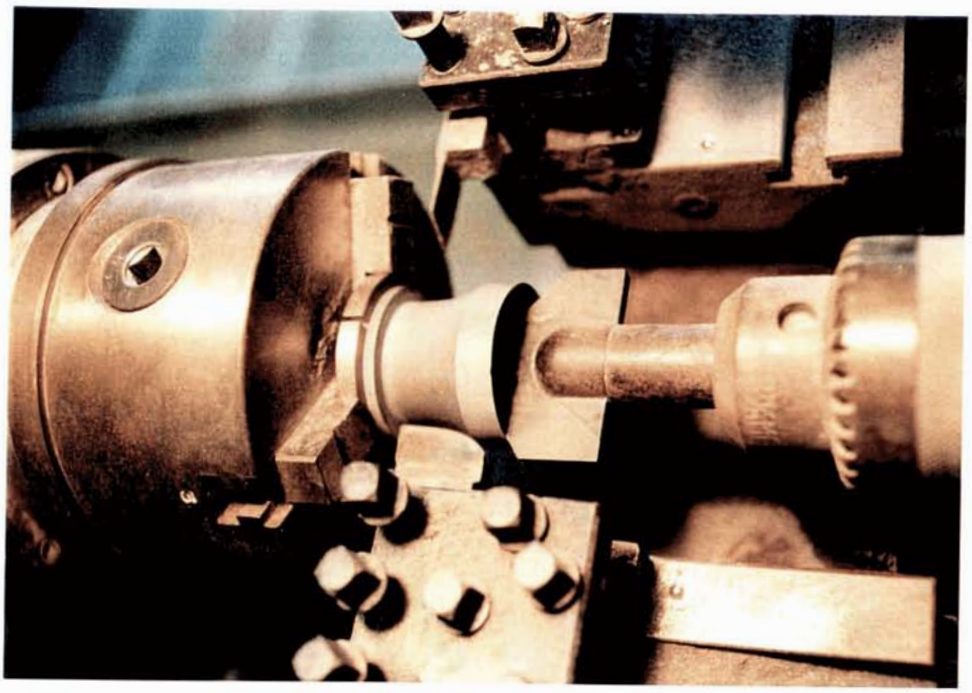

Fig. 2.9. The scene of manufacture of inner gasket.

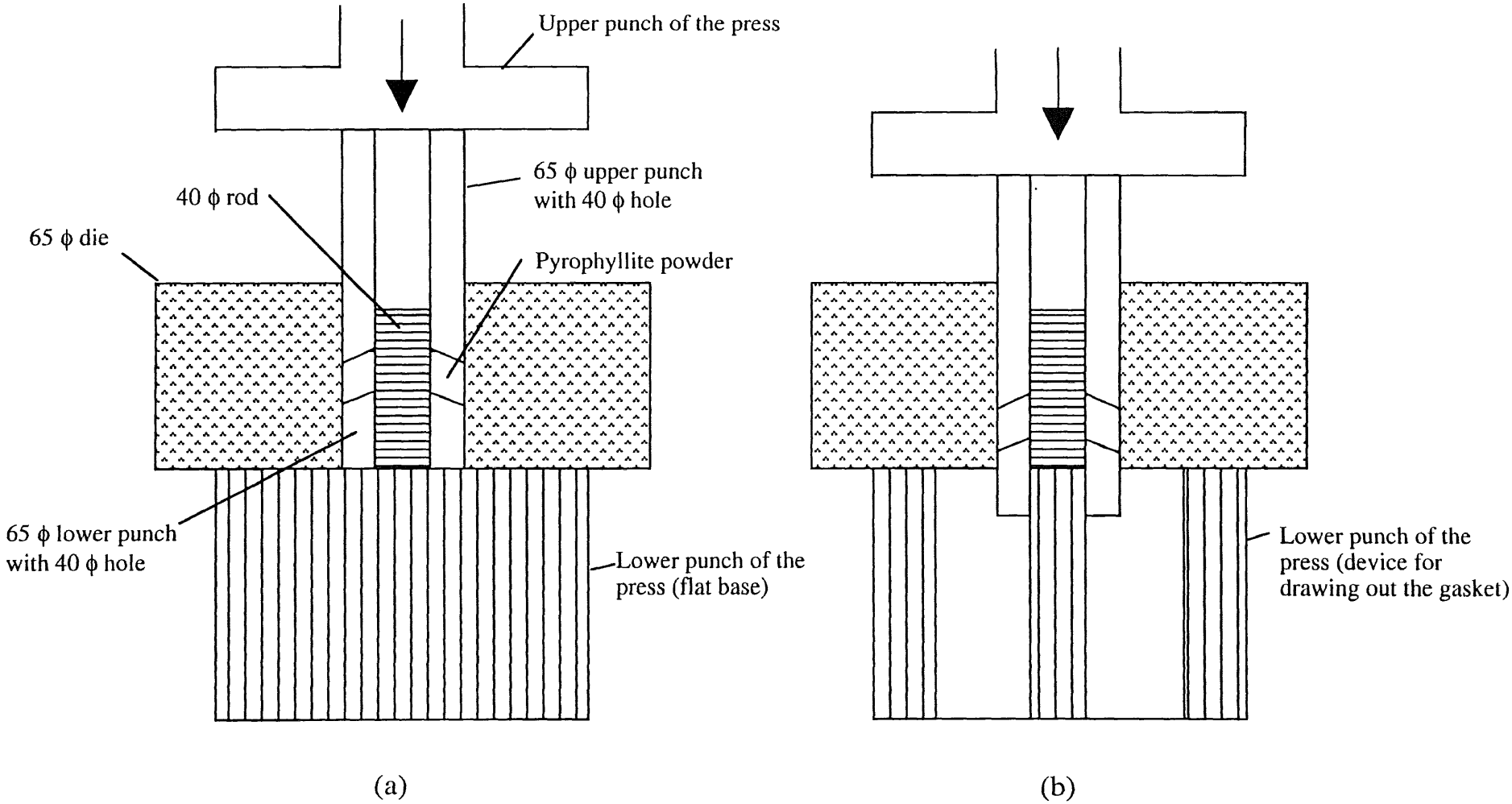

Fig. 2.10. The way of manufacture of outer pyrophyllite powder compact gasket

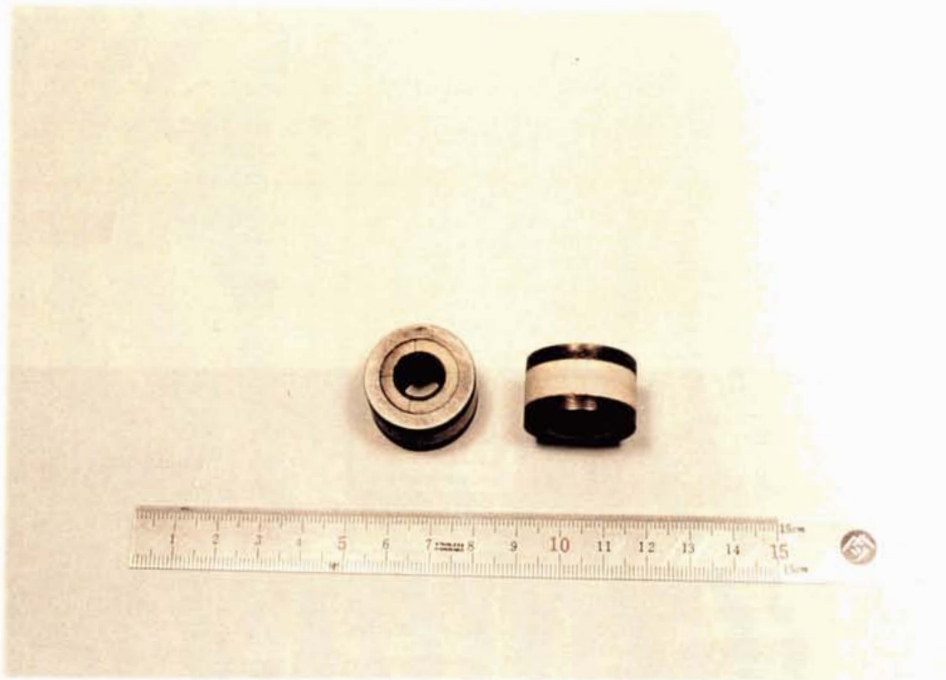

Fig. 2.11. The picture of the high pressure cell (outer part).

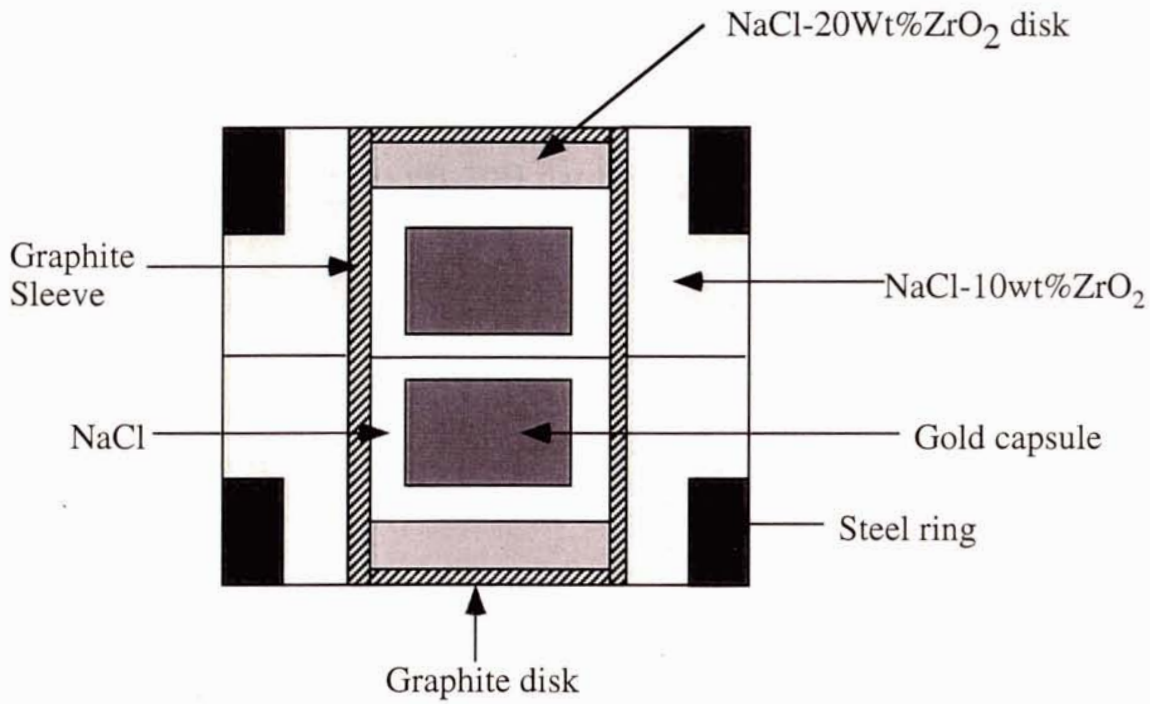

Fig. 2.12. The cross section of the high pressure cell

Fig. 2.13. The picture of the FB-30H flat-belt-type high pressure apparatus.

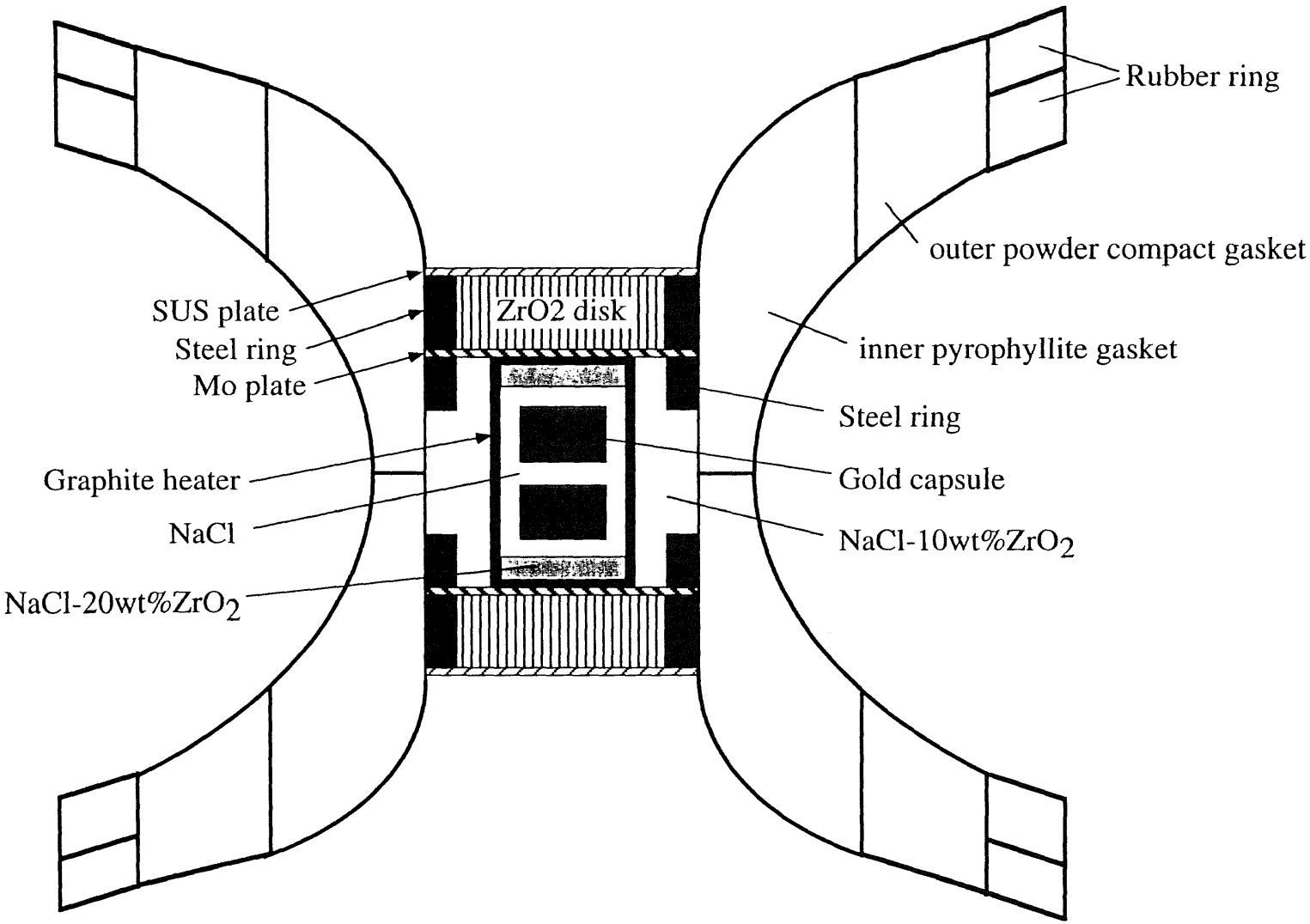

Fig.2.14. FB-30H sample assembly for high pressure experiment

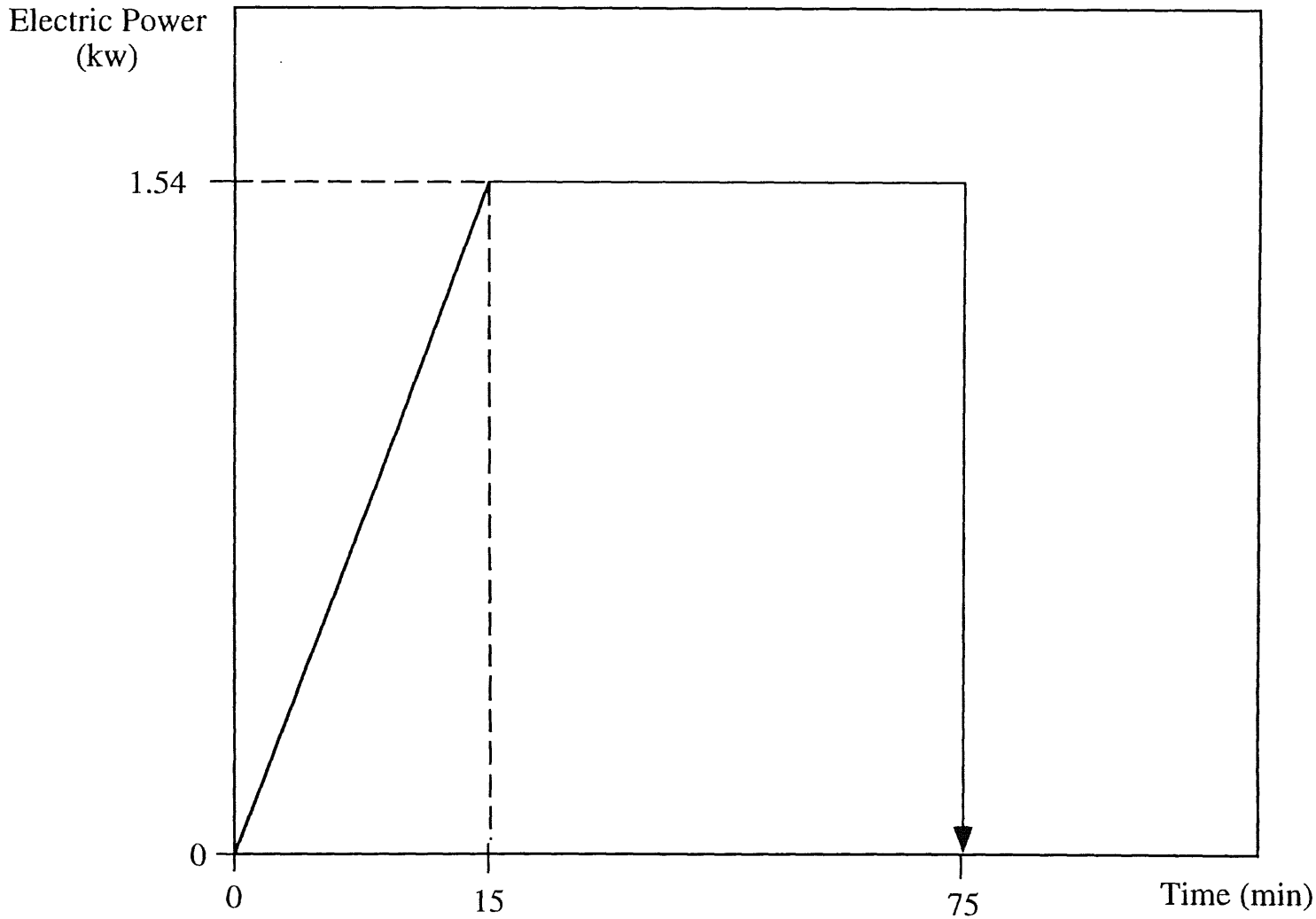

Fig. 2.15. An example of heating program patterns.

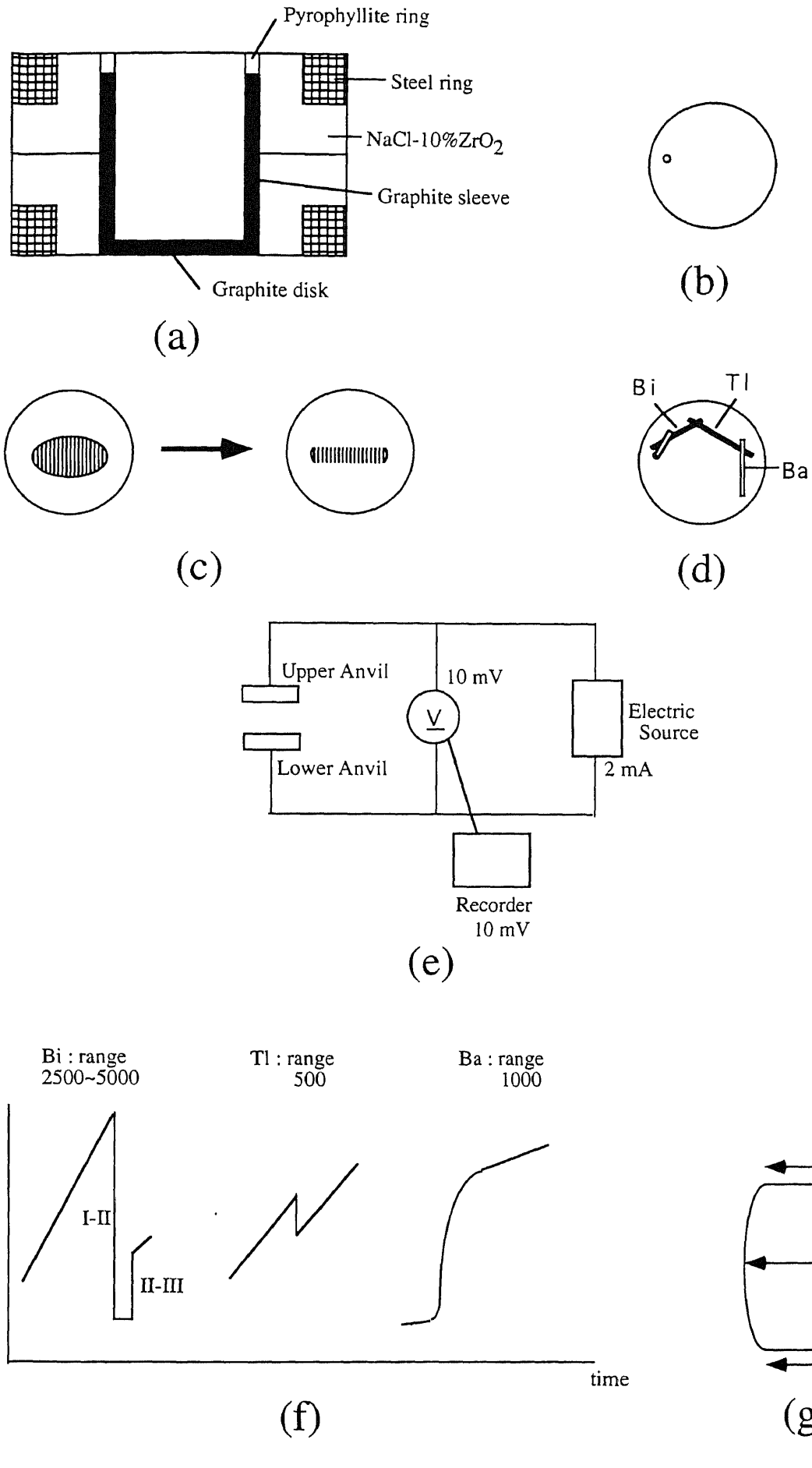

Fig. 2.16. The related figures of pressure calibration.

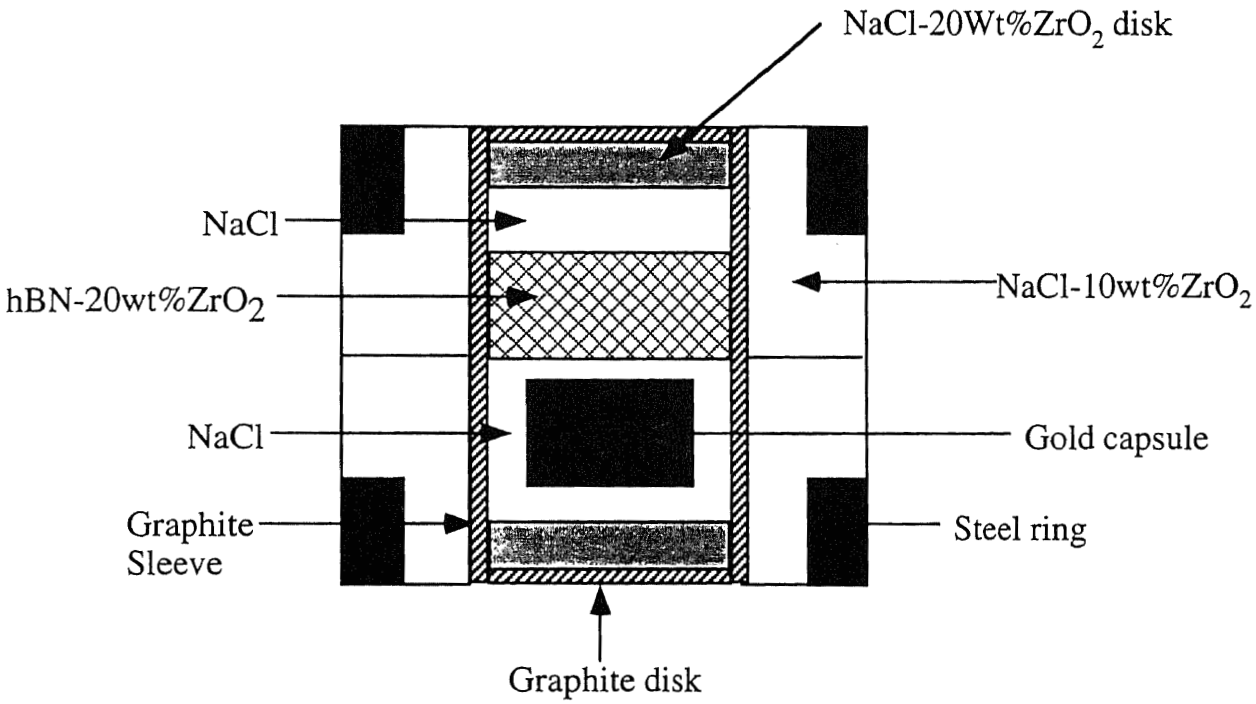

Fig. 2.17. The cross section of the high pressure cell for temperature calibration.

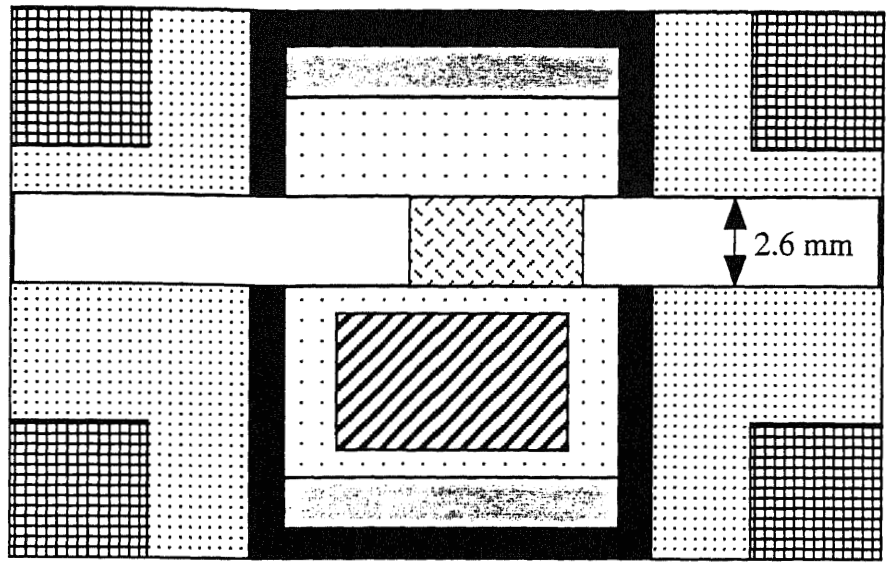

(a)

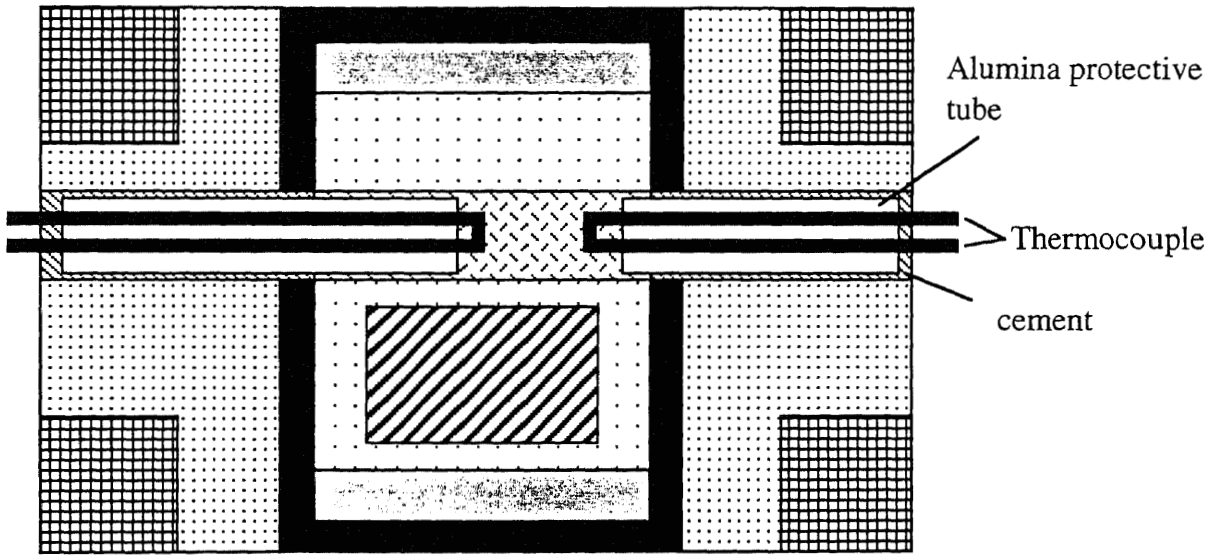

(b)

Fig. 2.18. The cross section of the high pressure cell. After drilled in the center of the hBN-20wt%ZrO2 disk (a) and after inserted the thermocouple (b).

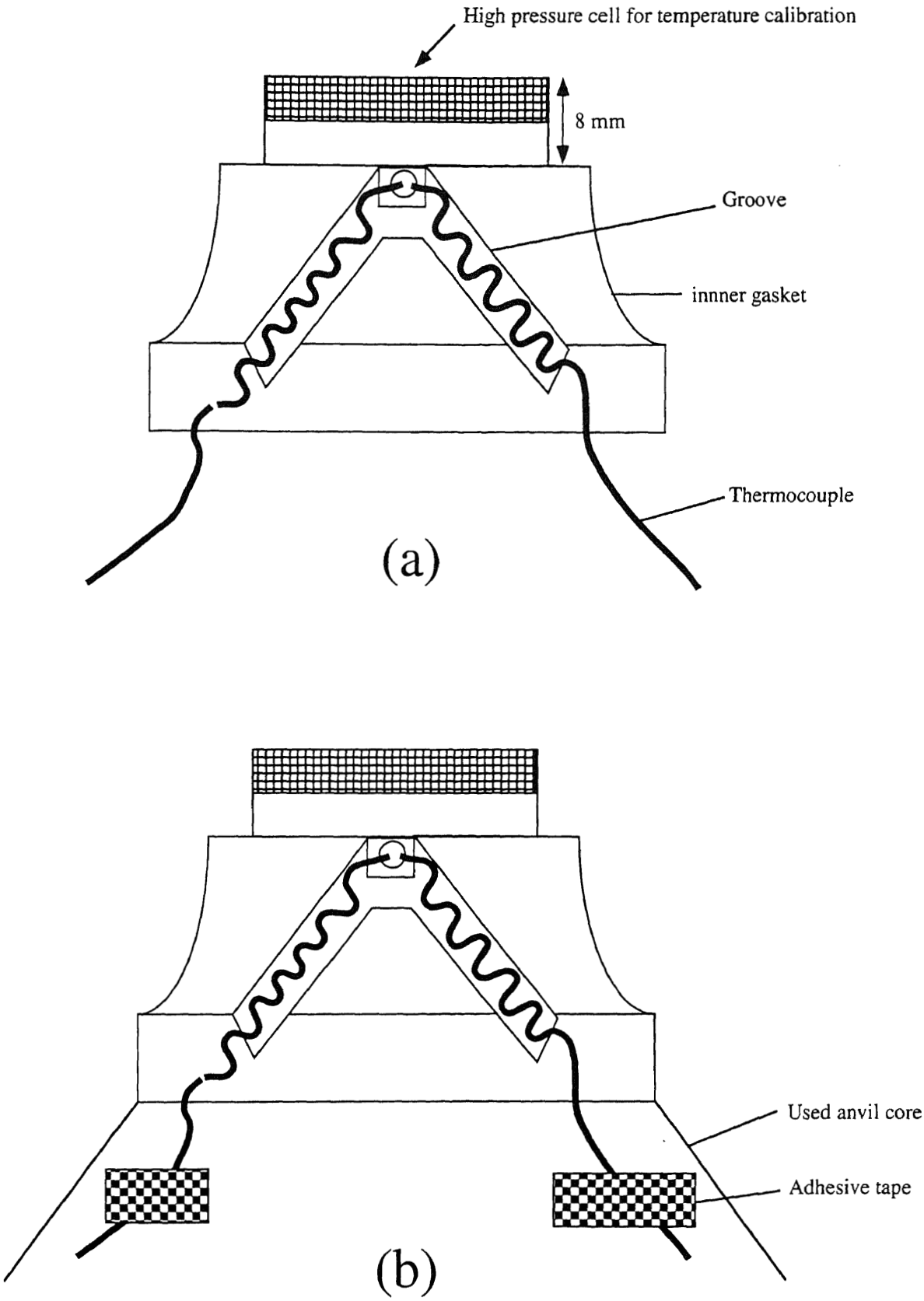

Fig. 2.19. The side view of the inner gasket with high pressure cell for temperature calibration.

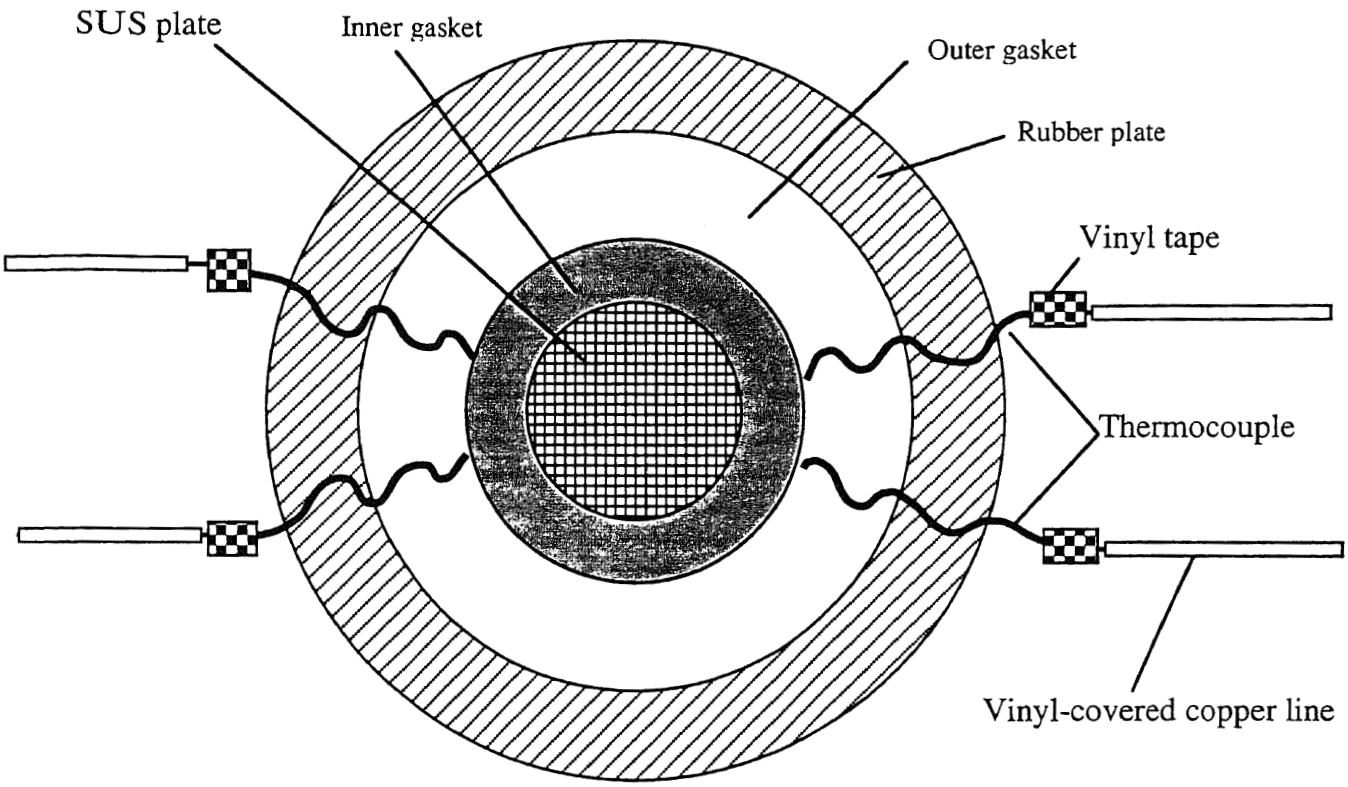

Fig. 2.20. The setting on the cylinder for temperature calibration.

3. High pressure synthesis and superconducting properties of new series of high-Tc superconductors, $(Cu_{0.5}C_{0.5})_mBa_{m+1}Ca_{n-1}Cu_nO_{2(m+n)+1}$

3.1 New oxycarbonate superconductors $(Cu_{0.5}C_{0.5})Ba_2Ca_{n-1}Cu_nO_{2n+3}$ (n=3,4) prepared at high pressure

In 1993, research group at Electrotechnical Laboratory, Japan have reported a new high pressure stable superconductor with T_c=117 K in the Ag-Ba-Ca-Cu-O system [20]. Though they suggested that the superconductor is the Ag-based 1234 isostructural to Tl(or Hg)-1234, its exact composition and structure were not given. Moreover, it was questionable if the superconductor includes silver.

To clarify these problems, we carried out phase search experiments of the system under high pressure. We isolated successfully two superconductors having T_c's, 67 and 117 K in which the latter seemed to correspond to the superconductor in question. Chemical and structural analysis indicated, however, that both phases did not include silver, at all, but instead, included carbon and "excess" copper.

The first superconductor including carbon, $(Ba,Sr)_2(Cu,C)_2O_y$ was reported in 1992 by Kinoshita and Yamada [13]. After their discovery, various kinds of oxycarbonate superconductors have been found by several groups [21-33]. Here, we report two new oxycarbonate superconductors, $(Cu_{0.5}C_{0.5})Ba_2Ca_2Cu_3O_{9\pm\delta}$ and $(Cu_{0.5}C_{0.5})Ba_2Ca_3Cu_4O_{11\pm\delta}$ which were found by chance in the process of phase search for the Ag-Ba-Ca-Cu-O system. The latter phase has T_c of 117 K which is the highest value among oxycarbonate superconductors found thus far.

3.1.1 . Experimental

A precursor having a composition "$Ba_2CaCu_2O_5$" was prepared from BaO_2, $CaCO_3$ (99.9%) and CuO (99.9%) at 850 °C in air for 4 days with several intermediate grindings. The precursor thus obtained was ground together with Ca_2CuO_3, CuO and Ag_2O (reagent grade) to obtain starting mixtures "$AgBa_2Ca_2Cu_3O_{7.5}$" and "$AgBa_2Ca_3Cu_4O_{9.5}$" for high pressure synthesis. The mixtures were sealed in gold capsules and allowed to react in a flat-belt-type high pressure apparatus at 5 GPa, 1200 °C for 1 hour, and then quenched to room temperature.

Though dry-box technique was used to handle the precursor, we found that the resulting high pressure products included significant amount of carbon (see below). We suspect that our process in preparation of the precursor was not adequate to remove a carbonate completely. Indeed, there were a few weak peaks unidentified in the X-ray powder pattern of the precursor, though most of peaks could be indexed assuming a mixture of $BaCuO_2$ and CaO.

X-ray powder diffraction patterns were obtained by a diffractometer (Philips-PW1700) with Cu Kα radiation and lattice constants were determined from the patterns using the least squares method. High-resolution transmission electron microscope (HRTEM) observations were carried out using a microscope (type H-1500) operated at 1000 kV.

DC magnetic susceptibility data were collected by a SQUID magnetometer (Quantum Design) under the field-cooling condition at a magnetic field of 20 Oe. DC resistivities were measured by the standard four-probe method.

Atomic rations of Ba, Ca and Cu (and Ag) were determined by EPMA method. In addition, carbon contents were obtained using a carbon determinator (LECO, type WR12).

3.1.2. Results and discussion

Figures 3.1 (a,b) show the X-ray powder diffraction patterns of the high pressure products from the starting mixtures, "$AgBa_2Ca_2Cu_3O_{7.5}$" and "$AgBa_2Ca_3Cu_4O_{9.5}$", respectively. Most X-ray peaks in figs. 3.1 (a) and (b) could be indexed assuming tetragonal cells with a_t=3.859(1), c_t=14.766(5) Å and a_t=3.855(1), c_t=17.930(6) Å, respectively. In addition, any systematic extinction was not, in both cases, observed, suggesting a space group, P4/mmm. These crystal data imply that the former phase is isostructural to Tl(or Hg)-1223 [34] and the latter to Tl(or Hg)-1234 [35]. Hereafter, we call the former phase as (Cu,C)-1223 and the latter as (Cu,C)-1234 since they actually included carbon (and copper) instead of silver as revealed below.

Table 3.1 gives atomic ratios and carbon contents in (Cu,C)-1223 and 1234 determined by EPMA and carbon analysis. Though we carefully checked in EPMA measurement, any detectable signal of silver was not observed in both the (Cu,C)-1223 and 1234 phases. Most silver was found to extract as metal suggesting that Ag_2O worked only to increase oxygen pressure.

In (Cu,C)-1223, the observed atomic ratio, Cu/(Ba+Ca) deviated significantly from 3/4 which is expected for a 1223-type compound but is rather close to 3.5/4. The Ba/Ca ratio was close to unity consistent with the 1223-composition. On the other hand, it included noticeable amount of carbon (0.85 wt%). Similar results were obtained for (Cu,C)-1234; its Cu/(Ba+Ca) ratio was closer to 4.5/5 rather than 4/5 and carbon content was as large as 0.62 wt%. In (Cu,C)-1234, however, the Ba/Ca ratio was smaller than 2/3 expected for the 1234-composition, suggesting partial replacement of the Ba sites by Ca atoms.

Figures 3.2 and 3.3 give electron diffraction patterns and lattice images for (Cu,C)-1223. The h0l diffraction pattern in fig. 3.2 (b) is not

fully compatible with the simple tetragonal cell of P4/mmm but some extra spots appear indicating a superstructure having $a_S=2a_t$, $b_S=b_t$, $c_S=2c_t$ and a possible space group, Bmmm. In the lattice images projected along the [1 0 0] direction (fig. 3.3(a)) and the [0 1 0] direction (fig. 3.3(b)), we can distinguish Cu, Ba and Ca planes stacked consistent with the 1223-type structure. However, in the image of fig. 3.3(b), the plane between two Ba ones consists of two types of dots having dark and less dark contrast to give $2a_t$ periodicity. Similar dot with less dark contrast was, corresponding to a carbon site, often observed in oxycarbonate superconductors (see ref. 21, for instance). Taking into account the composition analysis in table 3.1, we concluded that this plane is occupied by Cu and C atoms alternated along the at-axis as -Cu-C-Cu-C-. The Cu-C sequence in the upper (or lower) tetragonal cells has a different phase, -C-Cu-C-Cu-, resulting in $2c_t$ periodicity in the superstructure. The ideal composition of this phase becomes, therefore, $(Cu_{0.5}C_{0.5})Ba_2Ca_2Cu_3O_{9\pm\delta}$. The 2a periodicity due to Cu-C ordering has been also reported for the 123-type oxycarbonate, $(Y,Ca)Sr_2(Cu,C)_3O_y$ [23], for instance.

Similar superstructure was observed in (Cu,C)-1234, as well. Though we have not obtained lattice images of (Cu,C)-1234 yet, electron diffraction patterns reveal that it has a superstructure with $a_S=2a_t$, $b_S=b_t$, $c_S=2c_t$ and a possible space group, Bmmm derived from the 1234-type tetragonal cell (see the h0l diffraction pattern in fig. 3.4). The plane between the Ba ones, therefore, consists of Cu and C located alternately along at-axis and the ideal composition becomes $(Cu_{0.5}C_{0.5})Ba_2Ca_3Cu_4O_{11\pm\delta}$. In fig. 3.5, structure models for (Cu-C)-1223 and 1234 are shown, based on the above results.

Figure 3.6 gives DC susceptibility data for (Cu,C)-1223 and 1234. The former phase shows sharp superconducting transition at 67 K, while

the latter seems to have two-step superconducting transitions at 117 and 95 K. The second transition at 95 K may be caused by other member of the series, like (Cu,C)-1245 included as a minor phase. Both samples showed diamagnetic susceptibilities large enough to assume bulk superconductivity.

Figure 3.7 indicates DC resistivity data for (Cu,C)-1223 and 1234. Both compounds show metallic behavior above T_c. The superconducting transition was very sharp in each sample and T_c's determined from the resistivity data were 67 K for (Cu,C)-1223 and 117 K for (Cu,C)-1234, consistent with the susceptibility data.

3.2 A new series of oxycarbonate superconductors $(Cu_{0.5}C_{0.5})_2Ba_3Ca_{n-1}Cu_nO_{2n+5}$ (n=4,5) prepared at high pressure

In previous paragraph, we described new oxycarbonate superconductors, $(Cu_{0.5}C_{0.5})Ba_2Ca_{n-1}Cu_nO_{2n+3}$ ((Cu,C)-12(n-1)n). Two members of the series with n=3 ((Cu,C)-1223) and n=4 ((Cu,C)-1234) were isolated.

In the X-ray pattern of (Cu,C)-1234, we found some extra peaks which suggested existence of a member with a higher n, such as (Cu,C)-1245. Therefore, we carried out phase search experiments under high pressure, expecting preparation of a new member of the series. We found, however, a completely different series of oxycarbonate superconductors, $(Cu_{0.5}C_{0.5})_2Ba_3Ca_{n-1}Cu_nO_{2n+5}$ ((Cu,C)-23(n-1)n). The members of the series with n=4 and 5 were prepared in bulk.

3.2.1.Experimental

A precursor having a composition "$Ba_2Ca_3Cu_4O_9$" was prepared from BaO_2, $CaCO_3$ (99.9%) and CuO (99.9%) at 850 °C in air for 12 days with several intermediate grindings. The precursor thus obtained was mixed together with $CaCO_3$, Ca_2CuO_3, CuO and Ag_2O (reagent grade) in a dry-box to obtain starting mixtures "$C_{0.5}Ba_2Ca_4Cu_{5.5}O_{13}$" and "$C_{0.6}Ba_2Ca_4Cu_{5.5}O_{13.2}$" for high pressure syntheses. Ag_2O was expected to work as an oxygen source. Though a small amount of carbon, about 0.3 wt%, was included in the precursor, we disregarded this. The mixtures were sealed in gold capsules and allowed to react in a flat-belt-type high pressure apparatus at 5 GPa, 1250 °C for 1 hour, and then quenched to room temperature.

X-ray powder diffraction patterns were obtained by a diffractometer (Philips-PW1800) with Cu Kα radiation and lattice constants were determined from the patterns using the least squares method. High resolution transmission electron microscope (HRTEM) observation was carried out using a microscope (type H-1500) operated at 1000 kV.

DC magnetic susceptibility data were collected by a SQUID magnetometer (Quantum Design) at a magnetic field of 20 Oe. DC resistivities were measured by the standard four-probe method.

3.2.2. Results and discussion

Figures 3.8(a,b) show the X-ray powder diffraction patterns of the high pressure products from the starting mixtures, "$C_{0.6}Ba_2Ca_4Cu_{5.5}O_{13.2}$" and "$C_{0.5}Ba_2Ca_4Cu_{5.5}O_{13}$", respectively. Major X-ray peaks in fig. 3.8(a) could be indexed assuming a tetragonal cell with a=3.855(3), c=21.87(1) Å. The X-ray peaks in fig. 3.8(b) could be, on the other hand, indexed assuming a mixture of two tetragonal

phases in which one was the same phase as that in fig. 3.8(a) while the other had lattice constants, a=3.857(1), c=25.067(7) Å. Systematic extinction was not observed in both cases, suggesting a space group, P4/mmm. Comparing the c-dimensions of these phases with those of (Cu,C)-1223 (14.766 Å) and (Cu,C)-1234 (17.930 Å), one may suppose that they are n=4, 5 members of the (Cu,C)-12(n-1)n series. However, HRTEM observation indicated clearly that they belong to a different homologous series of compounds. Hereafter we will call the phase with c≈21.9 Å as (Cu,C)-2334, while that with c≈25.1 Å as (Cu,C)-2345, since they are, as shown below, n=4, 5 members of the series, $(Cu_{0.5}C_{0.5})_2Ba_3Ca_{n-1}Cu_nO_{2n+5}$.

Figures 3.9(a,b) show electron diffraction (ED) patterns of the (Cu,C)-2334 phase. These ED patterns are compatible with an orthorhombic superlattice (possible space group Pmmm), a_S=2a, b_S=b and c_S=c for the tetragonal lattice described above. On the contrary, the (Cu,C)-12(n-1)n series of compounds have different superlattices, a_S=2a, b_S=b and c_S=2c with respect to the tetragonal subcells. In the lattice images of (Cu,C)-2334 shown in figs. 3.10(a,b), we can clearly distinguish three Ba, three Ca and four Cu planes stacked along the c axis. Two remaining metal planes between the Ba ones are the (Cu,C) planes. In the image in fig. 3.10(b) which corresponds to the ED pattern of fig. 3.9(b), ordering between Cu and C is observed; a dot with dark contrast and that with less dark contrast are placed alternately along the a axis giving the 2a periodicity. This kind of -Cu-C-Cu-C- ordering was seen in the (Cu,C)-12(n-1)n compounds or in a 123-type oxycarbonate [23]. In (Cu,C)-12(n-1)n, however, a (Cu,C) plane of upper or lower subcells has the opposite phase (-C-Cu-C-Cu-) resulting in the 2c periodicity as well as the 2a periodicity. On the contrary, every (Cu,C) plane has the same phase with respect to the Cu-C sequence in (Cu,C)-2334.

In fig. 3.11, the structure model of (Cu,C)-2334 is given based on the HRTEM images. The ideal composition of this phase becomes $(Cu_{0.5}C_{0.5})_2Ba_3Ca_3Cu_4O_{13}$.

The above results on the (Cu,C)-2334 phase suggest that the phase with c≈25.1 Å ("(Cu,C)-2345") has an ideal composition, $(Cu_{0.5}C_{0.5})_2Ba_3Ca_4Cu_5O_{15}$ and a structure shown in fig. 3.11. Though we have not obtained lattice images of "(Cu,C)-2345" yet, an n=5 slab was often seen as intergrowth in the n=4 structure (see fig. 3.10(b)). Moreover, we sometimes found an intermediate phase between (Cu,C)-2334 and (Cu,C)-2345 in HRTEM observation (we refer to this phase as (Cu,C)-23(3.5)(4.5)). Figures. 3.12 and 3.13 show ED patterns and a lattice image of such a phase in which the n=4 and n=5 slabs are stacked alternately along the c axis giving c≈46 Å. In addition, the 2a periodicity is seen derived from the Cu-C ordering. Though we have not confirmed this phase in X-ray patterns, it may be prepared in bulk by proper synthetic conditions.

One may still ask a question if the c≈25.1 Å phase is indeed (Cu,C)-2345 rather than (Cu,C)-1256, since we have not gotten the lattice images for it. In fig. 3.14, a- and c-dimensions are plotted against m, a sum of numbers of (Cu,C) and Cu planes in a unit formula (note that m is 7 for both compositions, (Cu,C)-2345 and (Cu,C)-1256). The c-dimensions of (Cu,C)-2334 (m=6) and "(Cu,C)-2345" (m=7) deviate upward from a straight line obtained for (Cu,C)-1223 (m=4) and (Cu,C)-1234 (m=5), probably due to higher numbers of Ba planes included in a subcell. This is compatible with the conclusion that "(Cu,C)-2345" is the n=5 member of the (Cu,C)-23(n-1)n series rather than the n=6 member of the (Cu,C)-12(n-1)n series. Similar positive deviation was observed in the a-dimension vs. m plot, as well.

The oxidation state of Cu in the ideal compositions, $(Cu_{0.5}C_{0.5})_2Ba_3Ca_{n-1}Cu_nO_{2n+5}$ is exactly 2+ which means that no carriers (holes) are doped. The real compositions may, therefore, differ from the ideal ones; introduction of excess oxygen and/or replacement of Cu for C may occur in the (Cu,C) planes of the superconducting phases. Indeed, mixing of Cu and C for one crystallographic site has been reported for $(Ba,Sr)_2(Cu,C)_2O_y$ [13].

In the structure models in Fig. 3.11, C_2O_5 groups are assumed to exist rather than isolated CO_3 groups. Since the oxygen positions within the (Cu,C) plane has not been determined, we can not exclude completely structural models which include isolated CO_3 groups. Neutron diffraction or vibrational spectroscopic studies may be helpful to answer this question.

The nominal compositions in the present syntheses were Ca-rich with respect to the ideal compositions. The excess Ca might be concentrated in impurity phases. In (Cu,C)-1234, on the other hand, Ba/Ca ratio determined by EPMA was substantially smaller than the ideal one indicating partial substitution of Ca for Ba. Such a substitution may occur in the present series of compounds, as well.

The present series of compounds are the first examples in which three BaO layers are included in a charge reservoir layer. This type of structural block appears to be unstable because of highly active Ba ions. It is worth noting that every Ba ion is bounded to one or two CO_3 groups in the structures in fig. 3.11. Insertion of CO_3 groups between the BaO planes and the ordered manner in the Cu-C sequence seem to play a definite role for stabilizing the block which consists of three BaO planes.

Figures 3.15 and 3.16 indicate DC susceptibility and DC resistivity data for the samples whose X-ray patterns are shown in figs. 3.8(a,b). Both samples indicated onset superconducting transition at 113 K and

large enough diamagnetic susceptibilities at 5 K to assume bulk superconductivity. Since the sample corresponding to fig. 3.8(a) (denoted as (Cu,C)-2334 in figs. 3.15 and 3.16) did not include the (Cu,C)-2345 phase, it is reasonable to assume that T_c (onset) of (Cu,C)-2334 is 113 K. On the other hand, the sample corresponding to fig. 3.8(b) (denoted as (Cu,C)-2334+2345) included both (Cu,C)-2334 and 2345 phases. This sample showed a larger diamagnetic susceptibility at 5 K than the sample of fig. 3.8(a). The susceptibility data of the zero-field-cooling condition appear to show two-step decreases at 113 K and near 90 K in which the latter may reflect the transition of (Cu,C)-2345. However, the second "transition" disappeared in the field-cooling condition resulting in a single transition at 113 K. The larger diamagnetic susceptibility at 5 K suggests that (Cu,C)-2345 is also superconducting with T_c near 110 K. We need to prepare a single-phase sample for the definite determination of T_c of (Cu,C)-2345.

3.3 A new oxycarbonate superconductor $(Cu_{0.5}C_{0.5})_2Ba_3Ca_2Cu_3O_{11}$ (T_c=91 K) prepared at high pressure

In previous paragraph, we described new series of oxycarbonate superconductors, $(Cu_{0.5}C_{0.5})_mBa_{m+1}Ca_{n-1}Cu_nO_{2(m+n)+1}$ [(Cu,C)-m(m+1)(n-1)n]. Thus far, n=3 and n=4 members have been prepared in bulk for the m=1 series, while n=4 and n=5 ones for the m=2 series. The m=2 series of compounds have unique structures in which three BaO planes are stacked separated by the (Cu,C) planes. This type of block is not seen in other superconductors. Ordering between the Cu and C atoms occurs in both m=1 and m=2 series resulting in superstructures with

a_S=2a, b_S=b and c_S=2c for m=1 while a_S=2a, b_S=b and c_S=c for m=2 with respect to tetragonal subcells, a, b and c.

In the X-ray pattern of (Cu,C)-2334, we sometimes found some extra peaks which suggested existence of another member. We continued phase-search experiments under high pressure and found a new member of the m=2 series.

In this paragraph, we report a new oxycarbonate superconductor, $(Cu_{0.5}C_{0.5})_2Ba_3Ca_2Cu_3O_{11}$ (T_c=91 K) which is a member of (Cu,C)-23(n-1)n series with m=2 and n=3. The Cu and C atoms are, in this phase, ordered in a different manner compared with other m=2 members.

3.3.1. Experimental

Starting materials for high pressure synthesis were $BaCuO_2$, BaO_2, $CaCO_3$ (99.9%), Ca_2CuO_3 and CuO (99.9%). The starting materials were mixed in a dry-box to obtain a mixture with a composition, "$C_{1.0}Ba_{2.5}Ca_{2.5}Cu_4O_{11.6}$". The oxygen and the carbon contents were adjusted exactly by controlling the amounts of BaO_2 and $CaCO_3$. The carbon included in BaO_2 and $BaCuO_2$ was taken into account in this procedure. In preliminary experiment, we tried the stoichiometric 2323 composition, "$C_{1.0}Ba_{3.0}Ca_{2.0}Cu_4O_{11}$". However, the (Cu,C)-2323 phase was not obtained from this composition. The mixture was sealed in a gold capsule and allowed to react in a flat-belt-type high pressure apparatus at 5 GPa, 1250 °C for 5 hours, then quenched to room temperature.

Atomic ratios of Ba, Ca and Cu were determined by the electron probe microanalysis (EPMA). Carbon contents were measured using a carbon determinator (LECO, type WR12).

X-ray powder diffraction pattern was obtained by a diffractometer (Philips-PW1800) with Cu Kα radiation and lattice constants were determined using the least squares method. High resolution transmission

electron microscope (HRTEM) observation was carried out using a microscope (type H-1500) operated at 1000 kV.

DC magnetic susceptibility data were collected by a SQUID magnetometer (Quantum Design) at a magnetic field of 20 Oe. DC resistivity was measured by the standard four-probe method.

3.3.2. Results and Discussion

Fig. 3.17 shows the X-ray powder diffraction pattern of the high pressure product from the starting mixture, "$C_{1.0}Ba_{2.5}Ca_{2.5}Cu_4O_{11.6}$". Major X-ray peaks in Fig. 3.17 could be indexed assuming a tetragonal cell with a=3.852(1), c=18.61(2) Å. They are close to the parameters of the subcell for (Cu,C)-1234, a=3.855 and c=17.93 Å. At the same time, however, the c-dimension suggests that the present phase may be (Cu,C)-2323, the m=2 and n=3 member of the series (compare 18.61 Å with 21.87 Å for (Cu,C)-2334 and 25.067 Å for (Cu,C)-2345). We can not, therefore, conclude definitely only from the X-ray pattern whether the phase is (Cu,C)-1234 or (Cu,C)-2323.

Figs. 3.18(a), (b) show electron diffraction (ED) patterns of the present phase. These ED patterns are compatible with a superstructure (possible space group Bmmm) having a_S=2a, b_S=b, c_S=2c with respective to the above-mentioned tetragonal lattice. This type of superstructure have been observed in (Cu,C)-12(n-1)n series while the (Cu,C)-23(n-1)n series have, at least for n=4, 5, different superlattices, a_S=2a, b_S=b and c_S=c. In the lattice images shown in Figs. 3.19(a), (b), however, we can distinguish three Ba planes stacked along the c-axis as well as three Cu and two Ca planes. This clearly shows that the present phase is not (Cu,C)-1234 but (Cu,C)-2323 in spite of the different type of superstructure.

Two (Cu,C) planes located between BaO ones making a pair. In the image in Fig. 3.19(b) which corresponds to the ED pattern of Fig. 3.18(b), ordering between Cu and C is observed; a dot with dark contrast and one with less dark contrast are placed alternately along the a-axis giving the 2a periodicity. In each double (Cu,C) plane, a C atom (Cu atom) is located just below a C atom (Cu atom) of an upper (Cu,C) plane, that is, the phase of the Cu-C sequence is the same within a double plane. In an adjacent double plane, however, the phase is different (i.e., -C-Cu-C-Cu- against -Cu-C-Cu-C-) which results in the 2c periodicity. Both (Cu,C)-2334 and 2345 has, in contrast to (Cu,C)-2323, single periodicity along c-axis (c_S=c) since every (Cu,C) plane has the same phase. In Fig. 3.20, a structure model of (Cu,C)-2323 is given, together with those of (Cu,C)-2334 and 2345. We have no information about oxygen positions in the (Cu,C) plane. Oxygen atoms of the (Cu,C) plane in Fig. 3.20 are, therefore, drawn just for eyes. According to the model, the ideal composition of (Cu,C)-2323 becomes $(Cu_{0.5}C_{0.5})_2Ba_3Ca_2Cu_3O_{11}$. The valence of Cu is exactly +2.0 based on this composition. Excess oxygen introduction and/or partial substitution of Cu for C may occur to produce carriers (holes) as in the case of $(Ba,Sr)_2(Cu,C)_2O_y$ [13].

To check cation ratios in the (Cu,C)-23(n-1)n phases, EPMA measurements were performed not only for the present phase but for the (Cu,C)-2334 and 2345 ones which had been prepared in the previous work. Table 3.2 gives the results where the Cu/(Ba+Ca) ratio is always close to (n+1)/(n+2) obtained for the ideal composition, $(Cu_{0.5}C_{0.5})_2Ba_3Ca_{n-1}Cu_nO_{2n+5}$. The Ba/Ca ratio is, on the contrary, generally smaller than the expected one, 3/(n-1). This indicates partial occupation of the Ba sites by the Ca atoms which may be a reason why we could not obtain (Cu,C)-2323 starting from the stoichiometric 2323 composition. Such a substitution occurs in the (Cu,C)-1234 phase, as well.

In Fig. 3.21, a- and c-dimensions of the tetragonal subcells of the (Cu,C)-m(m+1)(n-1)n phases are plotted against k, the sum of numbers of (Cu,C) and Cu planes in a unit formula. The c-dimension increases linearly with k for m=1 as well as for m=2, but the line obtained for m=2 is deviated upward compared with that for m=1. This seems reasonable because a m=2 series of compound includes higher numbers of Ba planes in a subcell. A more contrastive tendency is seen in variation of the a-dimension with k. It decreases with k in the m=1 series while increases in the m=2 series. Fig. 3.21 is an another evidence for that the present phase is not (Cu,C)-1234 but (Cu,C)-2323.

The above results cast an important problem on identification of the present series of compounds. A 23(n-1)n phase would have subcell parameters close to those of a 12n(n+1) (k=n+2 in both cases). Therefore, X-ray measurement is not always sufficient for identification of a phase though accurate lattice parameters would give useful information as discussed above. Moreover, even ED patterns of a phase may not provide conclusive evidence for the identification. Note that (Cu,C)-2323 has the different type of superstructure seen in neither (Cu,C)-2334 nor 2345. Observation of lattice images seems indispensable for the definite identification.

Fig. 3.22 gives DC susceptibility of the present sample. It indicates two-step superconducting transitions at 113 K and 91 K with a sufficiently large diamagnetic susceptibility at 5 K. As shown in Fig. 3.17, this sample included (Cu,C)-2334 as a minor phase. Since Tc of (Cu,C)-2334 is 113 K, we concluded that the second transition at 91 K reflects T_c of the (Cu,C)-2323 phase. Fig. 3.23 indicates DC resistivity of the sample which shows a rather broad but single step decrease near 113 K which suggests that the minor phase, (Cu,C)-2334 percolated through the sample. A metallic temperature dependence of the resistivity was observed above T_c.

Table 3.1. Results of chemical analysis for (Cu,C)-1223 and (Cu,C)-1234

Compound	atomic ratio					carbon (wt%)	
	Cu /(Ba+Ca)			Ba / Ca			
	Obs.	Calc.*	Calc.**	Obs.	Calc.	Obs.	Calc.*
(Cu,C)-1223	0.89±0.02	0.88	0.75	0.90±0.07	1.00	0.85	0.83
(Cu,C)-1234	0.89±0.03	0.90	0.80	0.51±0.05	0.67	0.62	0.70

* Based on the composition, $(Cu_{0.5}C_{0.5})Ba_2Ca_2Cu_3O_9$ or $(Cu_{0.5}C_{0.5})Ba_2Ca_3Cu_4O_{11}$.

**Based on the composition, ABa2Ca2Cu3O9 or ABa2Ca3Cu4O11 (A is a metal other than Cu).

Table 3.2. Results of electron microprobe analysis for (Cu,C)-23(n-1)n series

Compound	atomic ratio			
	Cu /(Ba+Ca)		Ba / Ca	
	Obs.	Calc.	Obs.	Calc.
(Cu,C)-2323	0.782±0.008	0.80	0.99±0.003	1.50
(Cu,C)-2334	0.828±0.002	0.833	0.62±0.01	1.00
(Cu,C)-2345	0.856±0.003	0.857	0.54±0.01	0.75

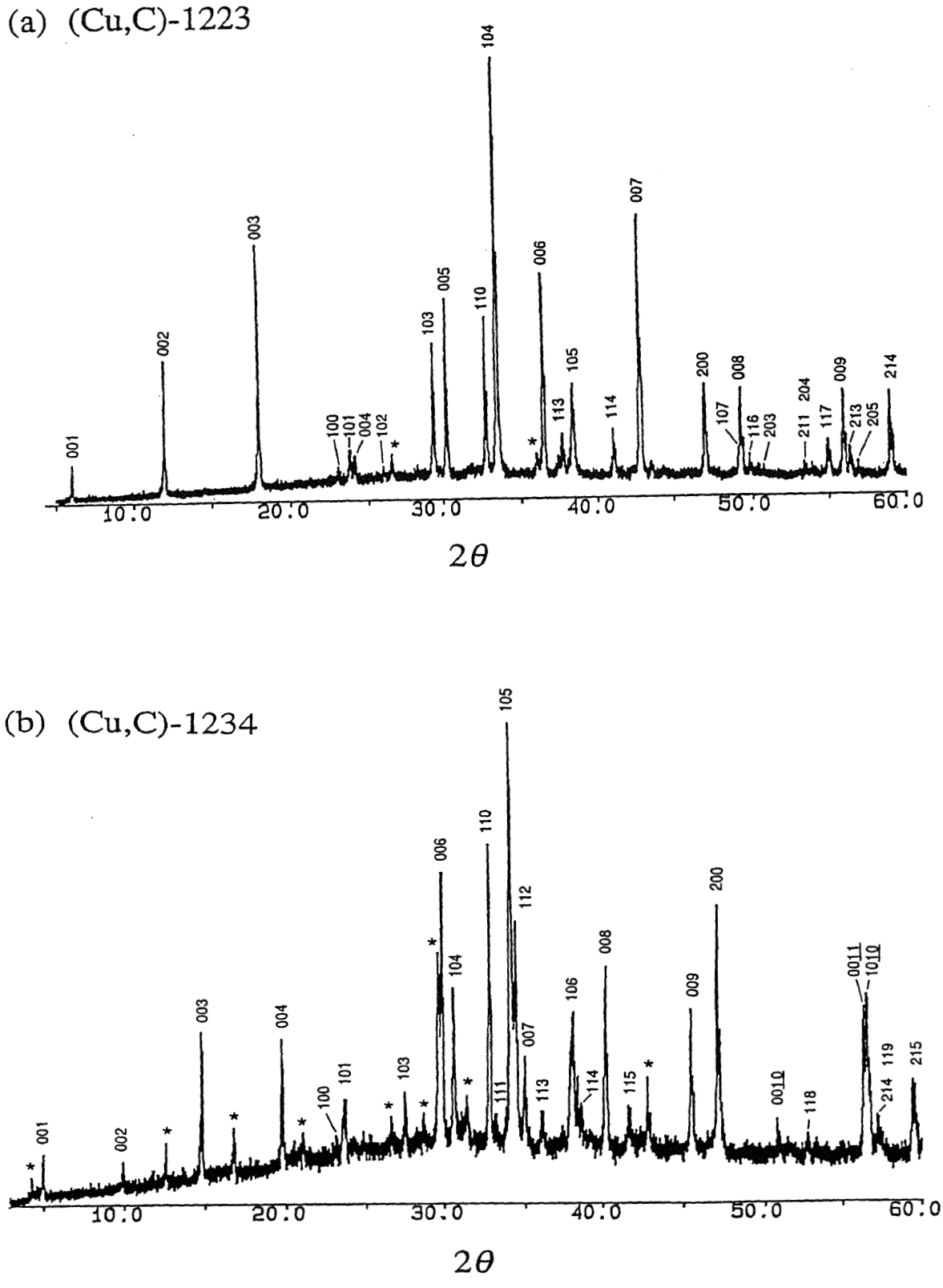

Fig. 3.1. Powder X-ray patterns of (Cu,C)-1223 (a) and 1234 (b) phases. Peaks due to impurity phases are labeled by "*". Indexes are given based on the tetragonal subcells with a_t=3.859(1), c_t=14.766(5) Å for (Cu,C)-1223 and a_t=3.855(1), c_t=17.930(6) Å for (Cu,C)-1234.

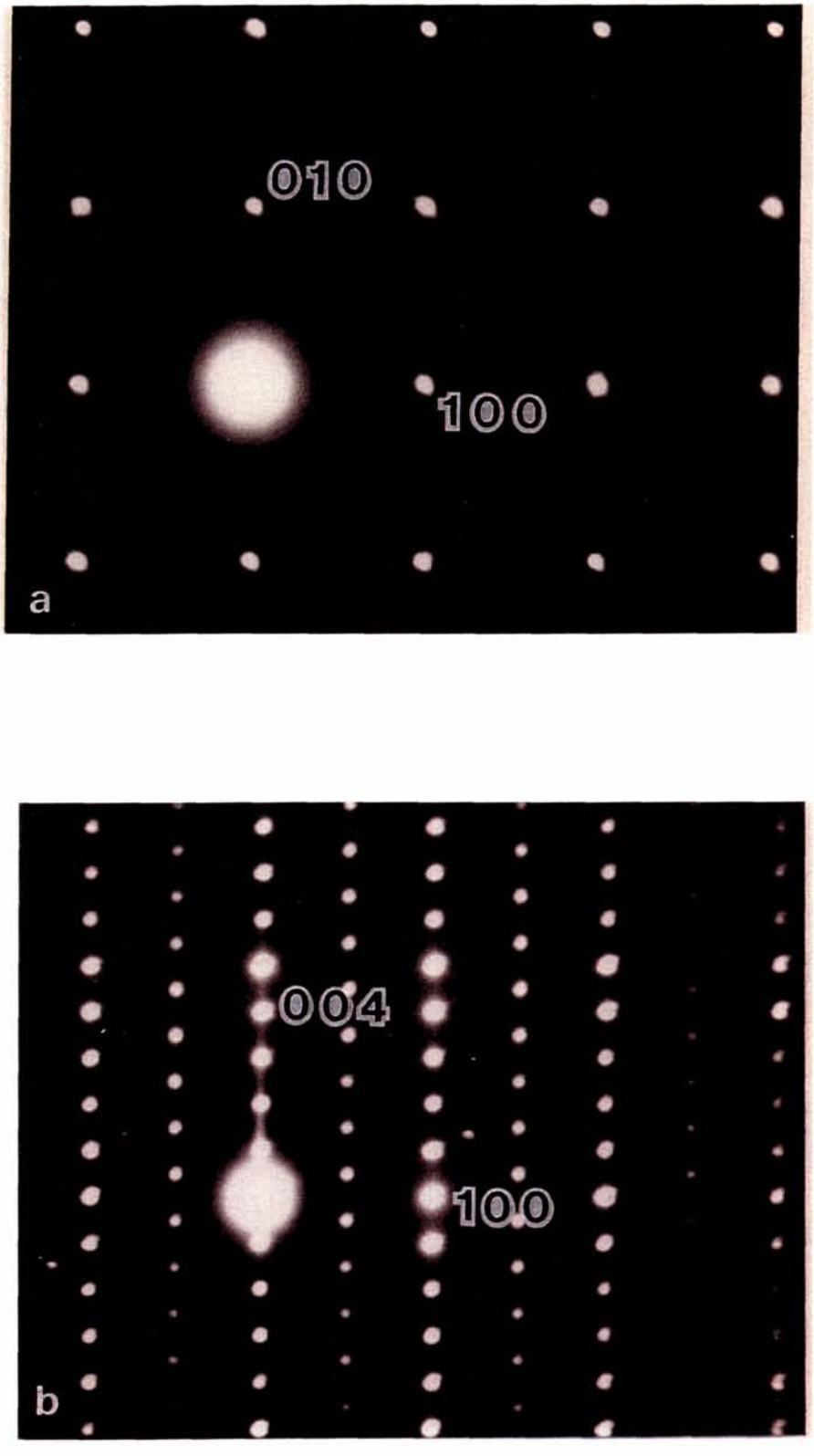

Fig. 3.2. The *hk0* (a) and *h0l* (b) electron diffraction patterns of (Cu,C)-1223. Indexes are given based on the tetragonal subcell.

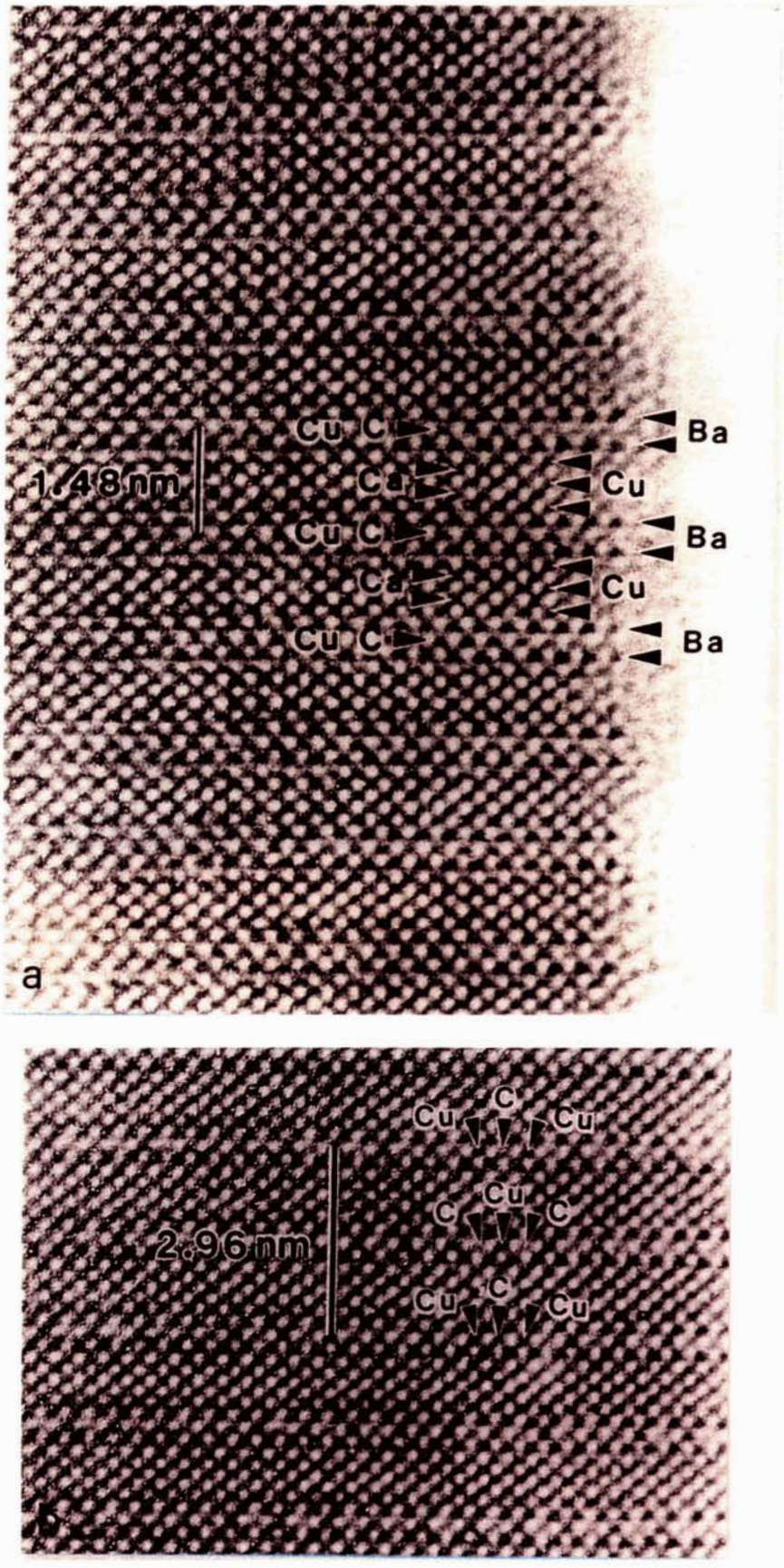

Fig. 3.3. HRTEM images of (Cu,C)-1223 projected along the [1 0 0] direction (a) and along the [0 1 0] direction (b).

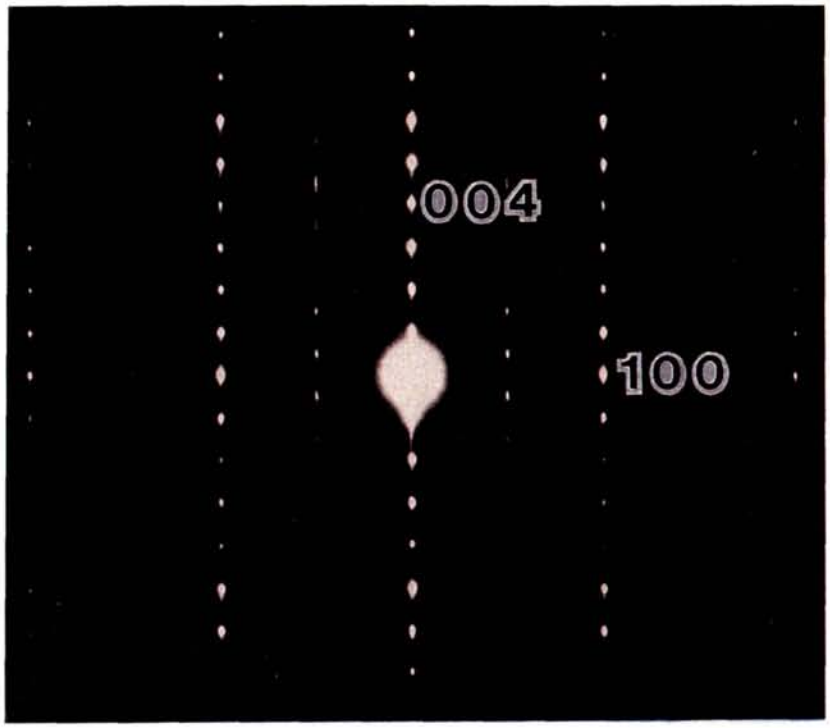

Fig. 3.4. The *h0l* electron diffraction pattern of (Cu,C)-1234. Indexes are given based on the tetragonal subcell.

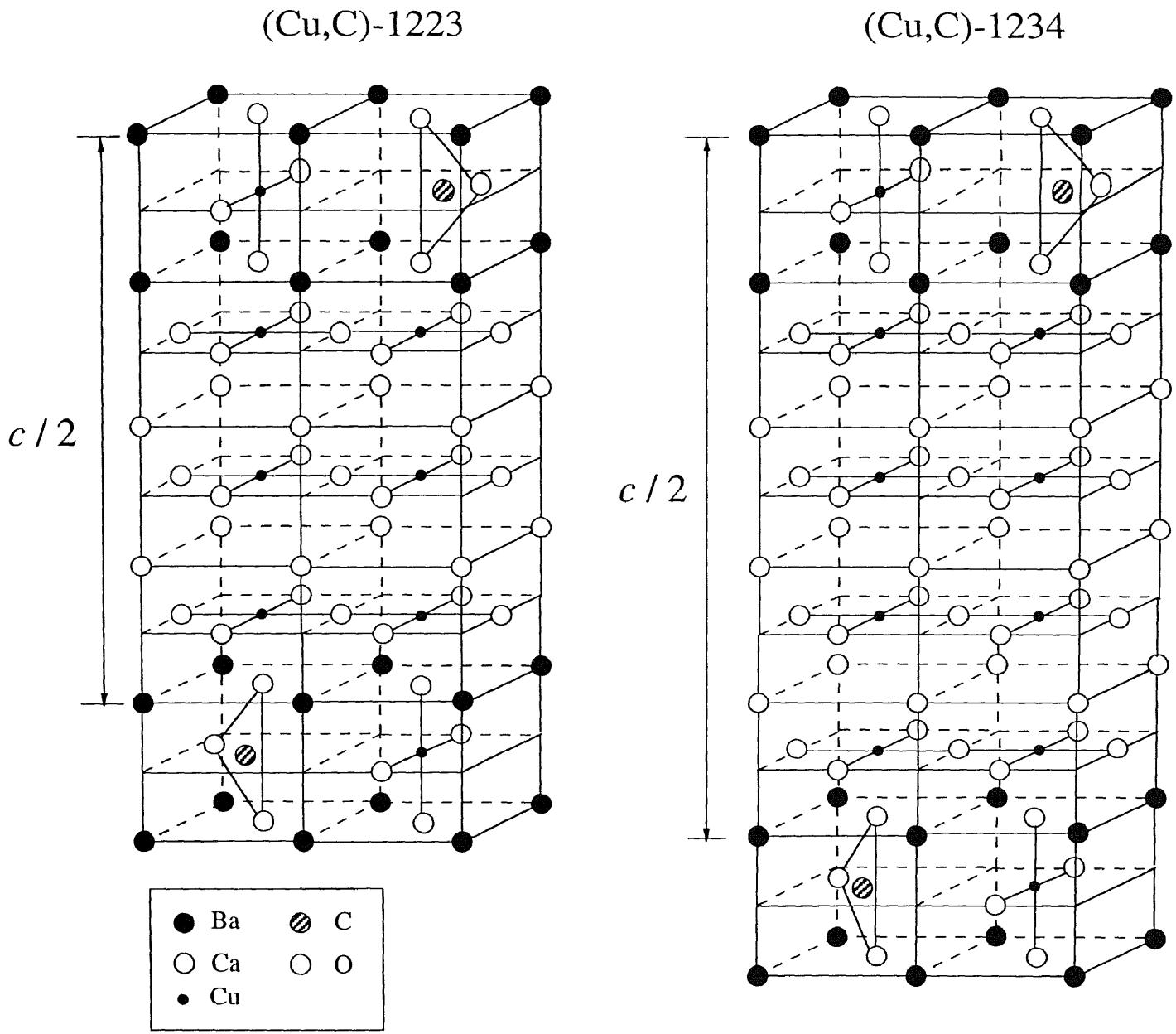

Fig. 3.5. Crystal structures of $(Cu_{0.5}C_{0.5})Ba_2Ca_2Cu_3O_{9\pm\delta}$ and $(Cu_{0.5}C_{0.5})Ba_2Ca_3Cu_4O_{11\pm\delta}$.

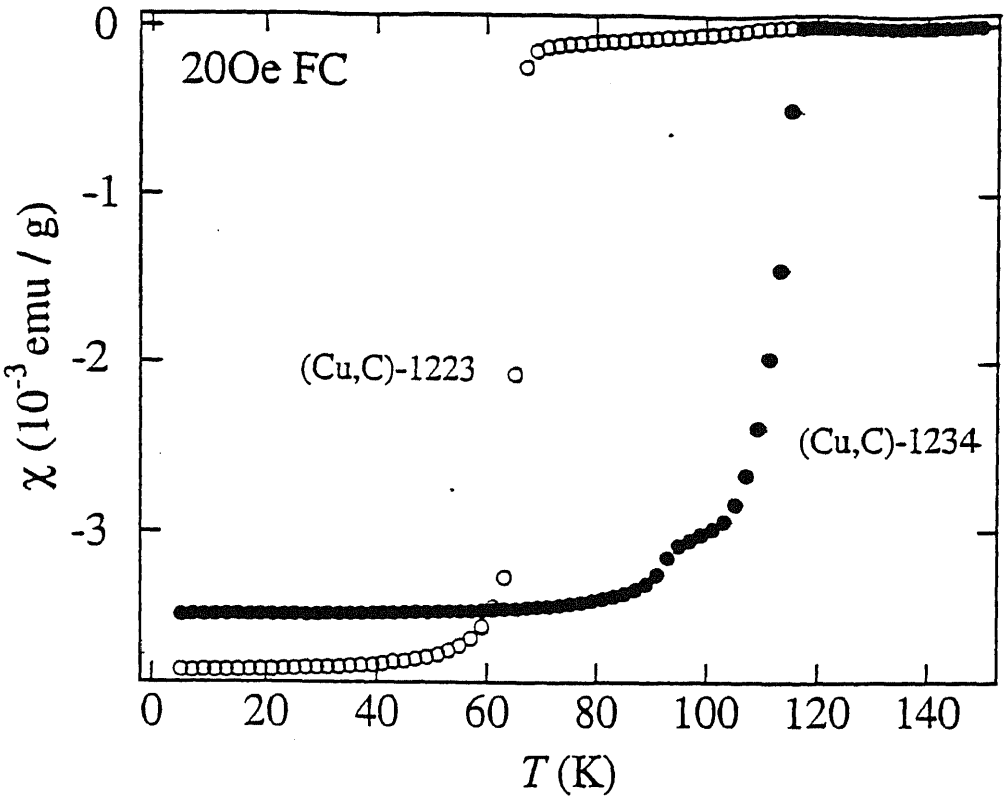

Fig. 3.6. DC susceptibility data of $(Cu_{0.5}C_{0.5})Ba_2Ca_2Cu_3O_{9\pm\delta}$ and $(Cu_{0.5}C_{0.5})Ba_2Ca_3Cu_4O_{11\pm\delta}$.

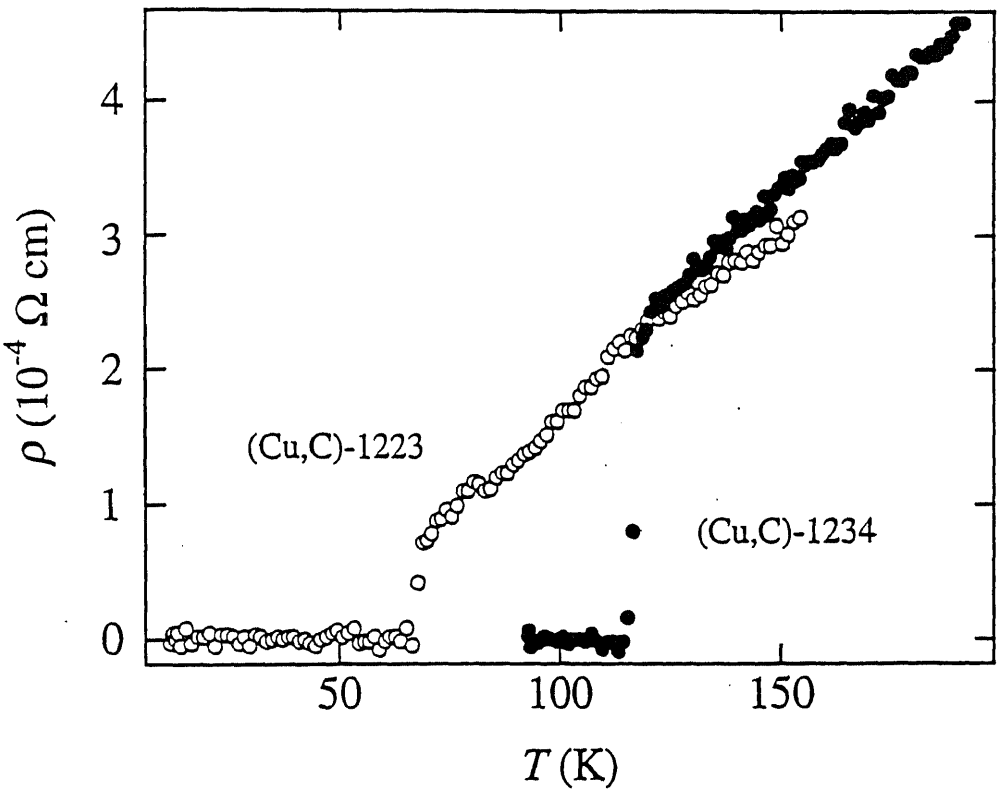

Fig. 3.7. Temperature dependences of DC resistivities of $(Cu_{0.5}C_{0.5})Ba_2Ca_2Cu_3O_{9\pm\delta}$ and $(Cu_{0.5}C_{0.5})Ba_2Ca_3Cu_4O_{11\pm\delta}$.

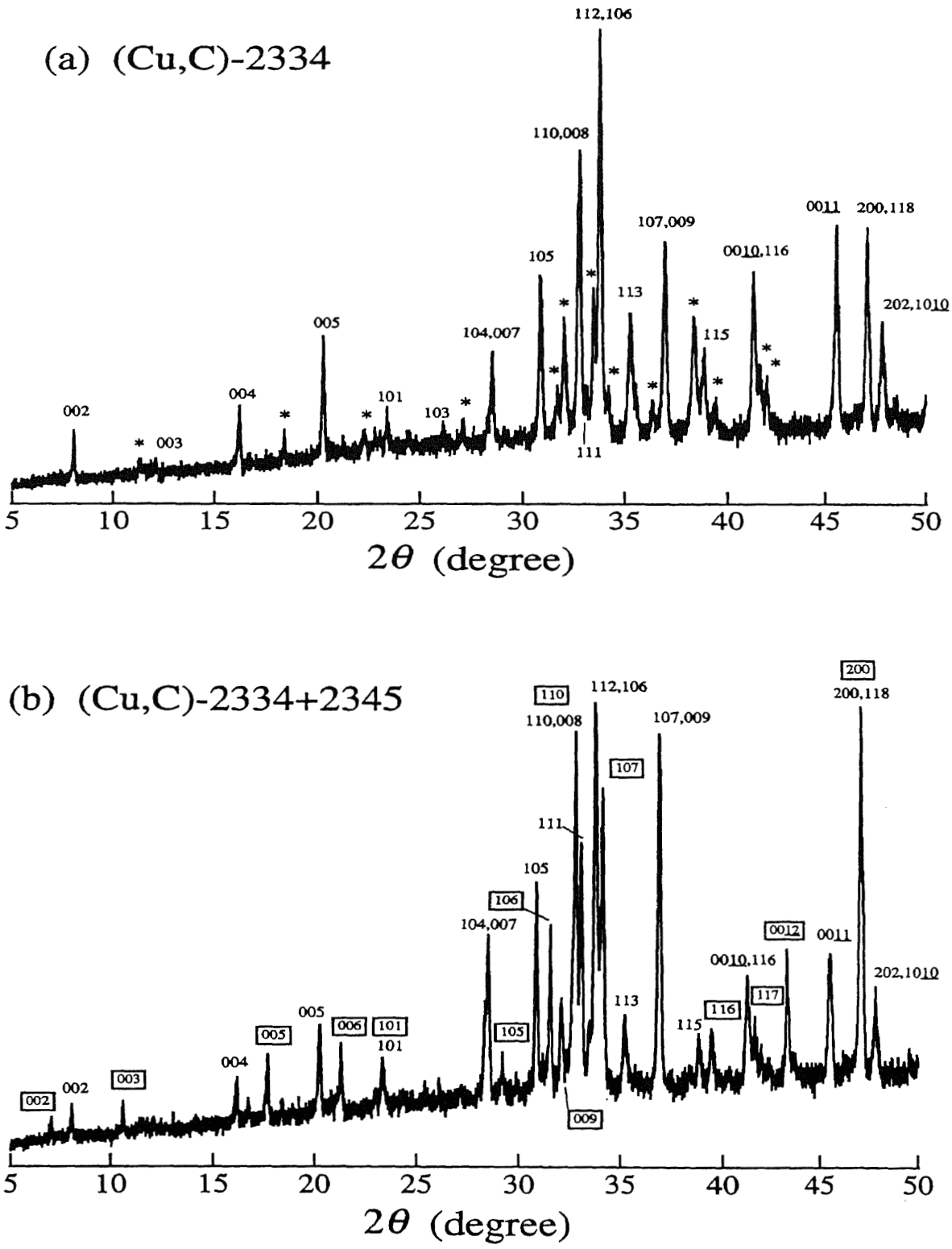

Fig. 3.8. Powder X-ray patterns of samples from starting mixtures of "$C_{0.6}Ba_2Ca_4Cu_{5.5}O_{13.2}$" (a) and "$C_{0.5}Ba_2Ca_4Cu_{5.5}O_{13}$" (b). Peaks due to impurity phases are labeled by "*". Indexes are given based on the tetragonal subcell with a=3.855(3), c=21.87(1) Å and that with a=3.857(1), c=25.067(7) Å (the latter indexes are in boxes).

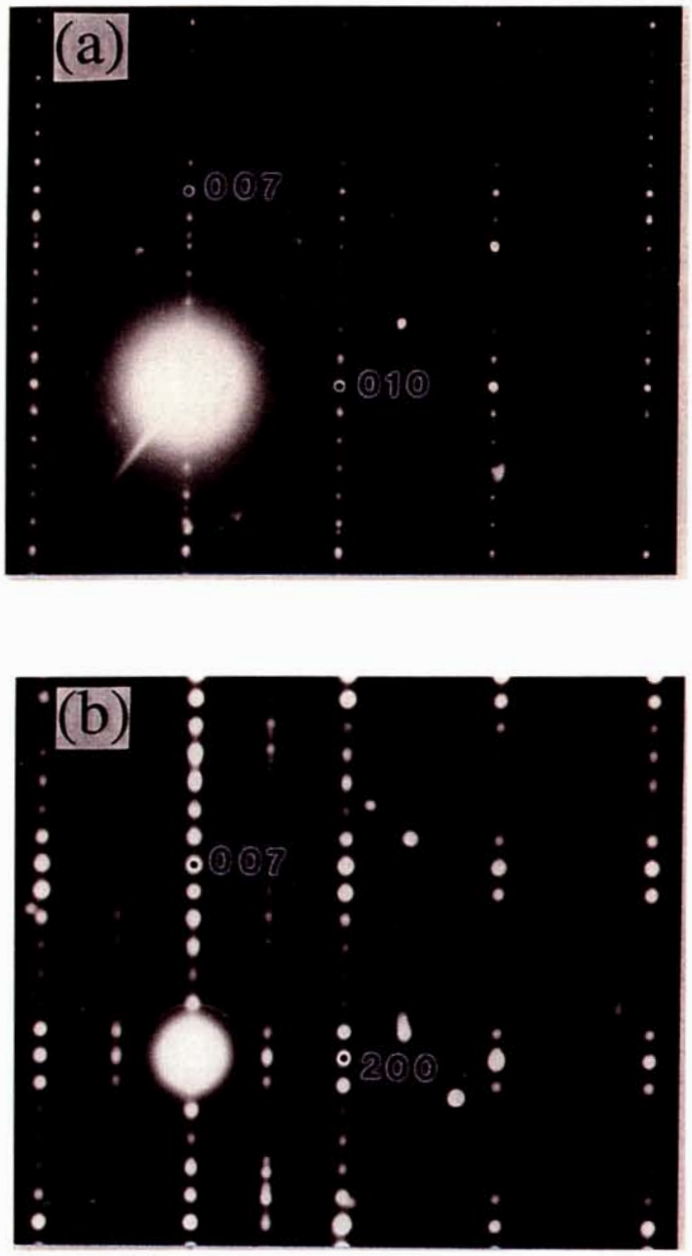

Fig. 3.9. The *0kl* (a) and *h0l* (b) electron diffraction patterns of (Cu,C)-2334. Indexes are given based on the orthorhombic superlattice, a_S=2a, b_S=b and c_S=c.

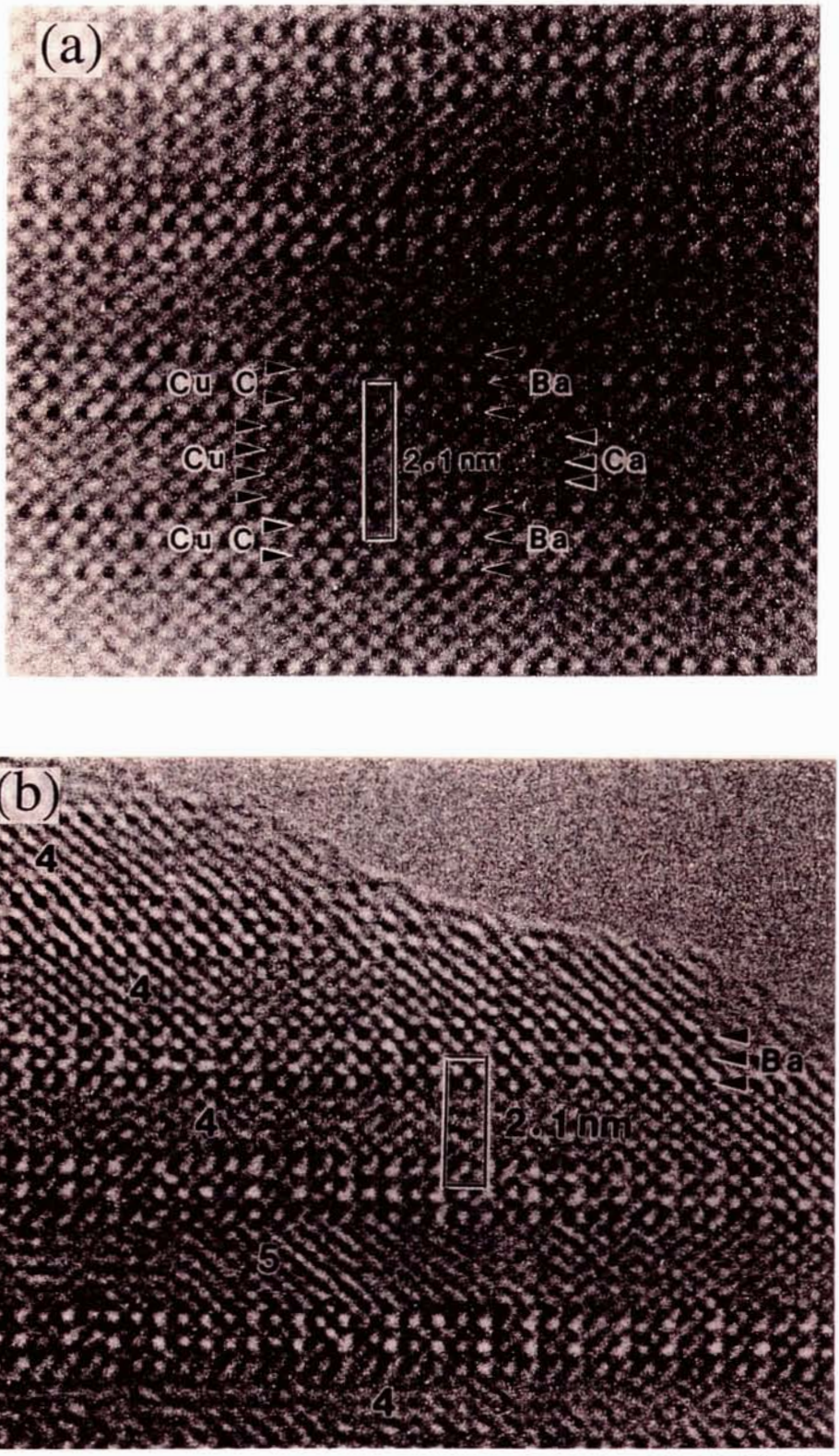

Fig. 3.10. HRTEM image of (Cu,C)-2334 projected along the [1 0 0] direction (a) and along the [0 1 0] direction (b). The number in Fig. 3.10(b) indicates the number of Cu planes.

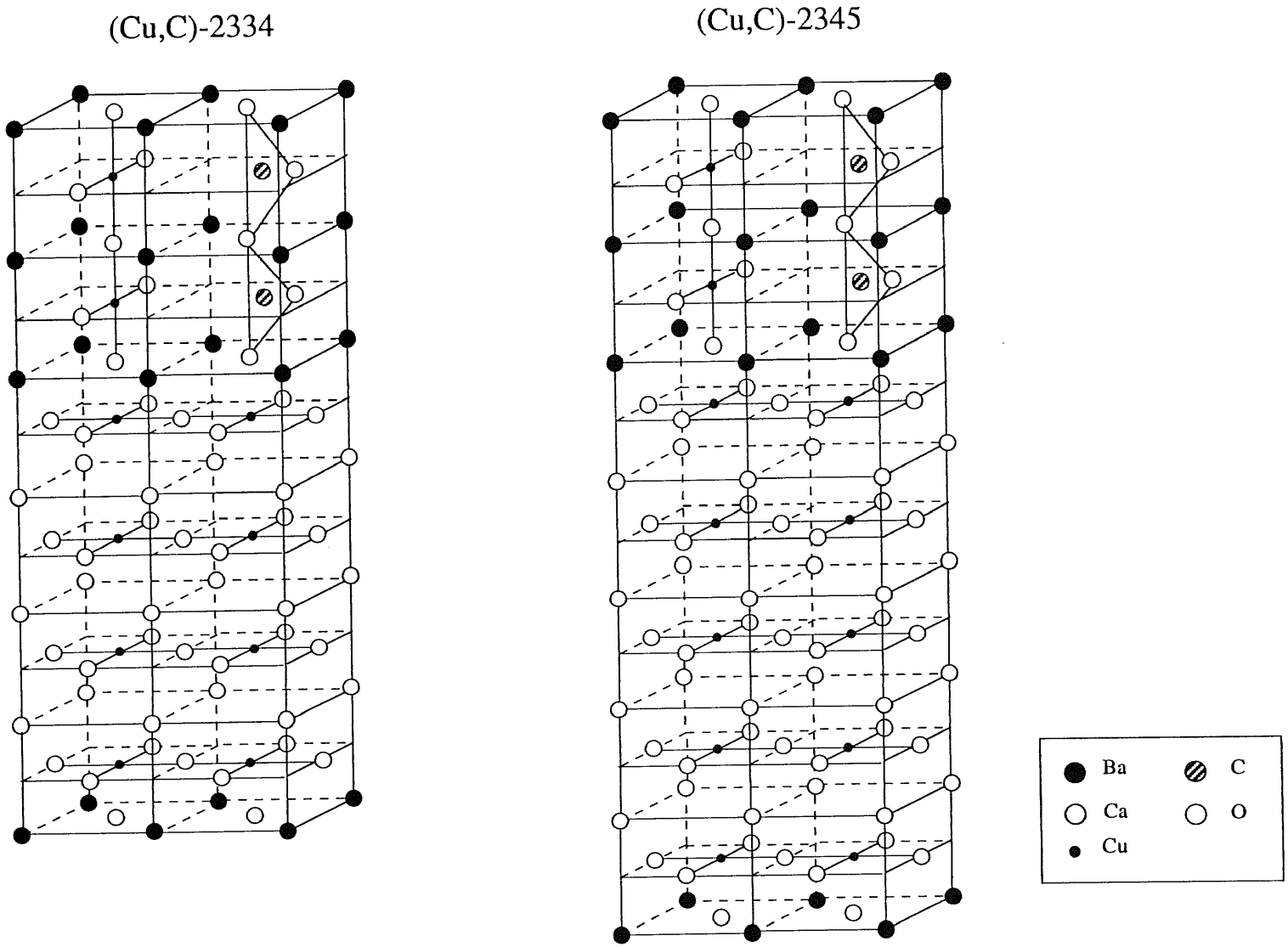

Fig. 3.11. Crystal structures of $(Cu_{0.5}C_{0.5})_2Ba_3Ca_3Cu_4O_{13}$ ((Cu,C)-2334) and $(Cu_{0.5}C_{0.5})_2Ba_3Ca_4Cu_5O_{15}$ ((Cu,C)-2345).

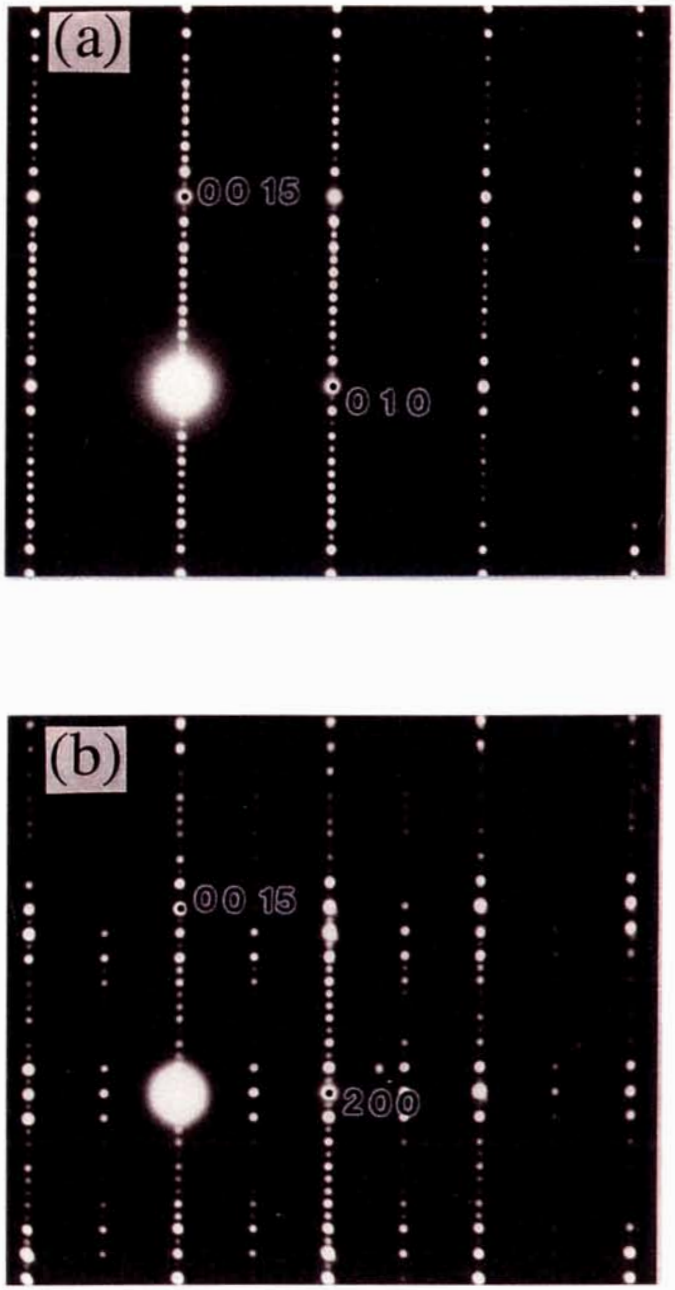

Fig. 3.12. The *0kl* (a) and *h0l* (b) electron diffraction patterns of the intermediate phase, (Cu,C)-23(3.5)(4.5). Indexes are given based on the superlattice, a≈7.7 Å, b≈3.9 Å and c≈46 Å.

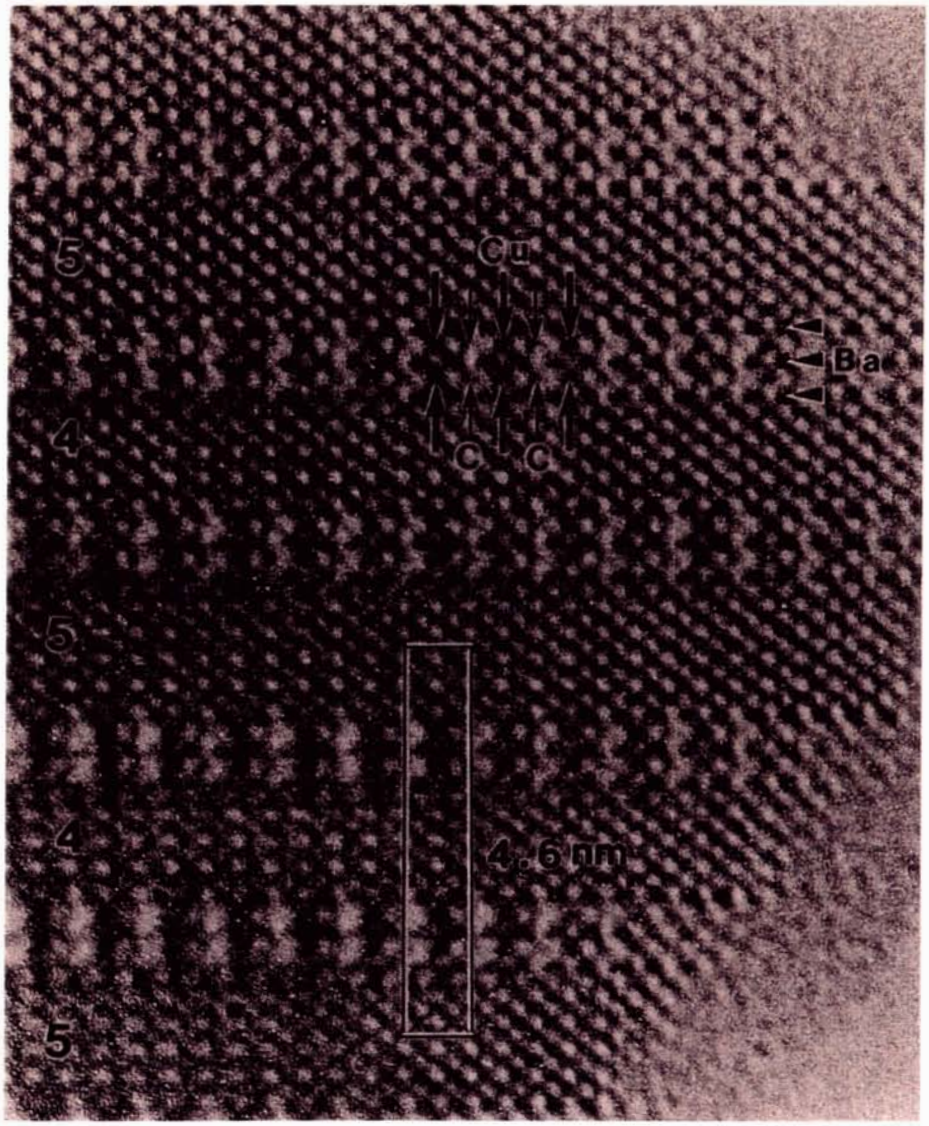

Fig. 3.13. HRTEM image of (Cu,C)-23(3.5)(4.5) projected along the [0 1 0] direction. The number in the figure indicates the number of Cu planes.

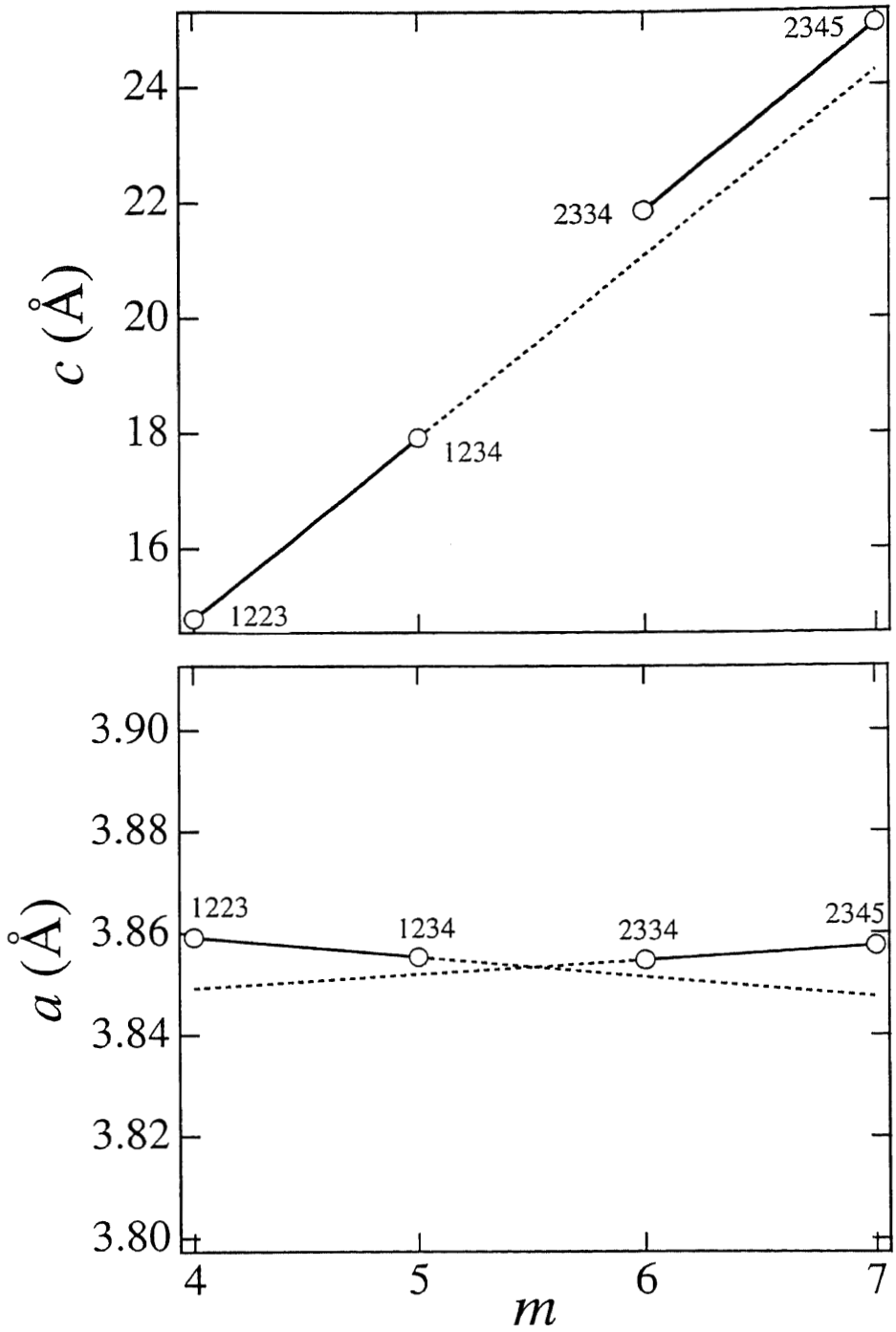

Fig. 3.14. The variations of the lattice constants of the tetragonal subcell as functions of m, the sum of numbers of (Cu,C) and Cu planes in a unit formula.

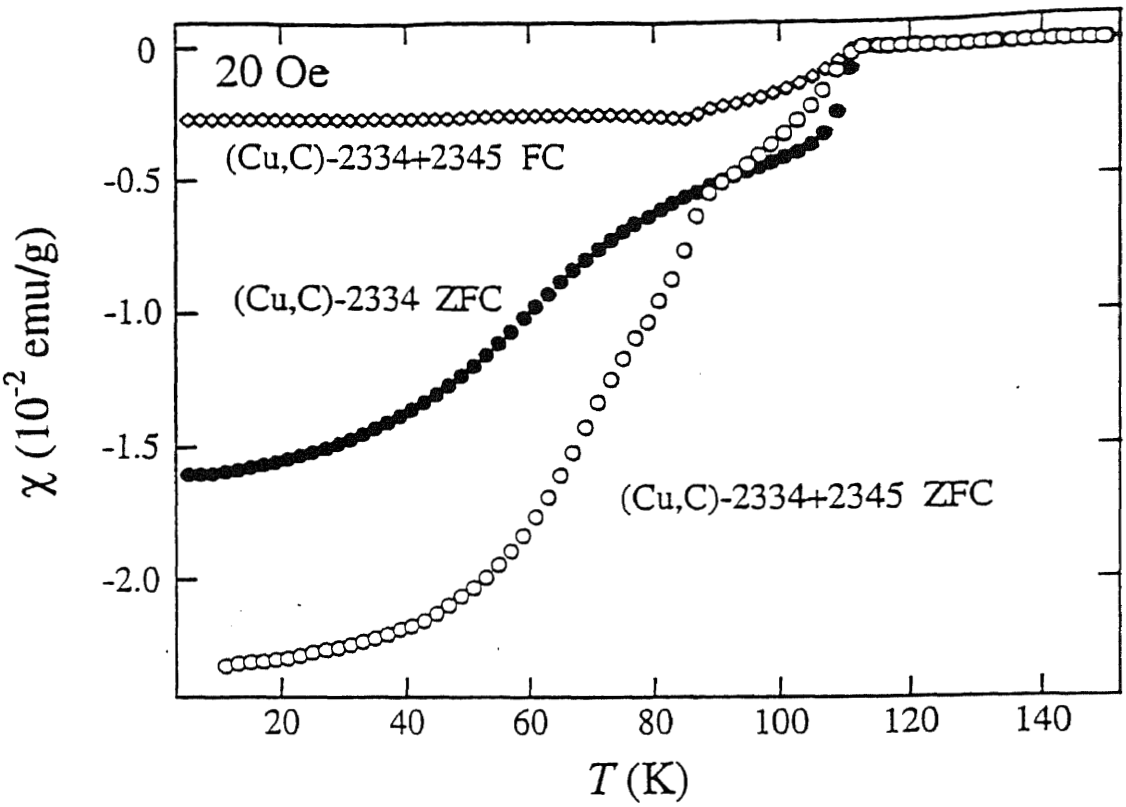

Fig. 3.15. DC susceptibility data of samples corresponding toFig. 3.8(a) (denoted as (Cu,C)-2334) and to Fig. 3.8(b) (denoted as (Cu,C)-2334+2345).

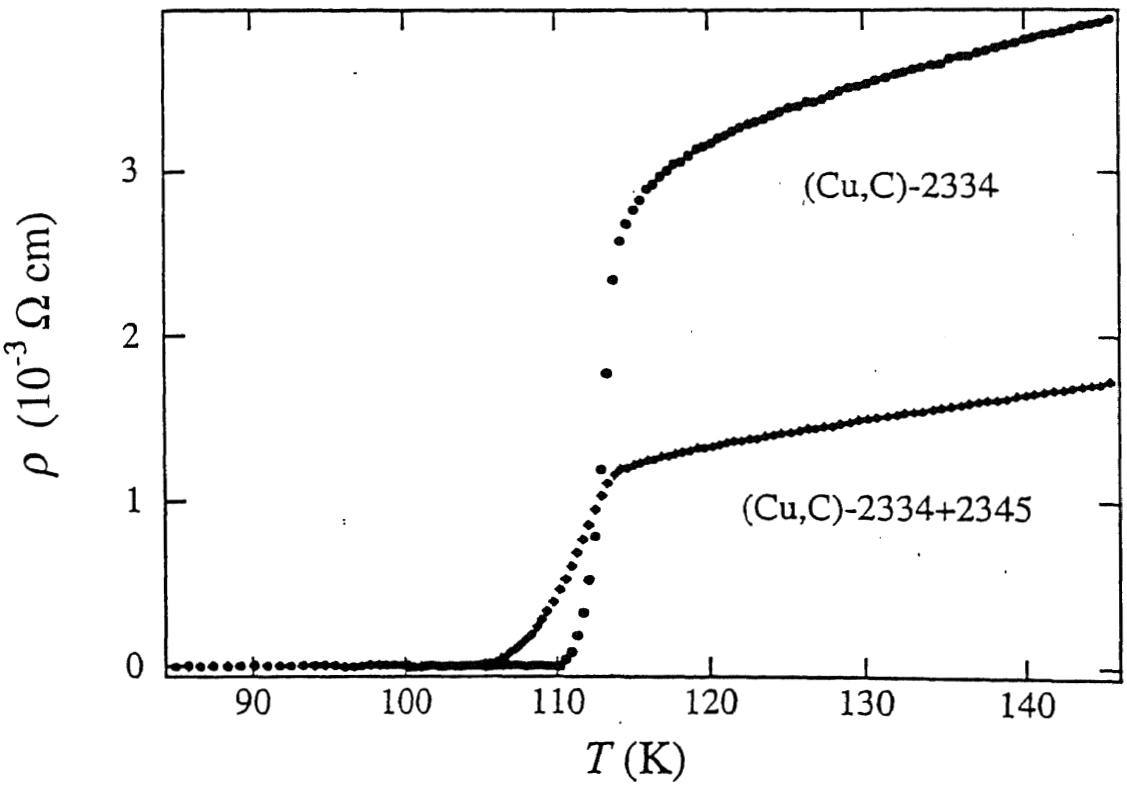

Fig. 3.16. DC resistivities of samples corresponding to Fig. 3.8(a) (denoted as (Cu,C)-2334) and to Fig. 3.8(b) (denoted as(Cu,C)-2334 +2345).

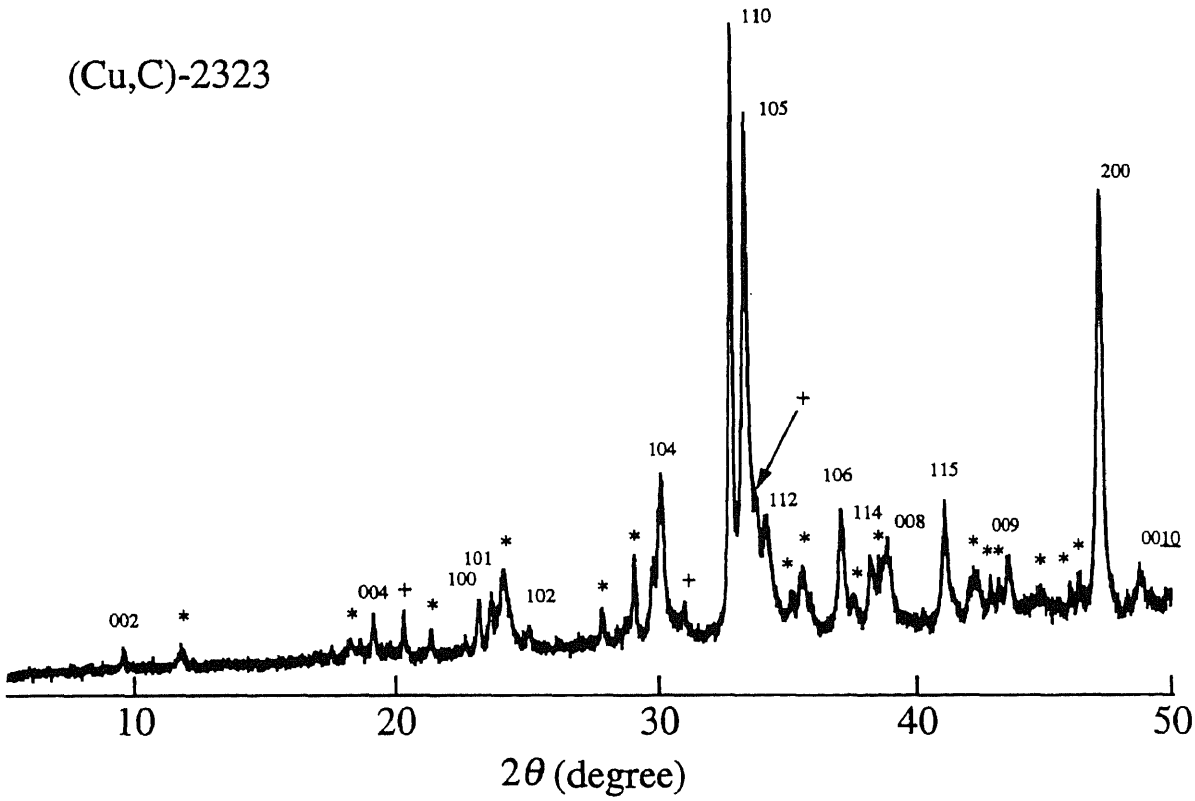

Fig. 3.17. Powder X-ray pattern of the sample having the nominal composition, "$C_{1.0}Ba_{2.5}Ca_{2.5}Cu_4O_{11.6}$". Peaks due to (Cu,C)-2334 are labeled by "+" while those due to unknown impurity phase(s) by "*". Indexes are given based on the tetragonal subcell with a=3.852(1), c=18.61(2) Å.

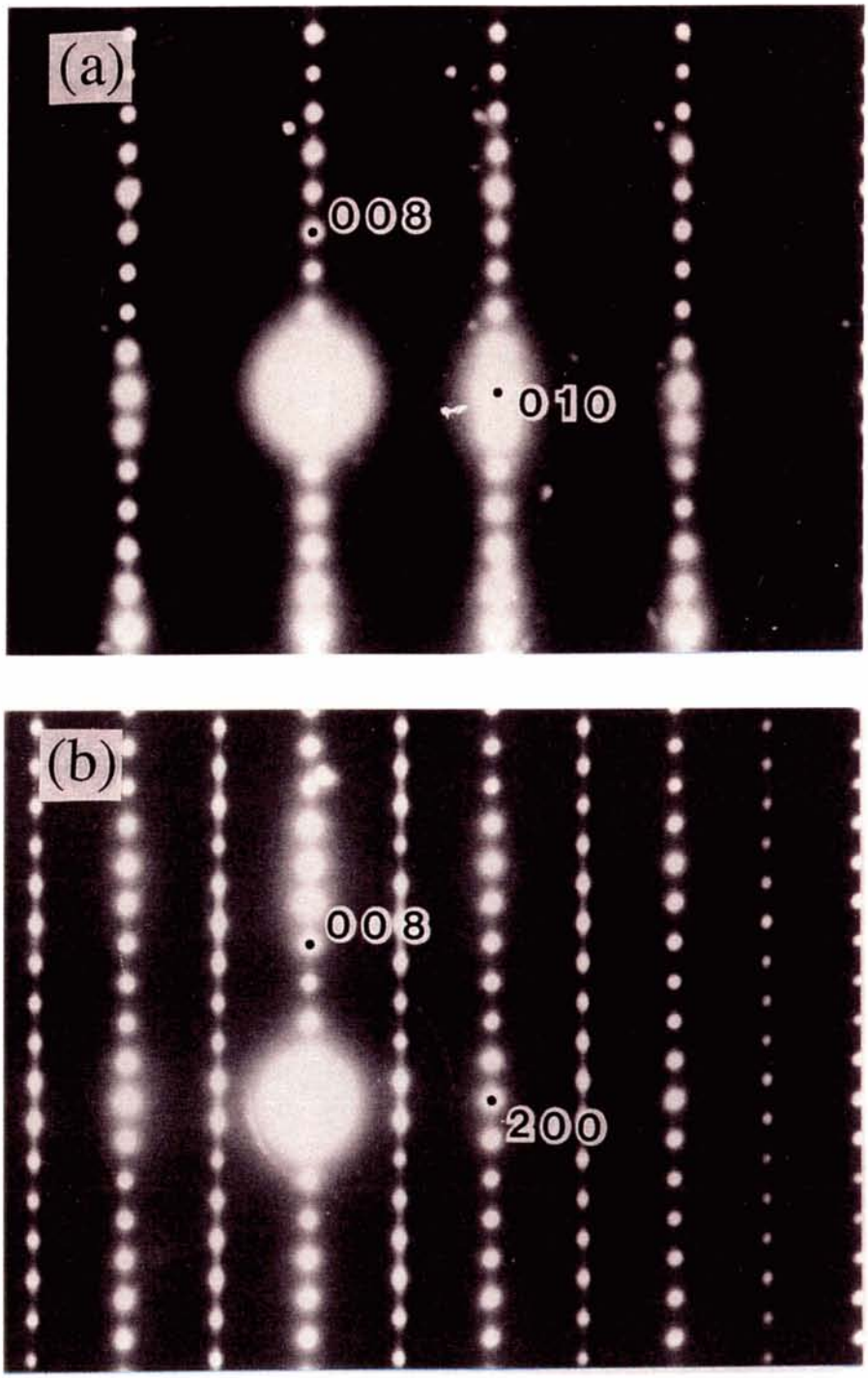

Fig. 3.18. The *0kl* (a) and *h0l* (b) electron diffraction patterns of (Cu,C)-2323. Indexes are given based on the superlattice, a_S=2a, b_S=b, c_S=2c.

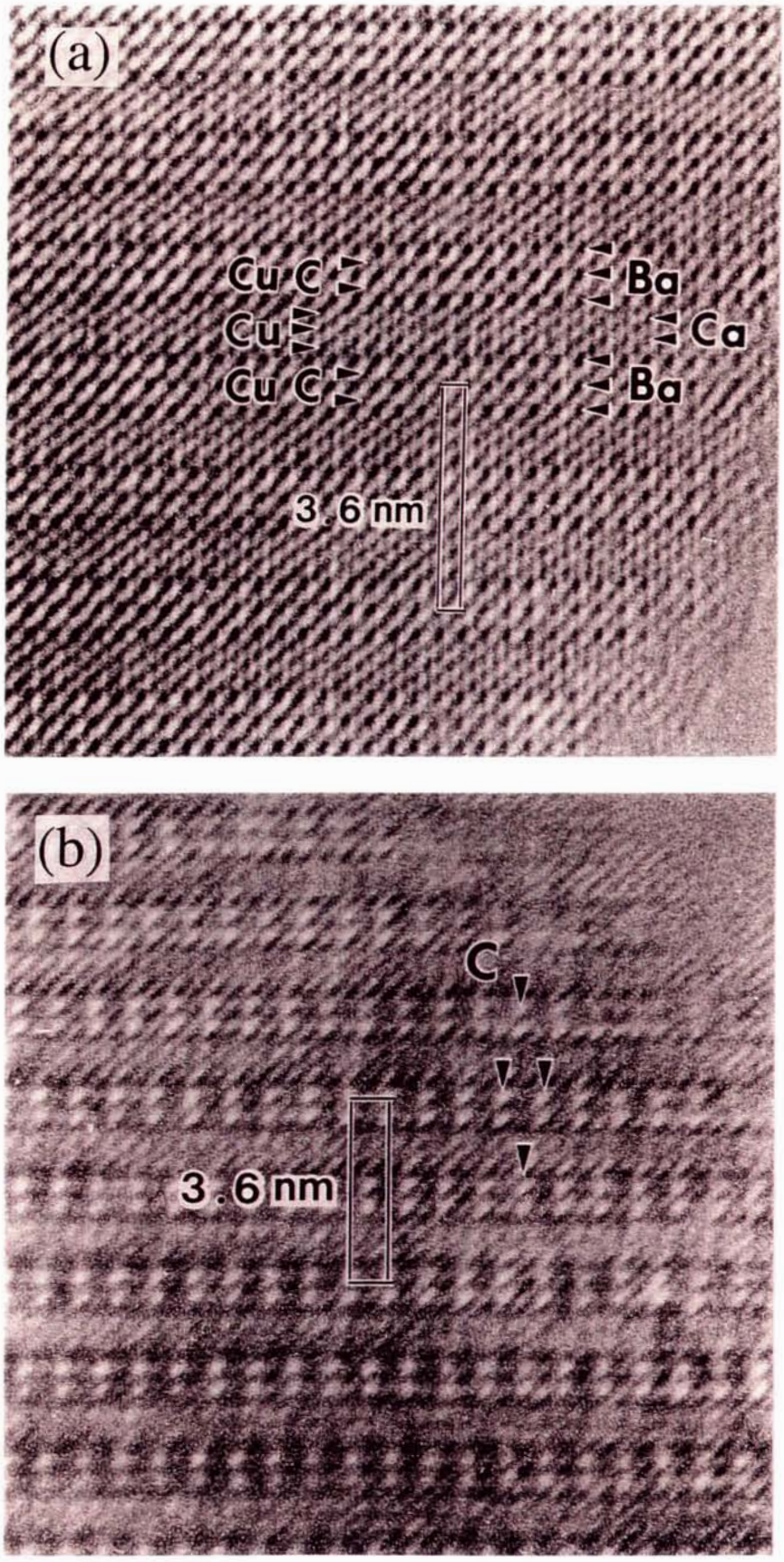

Fig. 3.19. HRTEM image of (Cu,C)-2323 projected along the [1 0 0] direction (a) and along the [0 1 0] direction (b).

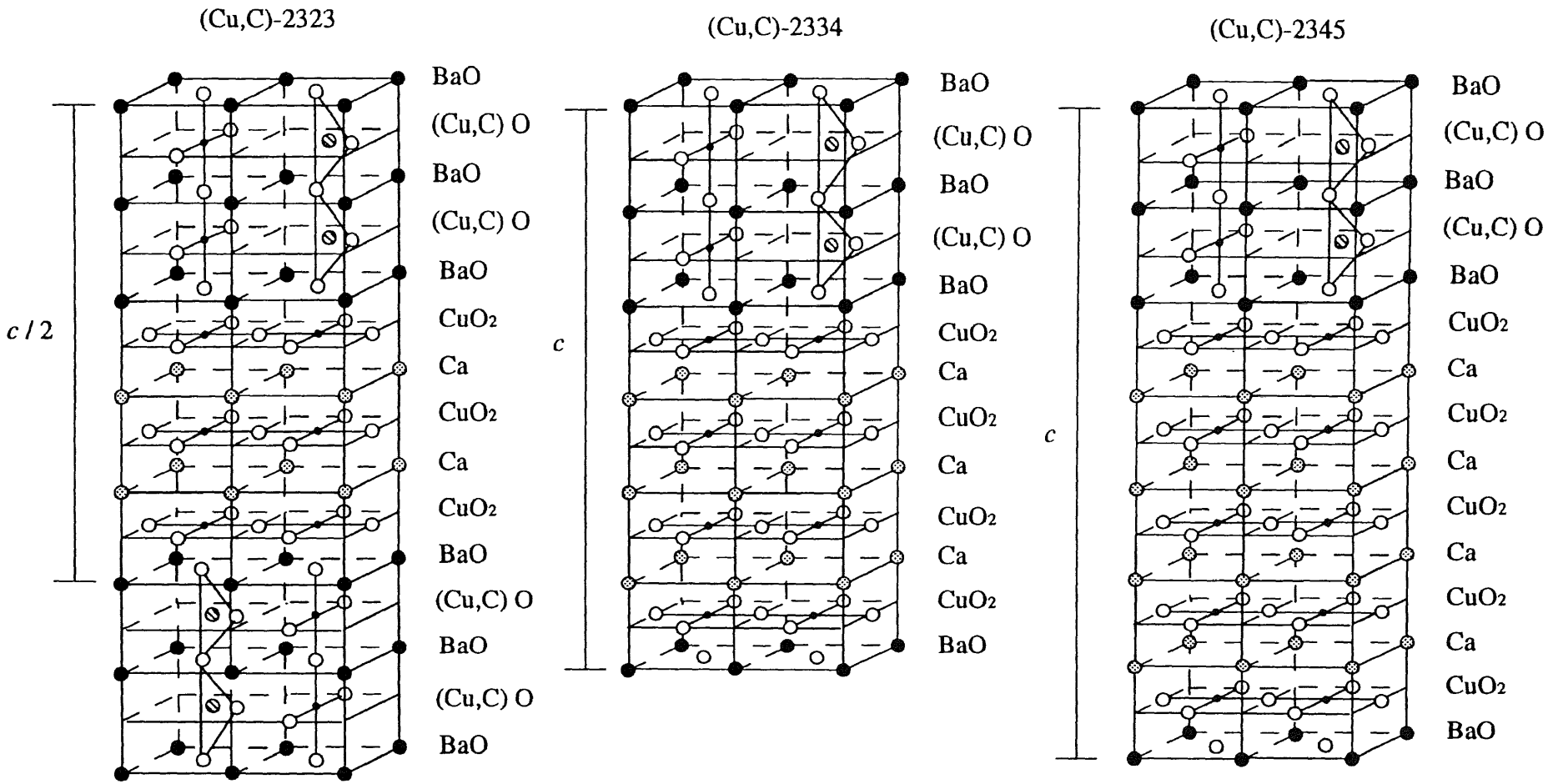

Fig. 3.20. Crystal structure of $(Cu_{0.5}C_{0.5})_2Ba_3Ca_{n-1}Cu_nO_{2n+5}$ (n=3,4,5).

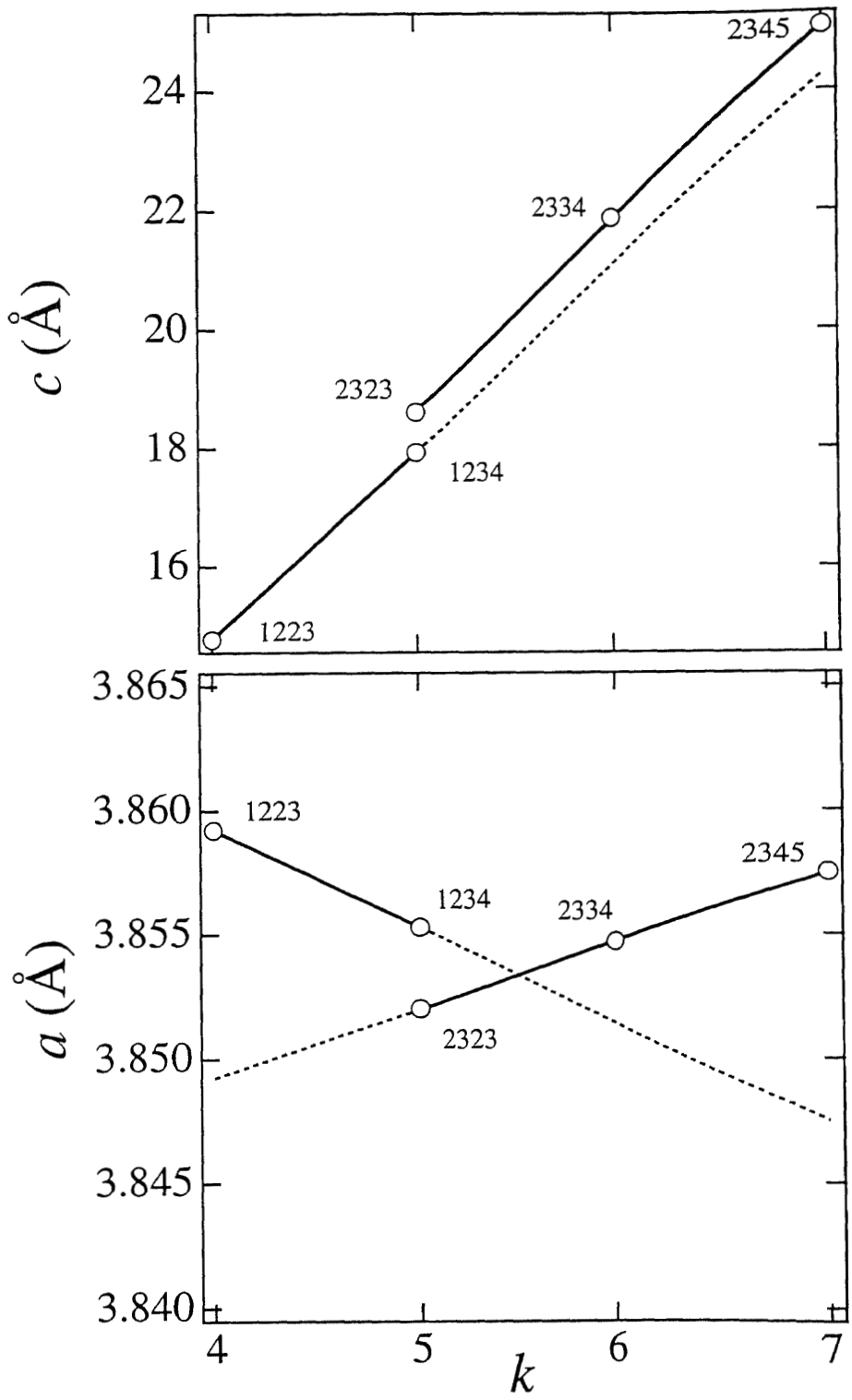

Fig. 3.21. The variations of the lattice constants of the tetragonal subcell as function of k, the sum of numbers of (Cu,C) and Cu planes in a unit formula.

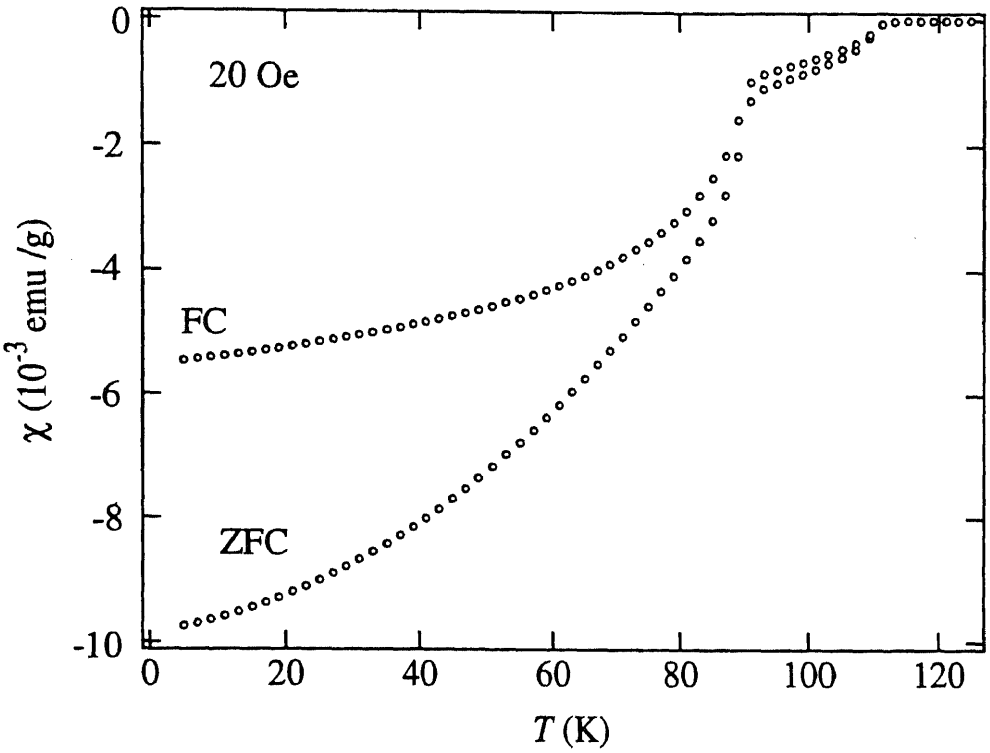

Fig. 3.22. DC susceptibility data for the "$C_{1.0}Ba_{2.5}Ca_{2.5}Cu_4O_{11.6}$" sample.

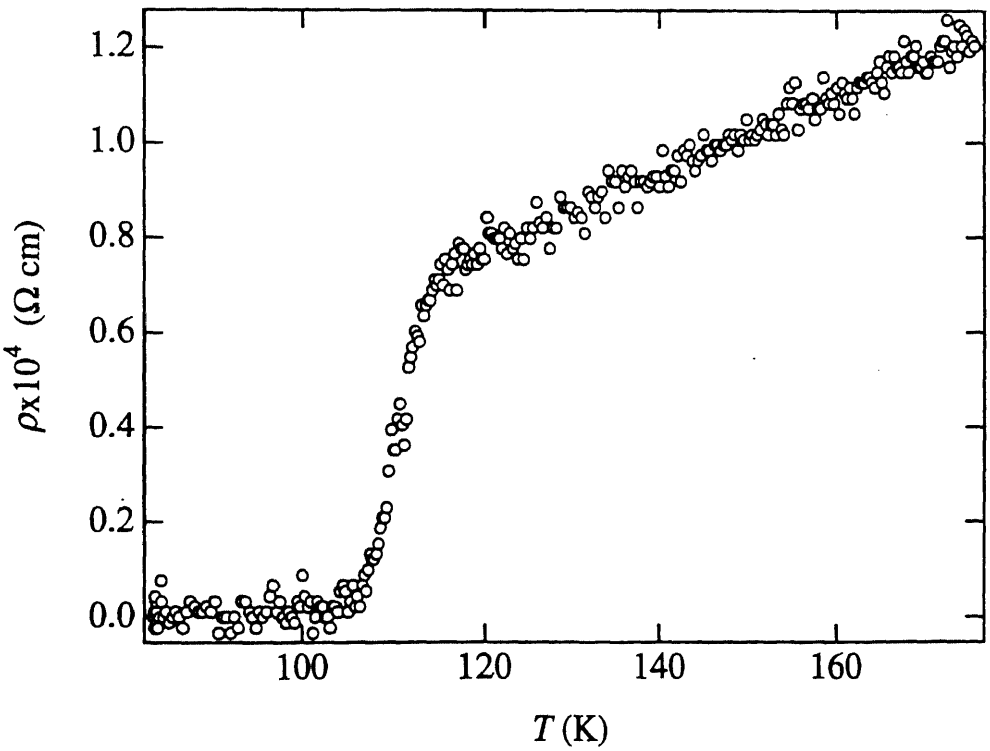

Fig. 3.23. Temperature dependence of DC resistivity for the "$C_{1.0}Ba_{2.5}Ca_{2.5}Cu_4O_{11.6}$" sample.

4. High pressure synthesis and superconducting properties of new series of high-Tc superconductors, $BSr_2Ca_{n-1}Cu_nO_{2n+3}$ (n=3 ~ 5).

Thus far, several investigations have been done on oxyborate cuprate superconductors. Zhu et al. studied the (B,Cu)-1212 system, $(B_xCu_{1-x})Sr_2YCu_2O_7$ and prepared a solid solution with x=0.1-0.9 [36]. Though this Sr-based solution was not a superconductor, the Ba-substituted system, $(B_{0.5}Cu_{0.5})(Sr,Ba)_2YCu_2O_7$, showed superconductivity below 51 K [36]. Under high pressure, Uehara et al. substituted B for C in oxycarbonate compounds to obtain a homologous series of superconductors, $(B_xC_{1-x})Sr_2(Ca,Sr)_{n-1}Cu_nO_y$ (n=1,2,3) [37]. They claimed that such a substitution is effective to introduce carriers (holes) into an oxycarbonate compound.

Successful high pressure syntheses of superconductors such as $(Cu,C)m Ba_{m+1}Ca_{n-1}Cu_nO_{2(m+n)+1}$, $(Cu,S)Sr_2Ca_{n-1}Cu_nO_y$ [38] and $MSr_2Ca_{n-1}Cu_nO_{2n+3}$ (M=Al, Ga) [39-40] suggests that if there is a 1212 phase under ambient pressure, 12(n-1)n (n>2) phases may be stabilized under high pressure. Combining this idea with the previous report by Zhu et al. [36], Takayama-Muromachi et al. applied high pressure synthesis to the B-Sr-Ca-Cu-O system to find a new oxyborate superconductor, $BSr_2Ca_3Cu_4O_{11}$ (B-1234) [41]. Its structure is closely related to that of Tl (or Hg)-1234; the Tl (or Hg) site is occupied by B. HRTEM observation indicated that there were intergrowths of $BSr_2Ca_{n-1}Cu_nO_{2n+3}$ (B-12(n-1)n) up to n=6. This suggests that there exist the homologous series of compounds and a phase with n≠4 can be prepared in bulk by adjusting synthetic conditions. In this chapter, we discuss a new oxyborate superconductors, $BSr_2Ca_2Cu_3O_9$ and $BSr_2Ca_4Cu_5O_{13}$ which are n=3 and 5 members of the series.

4.1. Experimental

Starting materials for high pressure synthesis were $SrCuO_2$, SrO_2, Ca_2CuO_3, B_2O_3 (99.9%) and CuO (99.9%). These materials were mixed in an agate mortar to obtain starting mixtures for high pressure synthesis. The mixture was sealed in a gold capsule and allowed to react in a flat-belt-type high pressure apparatus at 6 GPa, and at 1200 ~ 1300 °C for 1 hour, then quenched to room temperature. Carbon contents of the high pressure products were measured using a carbon determinator (LECO, type WR12).

X-ray powder diffraction pattern was obtained by a diffractometer (Philips-PW1800) with Cu Kα radiation and lattice constants were determined using the least squares method. High resolution transmission electron microscope (HRTEM) observation was carried out using a microscope (type H-1500) operated at 1000 kV.

DC magnetic susceptibility data were collected by a SQUID magnetometer (Quantum Design) at a magnetic field of 20 Oe. DC resistivity was measured by the standard four-probe method.

4.2. Results and Discussion

The ideal composition of the B-1223 phase is $BSr_2Ca_2Cu_3O_9$. However, the Sr/Ca ratio may be different from the ideal one due to mutual substitution between Sr and Ca. Electron probe micro analysis gave the Sr/Ca ratio of 0.56 for the B-1234 phase which is smaller than the ideal one, 0.67 [41]. According to this result, we first tried Ca-rich nominal compositions $BSr_{1.5}Ca_{2.5}Cu_3O_y$ (y=9.0, 9.1, 9.2). The mixtures were heat treated at 1250 °C under 6 GPa. However, X-ray patterns of the products indicated that they did not contain the B-1223 phase at all but contained the B-1234 phase reported previously [41] and some unknown phase(s). Next, we tried the stoichiometric metal ratios, varying the

nominal oxygen content from y=9.0 to 9.5 with an interval of 0.1. The reaction temperature was 1200 °C. By this procedure, we found that the best oxygen content to prepare the B-1223 phase is y=9.1, though some unknown phase(s) was (were) still observed in the X-ray pattern. The starting mixture with y=9.1 was heat treated at another reaction temperatures of 1100 and 1300 °C. The result became better for 1300 °C while it became worse for 1100 °C. Fig. 4.1(a) shows the X-ray powder diffraction pattern of the sample obtained at 1300 °C starting from the "best" mixture, $BSr_2Ca_2Cu_3O_{9.1}$. Major X-ray peaks in Fig. 4.1(a) could be indexed assuming a tetragonal cell with a=3.821(1), c=13.854(6) Å, compatible with the B-1223 structure.

For the B-1245 phase, we also tested the stoichiometric metal ratios with changing the oxygen content and found that a slightly oxygen-poor nominal composition, $BSr_2Ca_4Cu_5O_{12.9}$, gave a satisfactory result; Fig. 4.1(b) shows a X-ray pattern for a sample obtained at 1300 °C where most peaks could be indexed assuming a tetragonal cell with a=3.837(2), c=20.22(1) Å as expected for the 1245 structure. Not any systematic extinction was observed, in both X-ray patterns, suggesting the space group P4/mmm.

Fig. 4.2 shows the h0l electron diffraction (ED) pattern of the B-1223 phase. This ED pattern is consistent with the tetragonal lattice described above. Fig. 4.3 is a lattice image corresponding to the ED pattern in Fig. 4.2, where we can distinguish two Sr, two Ca and three Cu planes stacked between B planes having white contrast. Fig. 4.4(a), (b) show the h0l and hhl ED patterns of the B-1245 phase while Fig. 4.5 is a lattice image corresponding to the one in Fig 4.4(a). This image is consistent with the 1245 structure in which two Sr, four Ca, five Cu and one B planes are stacked along the c-axis. In Fig. 4.6, the structures of B-12(n-1)n phases are shown schematically. We have no information about

oxygen positions in the B plane. Oxygen atoms of the B plane in Fig. 4.6 are drawn in the case of three-fold coordination of the B, however, it is possible to have four-fold coordination.

The carbon analysis indicated that our high pressure samples included 0.15~0.16 wt.% C. The carbon content in the present B-1223 and B-1245 phases are, therefore, at most 0.07~0.10 per molecule, i.e., the plane with white contrast was confirmed to be the B plane, not a carbonate plane.

In Fig. 4.7, a- and c-dimensions of the B-12(n-1)n phases are plotted against n. The c-dimension increases linearly with a slope of 3.18 Å which corresponds to the thickness of the composite CuO_2-Ca plane and is consistent with values obtained for other series of superconductors prepared under high pressure [38-41]. The a-dimension looks to increase slightly with n but the increase is saturated already at n=5 which suggests that the a-dimension is essentially determined by the CuO_2 plane.

Fig. 4.8 gives DC susceptibilities of the B-1223 and B-1245 samples. Superconducting transitions occurred at 75 K in the B-1223 sample and 85 K in the B-1245 one. In addition, small diamagnetic susceptibilities were observed below 110 K in both samples. According to the previous report, T_c of the B-1234 phase is 110 K [41]. We concluded that a trace amount of the B-1234 phase contained in the samples caused the diamagnetic susceptibilities below 110 K. Fig. 4.9 indicates DC resistivities of the samples. Consistent with the susceptibility data, two-step decreases were observed in both cases near 110 K and at 75 or 85 K. Both showed metallic behavior above T_c.

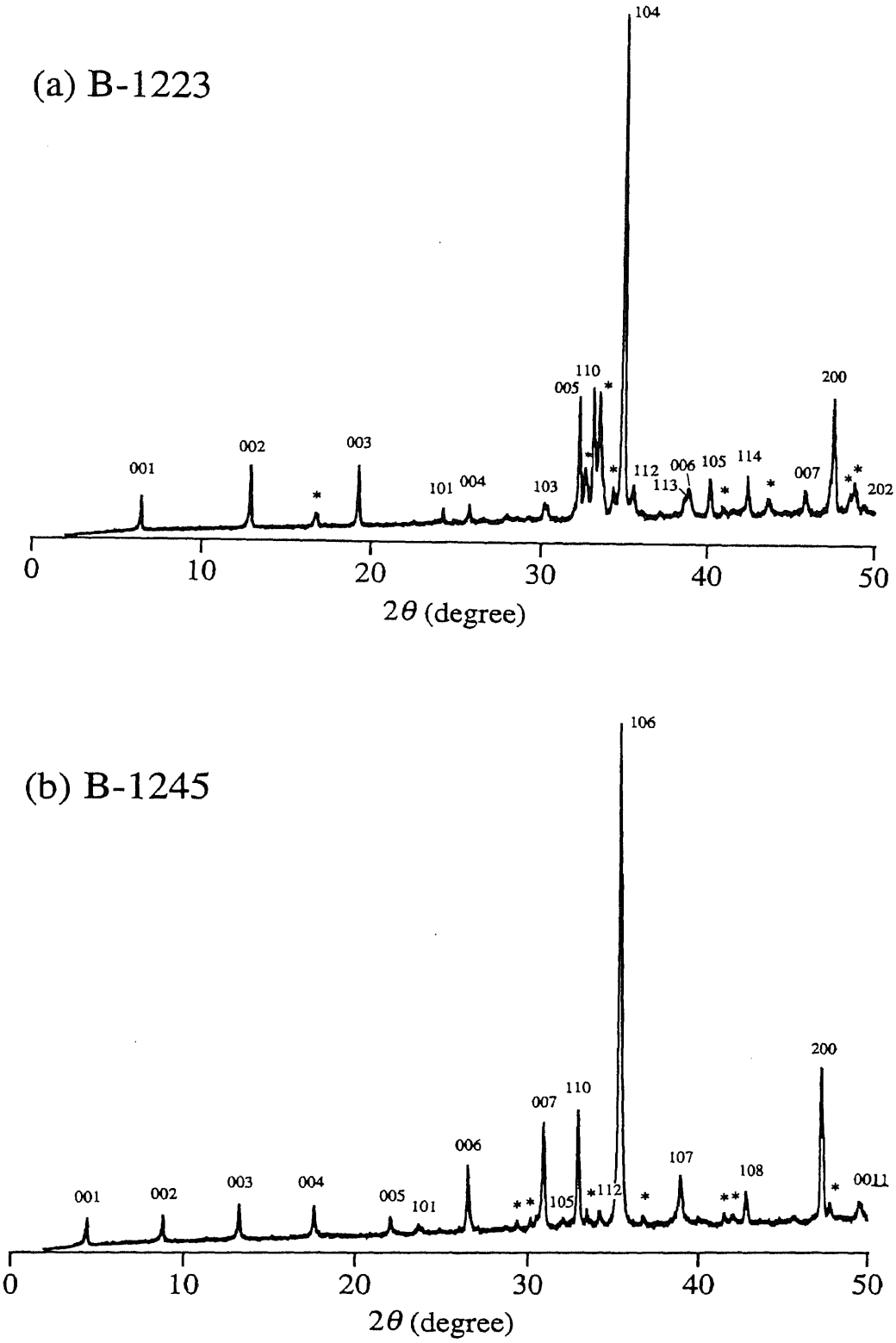

Fig. 4.1. Powder X-ray patterns of the samples having the nominal compositions, "$BSr_2Ca_2Cu_3O_{9.1}$" (a) and "$BSr_2Ca_4Cu_5O_{12.9}$" (b). Peaks due to unknown impurity phases are labeled by "*". Indexes are given based on the tetragonal cells with a=3.821(1), c=13.854(6) Å (a) and a=3.837(2), c=20.22(1) Å (b).

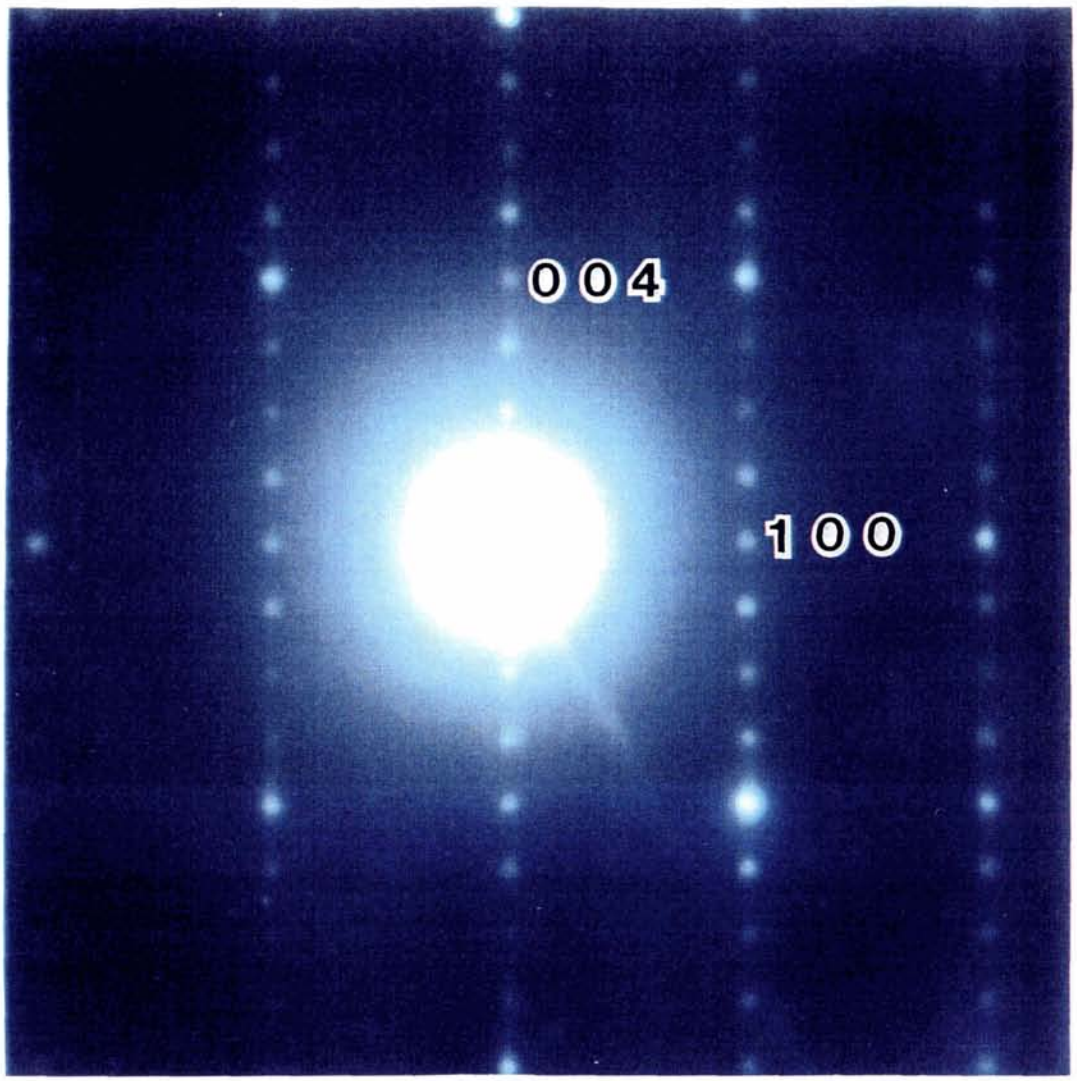

Fig. 4.2. The *h0l* electron diffraction pattern of the B-1223 phase.

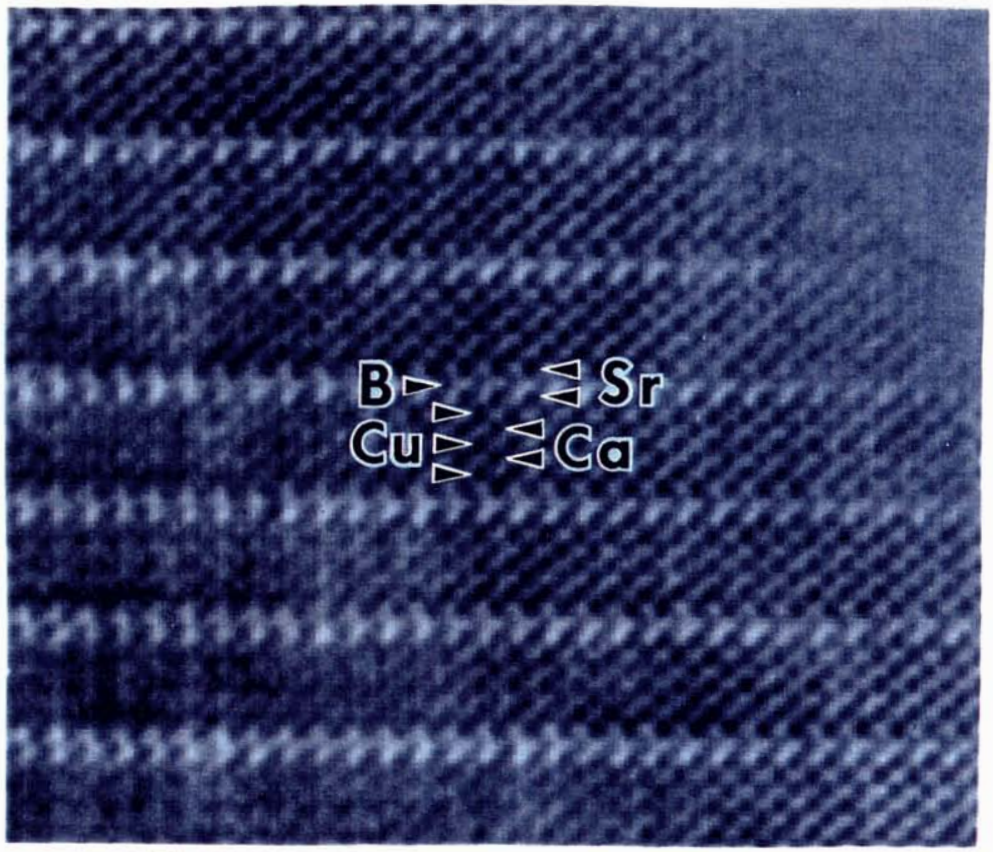

Fig. 4.3. HRTEM image of the B-1223 phase projected along [0 1 0].

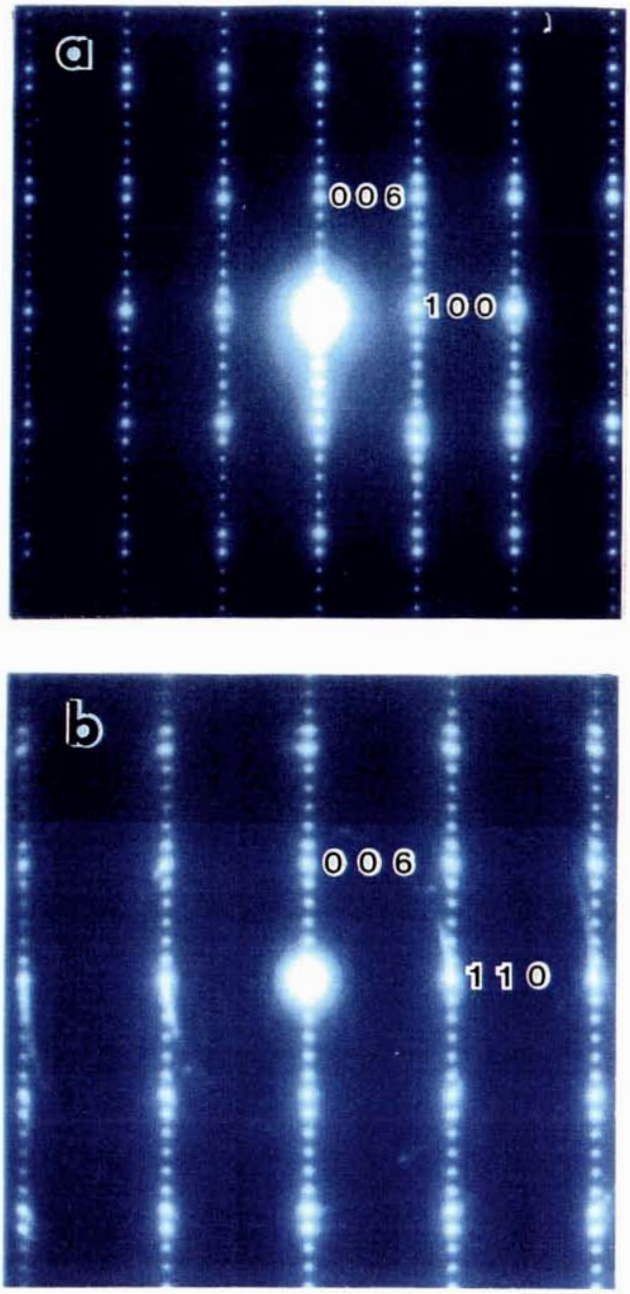

Fig. 4.4. The *h0l* (a) and *hhl* (b) electron diffraction patterns of the B-1245 phase.

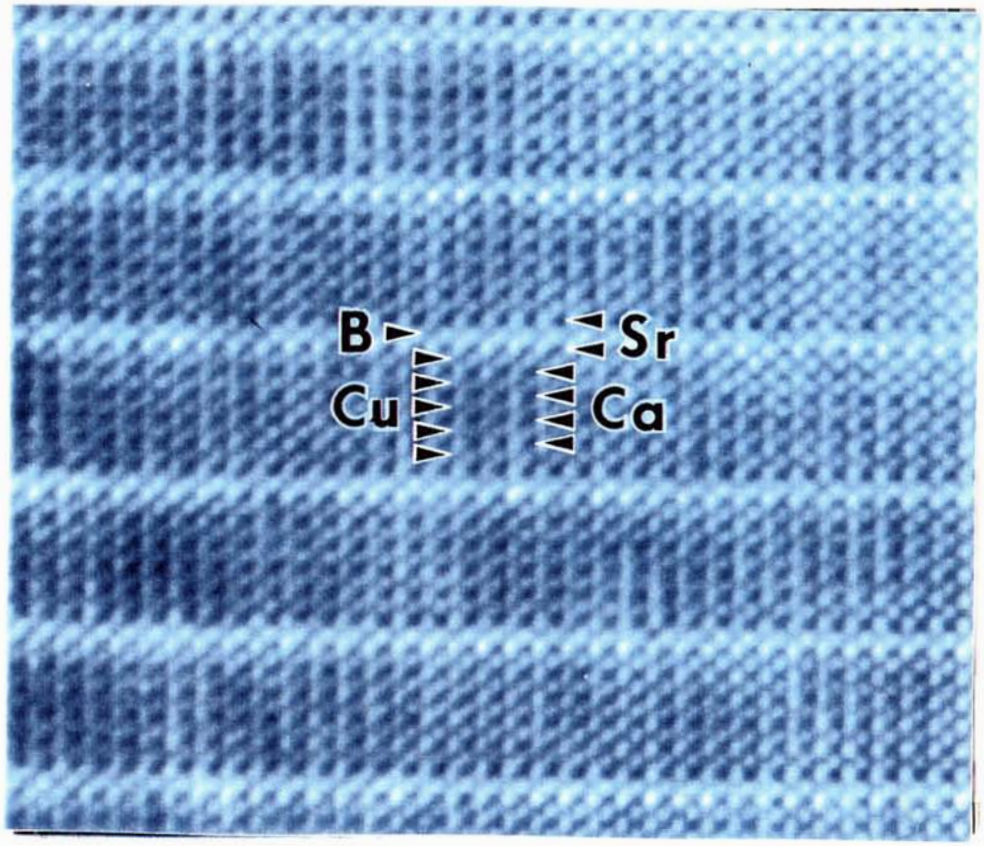

Fig. 4.5. HRTEM image of the B-1245 phase projected along [0 1 0].

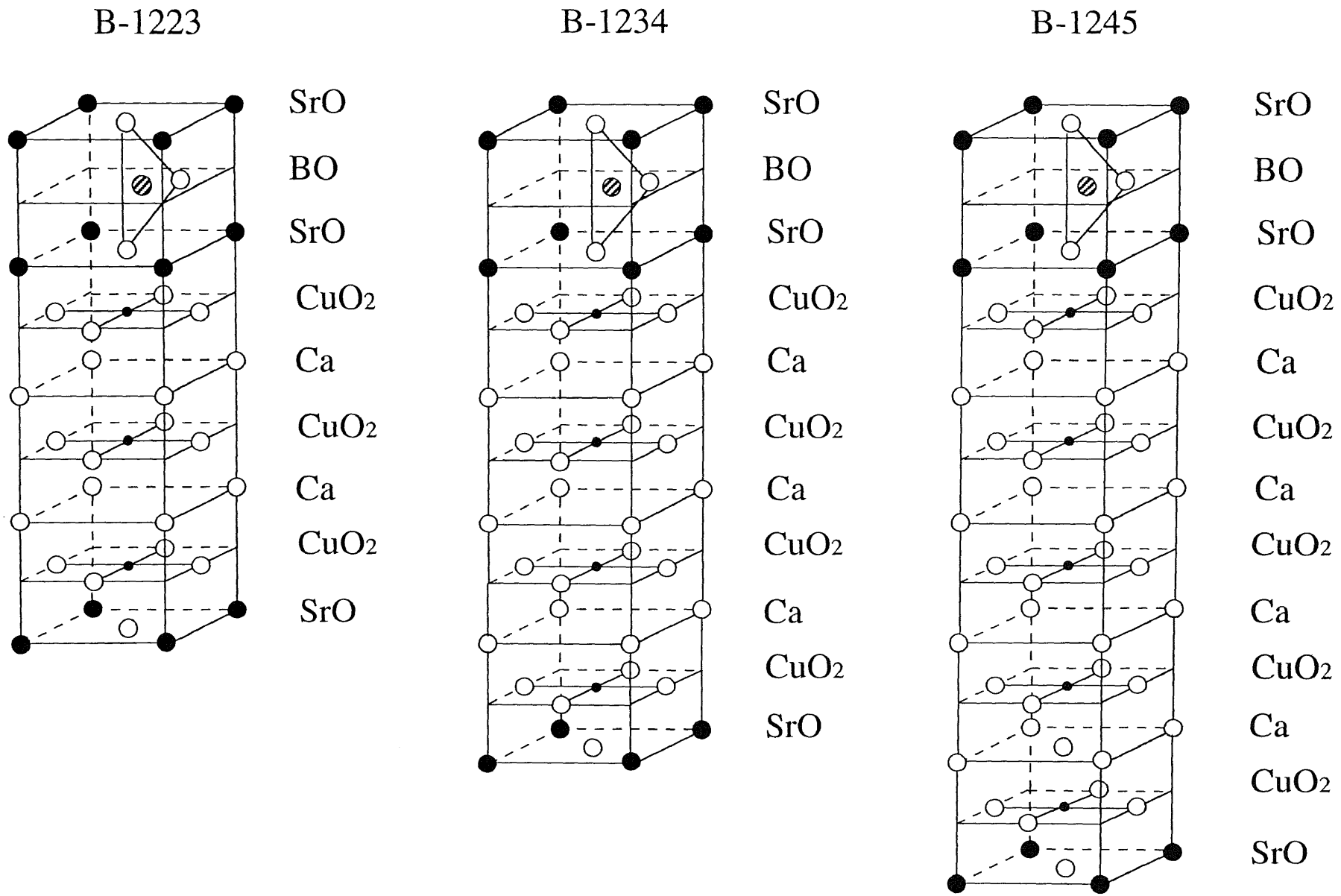

Fig. 4.6. Crystal structures of $BSr_2Ca_{n-1}Cu_nO_{2n+3}$ (n=3,4,5). The oxygen positions in the B plane are drawn for three-fold coordination of the B.

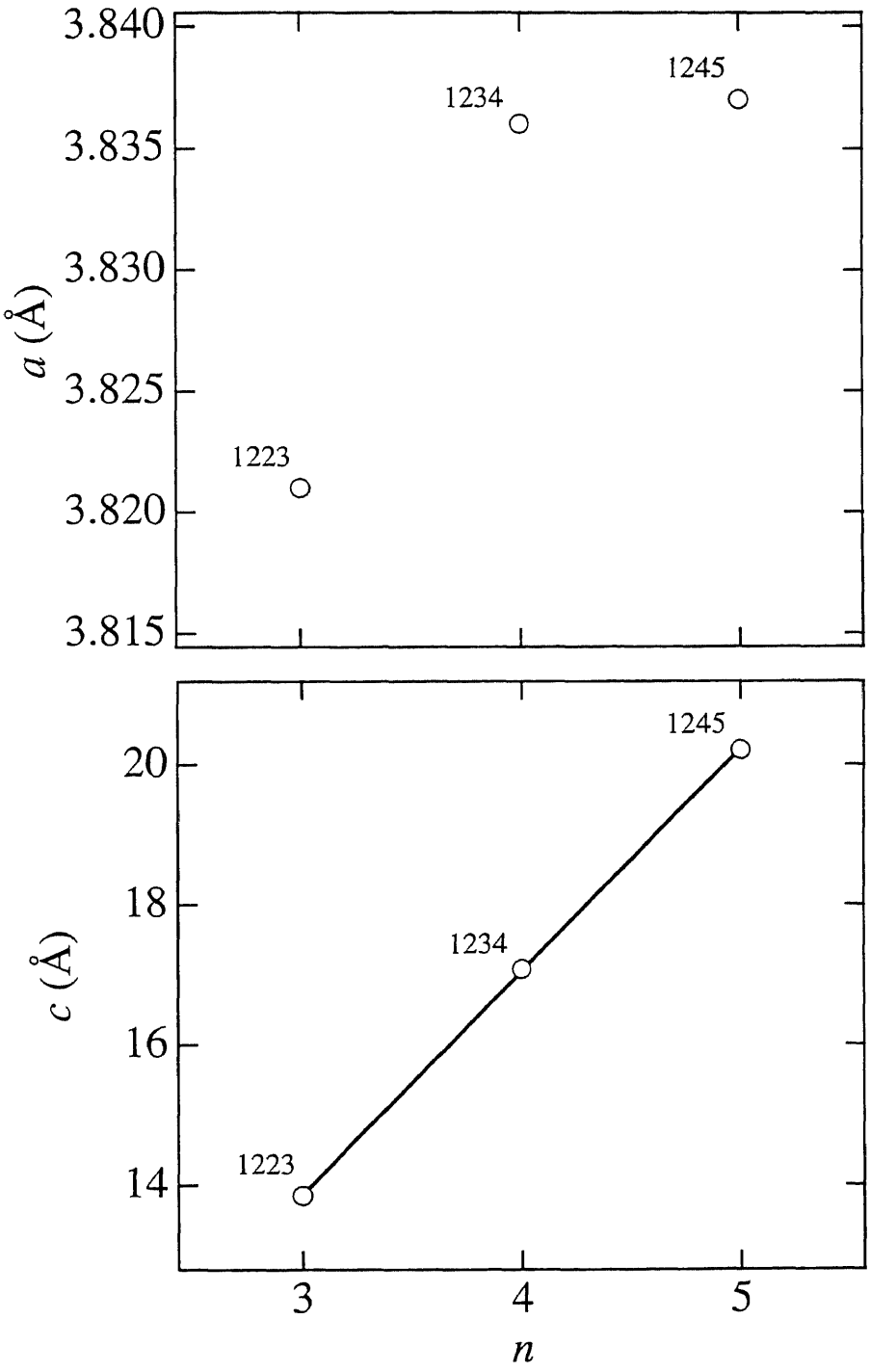

Fig. 4.7. The variations of the lattice constants of B-12(n-1)n as functions of *n*. The data for B-1234 were taken from Ref, [41].

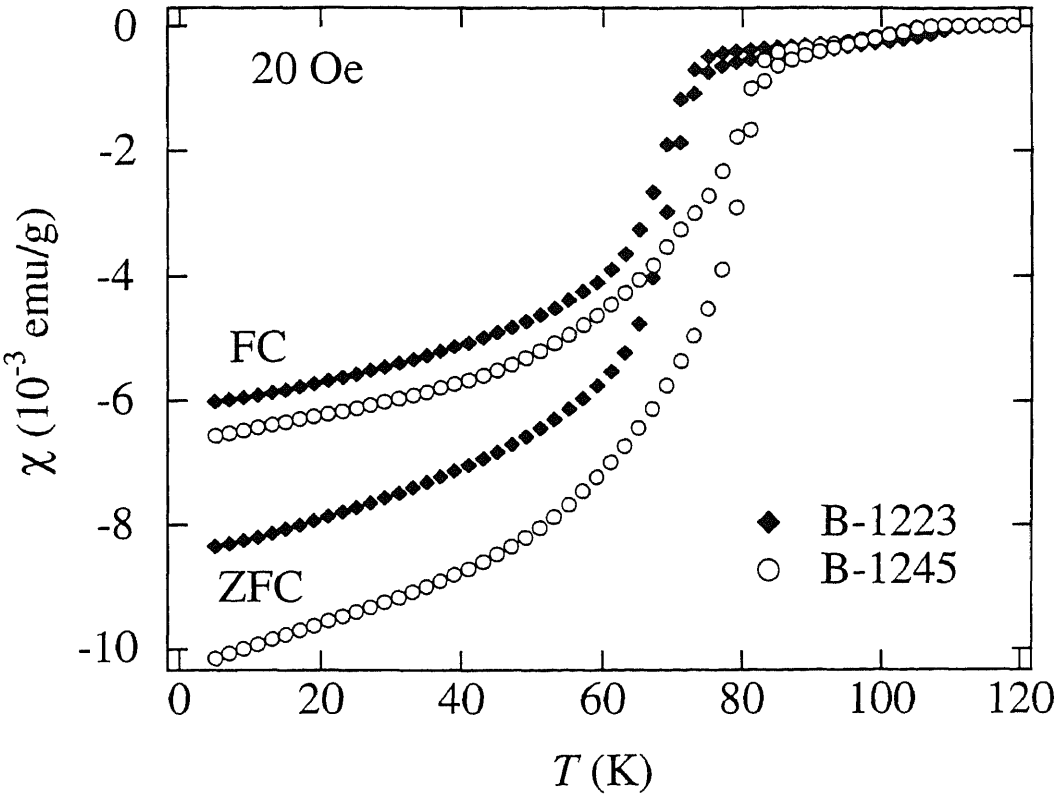

Fig. 4.8. DC susceptibility data of the samples corresponding to Fig. 4.1(a) (denoted as B-1223) and to Fig. 4.1(b) (denoted as B-1245).

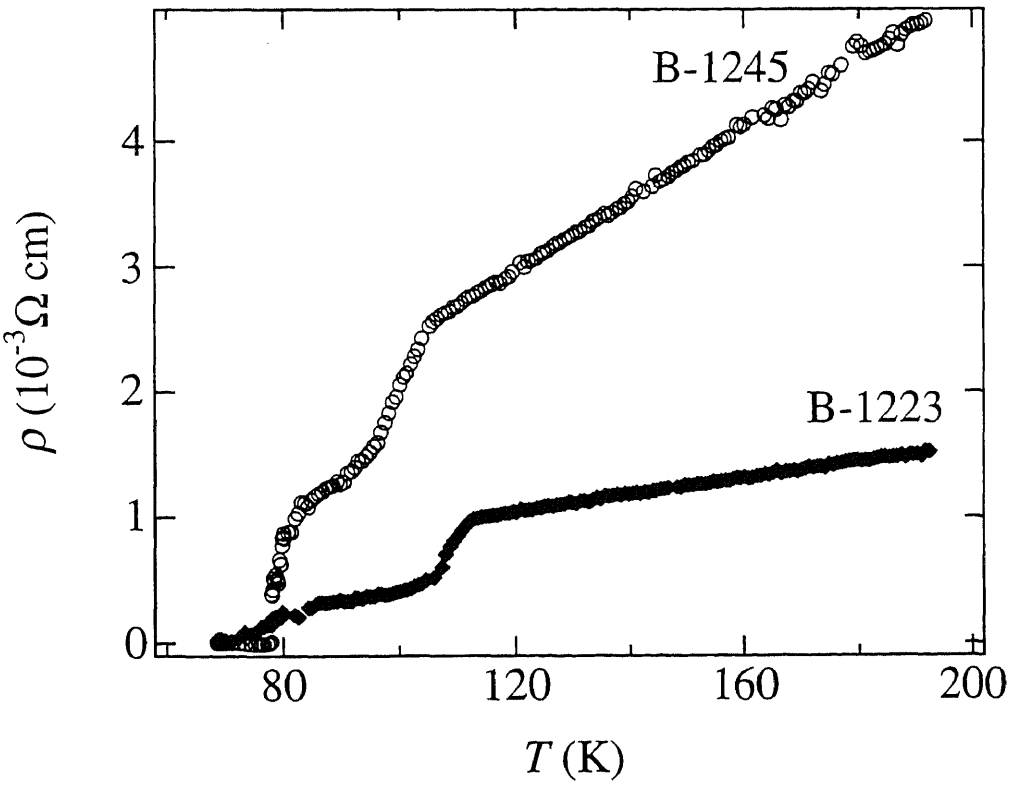

Fig. 4.9. DC resistivity of the samples corresponding to Fig.4.1(a) (denoted as B-1223) and to Fig. 4.1(b) (denoted as B-1245).

5. High pressure synthesis and superconducting properties of new series of high-Tc superconductors, $Sr_2Ca_{n-1}Cu_nO_{2n}X_2$ (X=O, F)

5.1 Superconductivity in the series of compounds $Sr_2Ca_{n-1}Cu_nO_y$ (n=1~4) prepared under high pressure

Sr-Cu-O system (or Sr-Ca-Cu-O system) is very interesting because there are superconductors having simple crystal structures consisting of only alkaline earth, copper and oxygen atoms. However, preparation of a single-phase sample is very hard under high pressure which sometimes makes it difficult to identify the superconducting phase definitely.

Hiroi et al. reported that n=1 and n=2 members of $Sr_{n+1}Cu_nO_{2n+1+\delta}$ showed superconductivity below 70 and 100 K, respectively [42]. On the other hand, Adachi et al. found similar homologous series, $Sr_2Ca_{n-1}Cu_nO_{2n+1+\delta}$ in the Sr-Ca-Cu-O system [43,44]. However, their superconducting samples were multiphase mixtures including members with n=2,3,4 and they did not decide T_c of each member separately. Laffez et al. investigated $Sr_2CuO_{3+\delta}$ varying amount of $KClO_3$ used as an oxidizing agent [45] and observed bulk superconductivity with T_c of 80 K. They did not, however, completely deny the possibility that the superconductivity was ascribed to a phase other than $Sr_2CuO_{3+\delta}$ [45]. Prouteau et al. also observed superconductivity with T_c=98 K in Sr-Ca-Cu-O system [46], but the superconducting phase was not identified. Han et al. prepared $Sr_2CuO_{3+\delta}$ sample at high pressure then heat treated at 310 °C in N_2 at ambient pressure [47]. After the N_2 annealing, T_c rose to 94 K from 70 K. However, the absolute diamagnetic susceptibility of their sample was not

so large implying a presence of a superconducting phase different from $Sr_2CuO_{3+\delta}$.

Shaked et al. [48] investigated $(Sr,Ca)CuO_2$ having the infinite-layer structure. According to them, the infinite-layer phase is not superconducting but the superconductivity reported [49] is ascribed to $Sr_{n+1}Cu_nO_{2n+1+\delta}$ ($n \geq 2$) phases included as impurity. Moreover, they suggested that the n=1 member of the series, $Sr_2CuO_{3+\delta}$ is not superconducting.

Shimakawa et al. analyzed crystal structure of $Sr_2CuO_{3+\delta}$ by neutron powder diffraction method and found that nearly half of the oxygen sites are vacant in the "CuO_2" plane [50]. This result cast serious question on the reports which insist superconductivity in $Sr_2CuO_{3+\delta}$.

In the present study, we reinvestigated the Sr-Ca-Cu-O system. Though we also failed to prepare single-phase samples, comparison of superconductivity of various samples enabled us to specify T_c's of n=2,3,4 phases of the $Sr_2Ca_{n-1}Cu_nO_{2n+1}$ series. Moreover, our results suggest strongly that the n=1 phase, $Sr_2CuO_{3+\delta}$ is not superconducting.

5.1.1. Experimental

Starting materials for high pressure synthesis were $SrCuO_2$, SrO_2 (or $KClO_3$), Ca_2CuO_3 and CuO (99.9%). These materials were mixed in an agate mortar to obtain starting mixtures. The mixture was sealed in a gold capsule and allowed to react in a flat-belt-type high pressure apparatus at 5~6 GPa, and at 900~1300 °C for 0.5~3 hours, then quenched to room temperature. SrO_2 was generally used as an oxidizing agent. Only $Sr_2CuO_{3+\delta}$ samples were prepared using $KClO_3$.

X-ray powder diffraction pattern was obtained by a diffractometer (Philips-PW1800) with Cu Kα radiation and lattice constants were determined using the least squares method. Profile fitting of the X-ray

pattern was done using intermediate Lorentzian as a profile shape function [51]. DC magnetic susceptibility data were collected for a pulverized sample by a SQUID magnetometer (Quantum Design) at a magnetic field of 20 Oe.

5.1.2. Results and discussion

Table 5.1 shows the synthetic conditions and superconducting properties of all samples prepared in the present study. Every high pressure product was a multi-phase mixture. In Table 5.1, only the phases belonging to the $Sr_2Ca_{n-1}Cu_nO_{2n+1}$ series are shown using a simplified notation, 02(n-1)n [44] since most of coexisting impurity phases could not be identified. It was sometimes hard to detect minor 02(n-1)n phases and only those identified definitely are shown in Table 5.1.

The superconducting transition temperature, T_c in the table is the onset value determined from the magnetic susceptibility data collected by the zero-field cooling method. When a sample showed two-step (or three-step) superconducting transitions, T_c of the second (and the third) transition is listed as well as the onset value. In addition, magnetic susceptibility at 5 K by the zero-field cooling method is given as a rough measure of the superconducting volume fraction.

The 02(n-1)n-phase formation was dependent not only on the nominal cation ratio but the oxygen content, pressure and temperature. For instance, different result was sometimes obtained after pressure or temperature was changed by the magnitude of 0.5 GPa or 50 °C, respectively.

Let us discuss first the n=1 phase, Sr_2CuO_y (0201 phase). We prepared two samples having different nominal oxygen contents, y=3.1 and 3.2 (sample No. hp-76-1 and hp-76-2, respectively) and compared their superconducting properties. Fig. 5.1(a) and Fig. 5.1(b) show the X-

ray powder diffraction patterns of the y=3.1 and 3.2 samples. Major X-ray peaks in Figs. 5.1(a), (b) could be indexed assuming the tetragonal 0201 lattice indicating that both samples contained the 0201 phase as a major one. It should be noted here that there are no significant differences in lattice parameters of the two samples: a=3.788(2), c=12.434(8) Å for y=3.1 and a=3.791(2), c=12.425(7) Å for y=3.2. This suggests strongly that compositions and oxygen contents of the 0201 phases in the two samples are very close to each other. Nevertheless, they showed quite different superconducting behaviors.

DC magnetic susceptibility data of both samples appear in Fig. 5.2. The y=3.1 sample showed a superconducting transition at ca. 70 K though superconducting volume fraction was rather small. This T_c is in good agreement with the value reported by Hiroi et al. [42]. However, superconductivity disappeared almost completely in the y=3.2 sample. The similarity in the lattice parameters and the small superconducting volume fraction cast doubt if the 0201 phase really becomes superconducting.

To check the possibility that the superconducting sample, the y=3.1 sample included a higher order phase with n>1, we compared very carefully the two X-ray patterns in Fig. 5.1. Fig. 5.3(a) and Fig. 5.3(b) show the enlargement of the patterns for a lower 2θ range where we noted two small peaks near 2θ=8.5° and 17° in the y=3.1 sample. They can be assigned as 002 and 004 reflections of the n=2 phase, $Sr_3Cu_2O_y$ (i.e., the Ca-free 0212 phase). Moreover, pattern fitting for the y=3.1 sample (Fig. 5.4(a)) revealed clearly that there is an additional peak near 2θ=31.8°, just beside the 103 peak of the 0201 phase. This 2θ angle corresponds to position of 105 reflection of the 0212 phase which has the second highest intensity and is not overlapped with the peaks of the 0201 phase. All these peaks assignable to the 0212 phase disappeared

completely in the nonsuperconducting sample with y=3.2 as shown in Fig. 5.3(b) and Fig. 5.4(b). If we assume the stoichiometric composition, $Sr_2Ca_{n-1}Cu_nO_{2n+2}$, average valence of Cu is higher in the n=1 phase than in the n=2 one. This suggests that the n=2 phase becomes stable in a relatively lower oxygen pressure range compared with the n=1 one. The disappearance of the 0212 phase in the y=3.2 sample seems, therefore, reasonable. It is also worth noting that T_c of the y=3.1 sample (70 K) is close to that of the Ca-containing 0212 phase (77 K, see below).

Shimakawa et al. found that nearly half of the oxygen sites are vacant in the "CuO_2" plane of the 0201 phase [50]. Together with their finding, the present results suggest strongly that the 0201 phase is not superconducting and the 70-K superconductivity reported previously [42] is ascribed to the 0212 phase contained as a minor phase.

We carried out many experiments with various conditions to prepare the 0212 phase (see table 5.1). However, it was quite difficult to get a good sample. Fig. 5.5 shows X-ray powder diffraction pattern of our "best" sample (No. 40-1-6) prepared at 5.5 GPa and 1050 °C for a nominal composition of $Sr_2CaCu_2O_{5.5}$. Though the pattern was very complicated, strong X-ray peaks could be indexed assuming a tetragonal cell with a=3.821(4), c=20.74(6) Å which are in good agreement with a≈3.86, c≈20.4 Å reported previously for the 0212 phase [44]. We concluded, therefore, that the 0212 phase was dominant in this sample.

Besides 0212, the 0201 and 0223 phases were also included in this sample as indicated by their 00ℓ peaks appearing in the lower 2θ region. Corresponding to this, two-step superconducting transitions were observed in DC magnetic susceptibility data at 109 and ≈77 K (Fig. 5.6) in which the latter transition showed larger diamagnetism.

Fortunately, a pretty good 0223 sample was obtained in the present study and its T_c was determined as 109 K as described below. Combined

this fact with the above results, we concluded that the transition at 77 K is ascribed to the 0212 phase.

When the starting mixture of $Sr_2CaCu_2O_{5.5}$ (the 0212 mixture described above) was heat treated at higher temperature of 1250 °C, volume fraction of the 0223 phase increased drastically (No. 40-2-5). Fig. 5.7 indicates the X-ray powder diffraction pattern of the sample in question; its major peaks could be indexed assuming a tetragonal cell with a=3.863(1), c=27.22(2) Å which are in good agreement with previous values, a≈3.86, c≈27.2 Å obtained for the 0223 phase [44]. Besides the 0223 phase, small amount of the 0212 and 0201 phases were contained in the sample. Various starting mixtures having 0223-type nominal compositions (No. 40-1-4, for instance, see table) were also tested with the object of preparing a better 0223 sample. However, the volume fractions of the 0223 phase were rather smaller in these specimens than in the 40-2-5 one.

DC susceptibility data for the 40-2-5 sample is given in Fig. 5.8. Almost single-step transition at 109 K with slight anomaly near 80 K is seen in this figure. The transition at 109 K is ascribed to the 0223 phase while the anomalous behavior near 80 K to the 0212 phase included as a minor component.

Hiroi et al. reported that the 0201 and Ca-free 0212 phases, i.e., $Sr_{n+1}Cu_nO_{2n+1+\delta}$ (n=1,2), showed superconducting transitions at 70 and 100 K, respectively [42]. It is worth noting that their T_c's of 0201 and 0212 are close to our values for 0212 and 0223, respectively. We suggest that their 0201 and 0212 samples contained the 0212 and 0223 phases, respectively as a minor component.

Fig. 5.9 indicates the X-ray powder diffraction pattern of the hp-73-2 sample. Its starting composition, $Sr_3CaCu_{2.8}O_{7.5}$ ($Sr_2(SrCa)Cu_{2.8}O_{7.5}$), was close to the n=3 composition. However, many

X-ray peaks in Fig. 5.9 could be indexed assuming a tetragonal cell with a=3.901(3), c=33.82(2) Å which indicated that the 0234 phase rather than 0223 was dominant in this sample.

DC susceptibility data of the hp-73-2 sample appear in Fig. 5.10. It showed main superconducting transition at 83 K which is assigned to T_c of the 0234 phase. Additional diamagnetism observed below 105 and ≈70 K is ascribed to minor phases of 0223 and 0212, respectively.

In Fig. 5.11, a- and c-dimensions of the 02(n-1)n phases are plotted against n. The c-dimension increases linearly with a slope of 6.4 Å and half of this gives a reasonable value of 3.2 Å as the thickness of the composite CuO_2-Ca plane [44]. The a-dimension also increases linearly with n with the slope of ≈0.4 Å. The good linearity on n both in a- and c-dimensions supports the present assignment of the X-ray patterns and identification of the phases.

Fig. 5.12 indicates the variation of T_c against n. Here, we used T_c data for the "best" samples described above. The T_c-n curve has a maximum at n=3 and similar tendency has been observed in other series of superconductors, in $Tl_2Ba_2Ca_{n-1}Cu_nO_{2n+4}$, for instance [52].

5.2 High pressure synthesis and superconductivity of new oxyfluoride superconductors, $Sr_2Ca_{n-1}Cu_nO_{2n+\delta}F_{2\pm y}$ (n=2, 3)

In 1994, a new superconductor including fluorine, $Sr_2CuO_2F_{2+\delta}$, was reported by Al-Mamouri et al. [53]. It was synthesized through the reaction of Sr_2CuO_3 with F_2 gas at ambient pressure and it showed superconducting transition at 46 K. The structure of this phase is essentially of K_2NiF_4 type and is closely related to that of $Sr_2CuO_{3+\delta}$

prepared under high pressure [42], i.e., the oxygen and interstitial sites of the "SrO" plane in $Sr_2CuO_{3+\delta}$ are occupied by fluorine atoms. An excess fluorine atom introduced into the interstitial site creates one hole which acts as a carrier.

This system has been reinvestigated by several groups to obtain essentially the same results [54,55]. However, the superconducting volume fraction estimated from magnetic susceptibility data still remains low.

Under high pressure, on the other hand, chlorine-based superconductors, $(Ca,M)_2Ca_{n-1}Cu_nO_{2n}Cl_2$ (M=Na or Sr, n=1,2) has been prepared [56-58] in which the n=1 phase corresponds to the above-mentioned fluorine superconductor if we disregard that carriers are created by the Na-substitution in the chlorine-based system.

Successful high pressure syntheses of the chlorine-based superconductors suggest that a homologous series of compounds, $Sr_2Ca_{n-1}Cu_nO_{2n+\delta}F_{2\pm y}$ with $n \geq 2$ may be stabilized under high pressure. Here, we discuss two new oxyfluoride superconductors prepared under high pressure, $Sr_2CaCu_2O_{4+\delta}F_{2\pm y}$ and $Sr_2Ca_2Cu_3O_{6+\delta}F_{2\pm y}$, which are the n=2,3 members of $Sr_2Ca_{n-1}Cu_nO_{2n+\delta}F_{2\pm y}$ series, respectively.

5.2.1. Experimental

Starting materials for high pressure syntheses were SrF_2 (99.9%), CaF_2 (99.9%), $SrCuO_2$, SrO_2, Ca_2CuO_3 and CuO (99.9%). These materials were mixed in an agate mortar to obtain starting mixtures for high pressure synthesis. The mixture was sealed in a gold capsule and allowed to react in a flat-belt-type high pressure apparatus at 5.5 GPa, and at 1250 °C for 3 hours, then quenched to room temperature.

X-ray powder diffraction pattern was obtained by a diffractometer (Philips-PW1800) with Cu Kα radiation and lattice constants were

determined using the least squares method. High resolution transmission electron microscope (HRTEM) observation was carried out using a microscope (type H-1500) operated at 1000 kV.

DC magnetic susceptibility data were collected by a SQUID magnetometer (Quantum Design) at a magnetic field of 20 Oe. DC resistivity was measured by the standard four-probe method.

5.2.2. Results and discussion

Table 5.2 shows synthetic conditions tried in the present study. Temperature and pressure were fixed at 1250 °C and 5.5 GPa, respectively. Every high pressure product was multi-phase mixture and only superconducting phase included is shown in Table 5.2 since most of coexisting impurity phases could not be identified. The superconducting transition temperature, T_c in the table is the onset value determined from the magnetic susceptibility data. Magnetic susceptibility at 5 K by the field cooling method is given as a rough measure of the superconducting volume fraction. In the following, we will describe in detail two samples having nominal compositions, $Sr_2CaCu_2O_{4.6}F_{2.0}$ and $Sr_2Ca_2Cu_3O_{6.2}F_{3.2}$.

Figs. 5.13 (a) and (b) show the X-ray powder diffraction patterns for the $Sr_2CaCu_2O_{4.6}F_{2.0}$ and $Sr_2Ca_2Cu_3O_{6.2}F_{3.2}$ samples, respectively. Major X-ray peaks in Figs. 5.13 (a) and (b) could be indexed assuming tetragonal cells with a=3.843(1), c=19.88(1) Å and a=3.840(1), c=26.17(1) Å, respectively. Hereafter, we call the former tetragonal phase as 0212-F and the latter as 0223-F according to their ideal compositions (see below).

Figs. 5.14 (a) and (b) shows the *hk0* and *h0l* electron diffraction (ED) patterns of the 0212-F phase. Space group, tetragonal I4/mmm is derived from systematic extinction of diffraction spots in these ED

patterns. Fig. 5.15 is a lattice image corresponding to the ED pattern in Fig. 5.14(b), where we can distinguish two Sr, one Ca and two Cu planes. Strong white contrast is seen near the Sr atom suggesting that the F atoms are concentrated in this part of the crystal. The HRTEM observations indicate that the ideal composition of 0212-F is $Sr_2CaCu_2O_4F_2$, the n=2 member of the $Sr_2Ca_{n-1}Cu_nO_{2n}F_2$ family.

Figs. 5.16(a) and (b) show the *hk0* and *h0l* ED patterns of the 0223-F phase while Fig. 5.17 is a lattice image corresponding to Fig 5.16(b). The ED patterns give the space group I4/mmm and the image is consistent with the 0223 structure in which two Ca and three Cu planes are stacked along the *c*-axis between double Sr planes. Strong white contrast is seen near the Sr atom as well as in 0212-F suggesting presence of SrF-SrF double planes. The ideal composition of 0223-F is, therefore, $Sr_2Ca_2Cu_3O_6F_2$.

According to Adachi *et al.* [44], the c-dimensions of $Sr_2Ca_{n-1}Cu_nO_{2(n+1)}$ series are 20.4 Å (n=2) and 27.2 Å (n=3). These values are appreciably larger than 19.88 Å (n=2) and 26.17 Å (n=3) in the present series of phases, respectively. This seems to reflect that apical oxygen atoms in $Sr_2Ca_{n-1}Cu_nO_{2(n+1)}$ are replaced by small F atoms in the present phases.

In Fig. 5.18, structure models of 02(n-1)n-F phases are shown schematically where the n=1 member was reported previously. The "SrF" double layers are supposed to include the interstitial fluorine and/or oxygen atoms. Moreover, partial substitution of the oxygen for the fluorine may occur, although, in Fig. 5.18, these complex features are disregarded.

Fig. 5.19 gives DC susceptibilities of the 0212-F and 0223-F samples. Both showed sharp superconducting transitions, at 99 K in the former sample and at 111 K in the latter with large enough diamagnetic

susceptibilities at 5 K to assume bulk superconductivity. Fig. 5.20 indicates DC resistivities of the two samples. A sharp decreases in resistivity were observed around 100 and 110 K for 0212-F and 0223-F, respectively consistent with the susceptibility data. Both samples showed metallic behaviors above T_c.

As shown in Table 5.2, T_c and the superconducting volume fraction (χ at 5 K) were strongly depend on the nominal cation and anion ratios. When the fluorine content increased with fixing the cation ratios and oxygen content, T_c got the maximum at an optimum fluorine content. In the $Sr_2CaCu_2O_4F_x$ series, for instance, maximum T_c was obtained at x=2.6. In the $Sr_2Ca_2Cu_3O_6F_x$ series, on the other hand, the x=3.2 sample showed the highest T_c of 109 K while the x=3.4 one was not superconducting.

Similar tendency was seen when the oxygen content was varied with fixing the cation rations and the fluorine content. In the $Sr_2CaCu_2O_zF_{2.0}$, for instance, an intermediate oxygen content of z=4.6 gave the highest T_c. As a result, T_c varied very widely depending on the nominal fluorine and oxygen contents, from 43 to 99 K in the 0212 phase and from 75 to 111 K in the 0223 phase. Though we could not calculate the hole concentration for each sample because of presence of coexisting impurity phases, the T_c variation described above seems to reflect variation of the hole (carrier) concentration.

To obtain a better 0212 sample, we changed the Sr/Ca ratio or Cu content in the starting mixture as shown in Table 5.2. However, this attempt was not successful; in many cases, it resulted in coexistence of two superconducting phases and impurity ones.

It should be noted that T_c's of the present series of phases are very high in spite of the presence of the apical fluorine atom. In particular, T_c of 0223-F, 111 K is comparable to the highest T_c observed in halogen-

free oxide superconductors. This fact clearly indicates that the structure and the carrier density of the CuO_2 plane are essential to determine T_c and the blocking layer is important so long as it is concerned with the creation of the carriers.

Table 5.1. Starting compositions, synthetic conditions, observed phases and superconducting properties of the high-pressure samples.

Sample No.	Starting composition	P (GPa)	Temp. (℃)	Phase	T_c (K)	χ at 5K (ZFC) (10^{-3} emu/g)
hp-76-1	$Sr_2CuO_{3.1}$ (with $KClO_3$)	6	900	0212,0201	73	-0.66
hp-76-2	$Sr_2CuO_{3.2}$ (with $KClO_3$)	6	900	0201	not superconducting	
hp-75-2	$Sr_2CaCu_2O_{5.4}$	6	1250	0223,0201	83,107	-2.83
hp-78-2	$Sr_2CaCu_2O_{5.4}$	6	1300	0212,0201	73,101	-1.94
hp-88-1	$Sr_2CaCu_2O_{5.5}$	5	900	0212,0201	97	-1.61
hp-84-1	$Sr_2CaCu_2O_{5.5}$	5	1050	0212,0201	101	-1.59
hp-86-1	$Sr_2CaCu_2O_{5.5}$	5	1200	0201	73,101	-0.75
40-1-6	$Sr_2CaCu_2O_{5.5}$	5.5	1050	0223,0212,0201	77,109	-2.83
40-2-5	$Sr_2CaCu_2O_{5.5}$	5.5	1250	0223,0212,0201	109	-3.09
40-5-2	$Sr_{1.5}Ca_{1.5}Cu_2O_{5.5}$	5.5	1250	0223,0201	*	*
40-5-1	$SrCa_2Cu_2O_{5.5}$	5.5	1250	0223,0201	*	*
hp-82-1	$Sr_2CaCu_2O_{5.5}$	6	900	0201	73	-0.09
hp-81-1	$Sr_2CaCu_2O_{5.5}$	6	950	0212,0201	99	-0.40
hp-74-1	$Sr_2CaCu_2O_{5.5}$	6	1050	0212,0201	97	-0.56
hp-77-1	$Sr_2CaCu_2O_{5.5}$	6	1100	0212,0201	99	-0.31
hp-89-1	$Sr_2CaCu_2O_{5.5}$	6	1200	0212,0201	87,109	-2.67
hp-75-1	$Sr_2CaCu_2O_{5.5}$	6	1250	0223,0201	107	-0.74

Table 5.1. cont.

hp-78-1	$Sr_2CaCu_2O_{5.5}$	6	1300	0201	107	-1.20
40-3-1	$Sr_2CaCu_2O_{5.7}$	5.5	1250	0223,0212	101	-2.54
40-5-3	$SrCa_2Cu_2O_{5.7}$	5.5	1250	0201	*	*
hp-74-2	$Sr_2CaCu_2O_{5.7}$	6	1050	0201	91	-0.45
hp-77-2	$Sr_2CaCu_2O_{5.7}$	6	1100	0201	91	-0.26
40-3-3	$Sr_2CaCu_2O_{5.9}$	5.5	1250	0223	103	-2.66
hp-67-1	$Sr_2CaCu_2O_{6.0}$	6	1250	0201	105	-0.92
hp-67-2	$Sr_2CaCu_2O_{6.1}$	6	1250	0201	105	-0.81
hp-65-1	$Sr_2CaCu_2O_{6.2}$	6	1250	0201	101	-1.00
hp-65-2	$Sr_2CaCu_2O_{6.5}$	6	1250	0201	101	-0.97
40-1-3	$Sr_2Ca_2Cu_3O_{7.2}$	5.5	1050	?	77,109	-1.57
40-1-4	$Sr_2Ca_2Cu_3O_{7.5}$	5.5	1050	?	101	-2.94
40-3-2	$Sr_2Ca_2Cu_3O_{7.5}$	5.5	1250	0223,0212,0201	85,109	-4.02
40-3-4	$Sr_{1.5}Ca_{2.5}Cu_3O_{7.5}$	5.5	1250	0223,0212,0201	75,105	-2.05
40-5-4	$Sr_{2.67}Ca_{1.33}Cu_3O_{7.8}$	5.5	1250	0201	*	*
40-5-5	$Sr_{2.67}Ca_{1.33}Cu_3O_{7.9}$	5.5	1250	0234,0223,0201	*	*
40-5-6	$Sr_{2.67}Ca_{1.33}Cu_3O_{8.0}$	5.5	1250	0234,0223,0201	*	*
hp-70-1	$Sr_{2.67}Ca_{1.33}Cu_3O_{8.3}$	5.5	1250	0234,0223,0201	101	-1.01
hp-70-2	$Sr_{2.67}Ca_{1.33}Cu_3O_{8.5}$	5.5	1250	?	*	*
hp-73-1	$Sr_{2.67}Ca_{1.33}Cu_{2.8}O_{7.5}$	5.5	1250	0234,0223,0212,0201	*	*
hp-73-2	$Sr_3CaCu_{2.8}O_{7.5}$	5.5	1250	0234,0223,0212,0201	70,83,105	-3.64

* not measured.

Table 5.2. Chemical composition of starting mixtures, observed phases and superconducting property of every samples.

sample No.	starting composition	phase	T_c (K)	χ at 5K (FC) (10^{-3} emu/g)
40-7-1	$Sr_2CaCu_2O_4F_{2.0}$	0212	43	-0.08
40-7-2	$Sr_2CaCu_2O_4F_{2.2}$	0212	79	-3.04
40-11-1	$Sr_2CaCu_2O_4F_{2.4}$	0212	83	-1.01
40-7-4	$Sr_2CaCu_2O_4F_{2.6}$	0212	93	-0.62
40-7-5	$Sr_2CaCu_2O_4F_{2.8}$	0212	89	-0.98
40-7-6	$Sr_2CaCu_2O_4F_{3.0}$	0212	85	-0.94
40-10-4	$Sr_2CaCu_2O_{4.2}F_{2.0}$	0212	83	-0.99
40-10-5	$Sr_2CaCu_2O_{4.4}F_{2.0}$	0212	93	-1.90
40-10-6	$Sr_2CaCu_2O_{4.6}F_{2.0}$	0212	99	-4.73
40-10-7	$Sr_2CaCu_2O_{4.8}F_{2.0}$	0212	83	-5.46
40-10-8	$Sr_2CaCu_2O_{5.0}F_{2.0}$	0212	53	-3.06
40-8-12	$Sr_2CaCu_2O_{3.9}F_{2.4}$	0201,0212	83	-0.08
40-8-1	$Sr_2CaCu_2O_{4.1}F_{2.4}$	0212	87	-1.43
40-8-2	$Sr_2CaCu_2O_{4.2}F_{2.4}$	0212	97	-3.09
40-8-3	$Sr_2CaCu_2O_{4.3}F_{2.4}$	0212	99	-3.66
40-10-1	$Sr_2CaCu_2O_{4.4}F_{2.4}$	0212	91	-5.43
40-10-2	$Sr_2CaCu_2O_{4.6}F_{2.4}$	0212	77	-3.82
40-10-3	$Sr_2CaCu_2O_{4.8}F_{2.4}$	0212	53	-2.87
40-8-4	$Sr_{2.7}Ca_{0.3}Cu_2O_{4.0}F_{2.4}$	0201,0212	79	-1.01
40-8-5	$Sr_{2.7}Ca_{0.3}Cu_2O_{4.1}F_{2.4}$	0201,0212	87	-1.79
40-8-6	$Sr_{2.7}Ca_{0.3}Cu_2O_{4.2}F_{2.4}$	0201,0212	89	-1.85
40-8-7	$Sr_{2.7}Ca_{0.3}Cu_2O_{4.3}F_{2.4}$	0201,0212	87	-1.21
40-8-8	$Sr_{2.4}Ca_{0.6}Cu_2O_{4.0}F_{2.4}$	0212	80	-2.31
40-8-9	$Sr_{2.4}Ca_{0.6}Cu_2O_{4.1}F_{2.4}$	0212	83,97	-5.92
40-8-10	$Sr_{2.4}Ca_{0.6}Cu_2O_{4.2}F_{2.4}$	0201	45,90	-1.45
40-8-11	$Sr_{2.4}Ca_{0.6}Cu_2O_{4.3}F_{2.4}$	0201,0212	80	-3.04
40-11-4	$Sr_{1.7}Ca_{1.3}Cu_2O_{4.3}F_{2.4}$	0212,0223	97,111	-5.83

Table 5.2. cont.

40-11-2	$Sr_2CaCu_{1.8}O_{4.1}F_{2.4}$	0212	99	-3.77
40-11-3	$Sr_2CaCu_{1.8}O_{3.9}F_{2.4}$	0212	89	-1.92
40-7-7	$Sr_2Ca_2Cu_3O_6F_{2.0}$	?	not superconducting	
40-7-8	$Sr_2Ca_2Cu_3O_6F_{2.2}$	0223	75	-0.19
40-7-9	$Sr_2Ca_2Cu_3O_6F_{2.4}$	0223	81	-0.21
40-7-10	$Sr_2Ca_2Cu_3O_6F_{2.6}$	0223	89	-3.97
40-7-11	$Sr_2Ca_2Cu_3O_6F_{2.8}$	0223	97	-4.22
40-7-12	$Sr_2Ca_2Cu_3O_6F_{3.0}$	0223	101	-4.26
40-10-9	$Sr_2Ca_2Cu_3O_6F_{3.2}$	0223	109	-4.03
40-10-10	$Sr_2Ca_2Cu_3O_6F_{3.4}$	?	not superconducting	
40-11-5	$Sr_2Ca_2Cu_3O_{6.6}F_{2.0}$	0223	103	-7.60
40-11-6	$Sr_2Ca_2Cu_3O_{6.2}F_{2.4}$	0223	49,77	-4.78
40-11-7	$Sr_2Ca_2Cu_3O_{6.4}F_{2.4}$	0212,0223	89	-3.16
40-11-8	$Sr_2Ca_2Cu_3O_{6.6}F_{2.4}$	0212	85	-0.77
40-11-9	$Sr_2Ca_2Cu_3O_{6.8}F_{2.4}$	?	not superconducting	
40-10-11	$Sr_2Ca_2Cu_3O_{6.2}F_{3.0}$	?	not superconducting	
40-10-12	$Sr_2Ca_2Cu_3O_{6.4}F_{3.0}$	?	not superconducting	
40-11-10	$Sr_2Ca_2Cu_3O_{6.2}F_{3.2}$	0223	111	-4.34
40-11-11	$Sr_2Ca_2Cu_3O_{6.4}F_{3.2}$	0223	111	-3.28
40-11-12	$Sr_2Ca_2Cu_3O_{6.6}F_{3.2}$	0223	111	-1.97

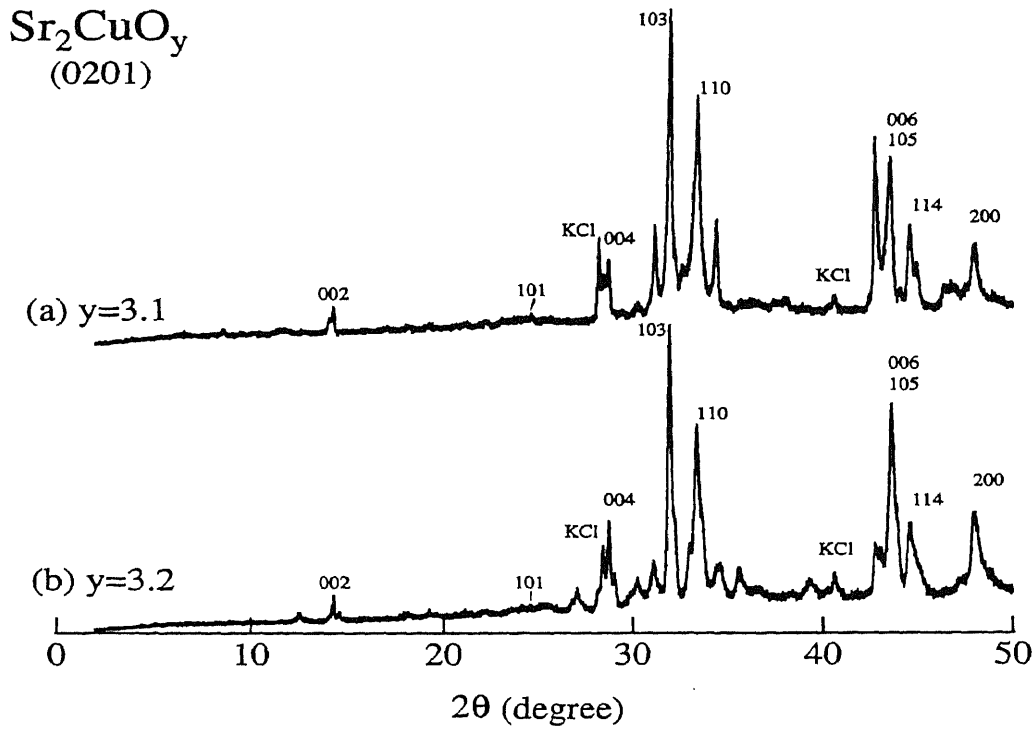

Fig. 5.1. Powder X-ray patterns of the samples having the nominal compositions, "$Sr_2CuO_{3.1}$" (a) and "$Sr_2CuO_{3.2}$" (b). Indexes are given based on the tetragonal cells with a=3.788(2), c=12.434(8) Å (a) and a=3.791(2), c=12.425(7) Å (b).

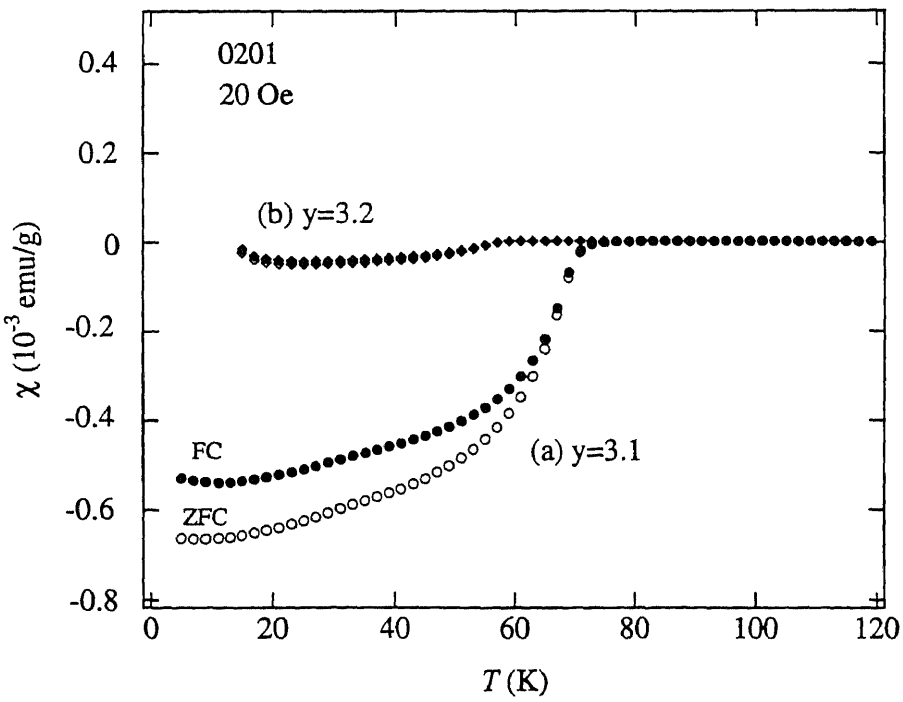

Fig. 5.2. DC magnetic susceptibility data of samples corresponding to Fig. 5.1(a) and to Fig. 5.1(b).

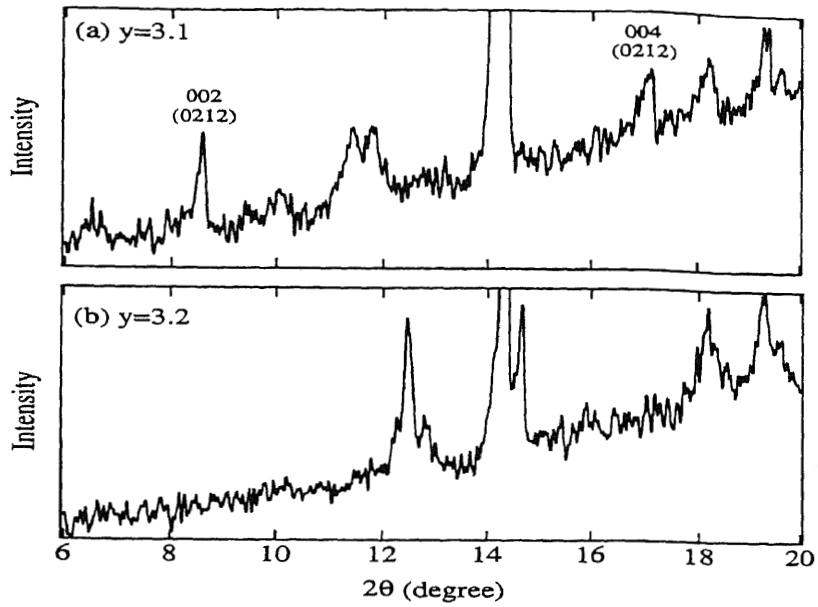

Fig. 5.3. The enlargement of the X-ray patterns in Fig. 5.1 for a lower 2θ range .

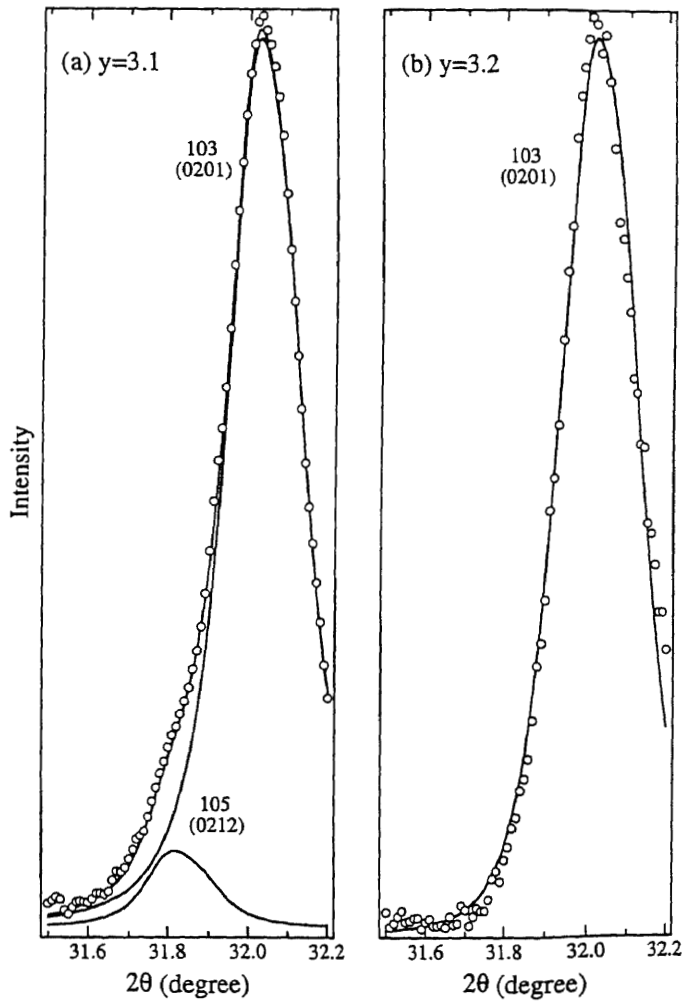

Fig. 5.4. Profile fitting of X-ray diffraction data in Fig.5.1 near 2θ=32°.

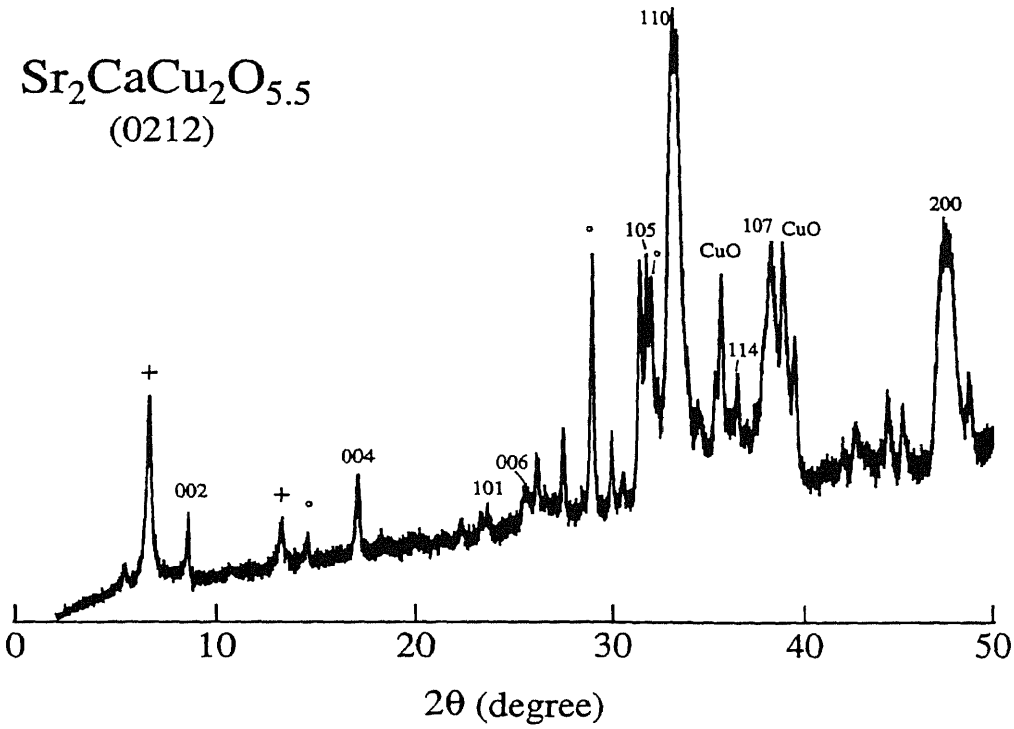

Fig. 5.5. Powder X-ray pattern of the 40-1-6 sample having the nominal composition, "$Sr_2CaCu_2O_{5.5}$". Indexes are given based on the tetragonal cells with a=3.821(4), c=20.74(6) Å. Peaks due to 0201 and 0223 phases are denoted by "°" and "+", respectively.

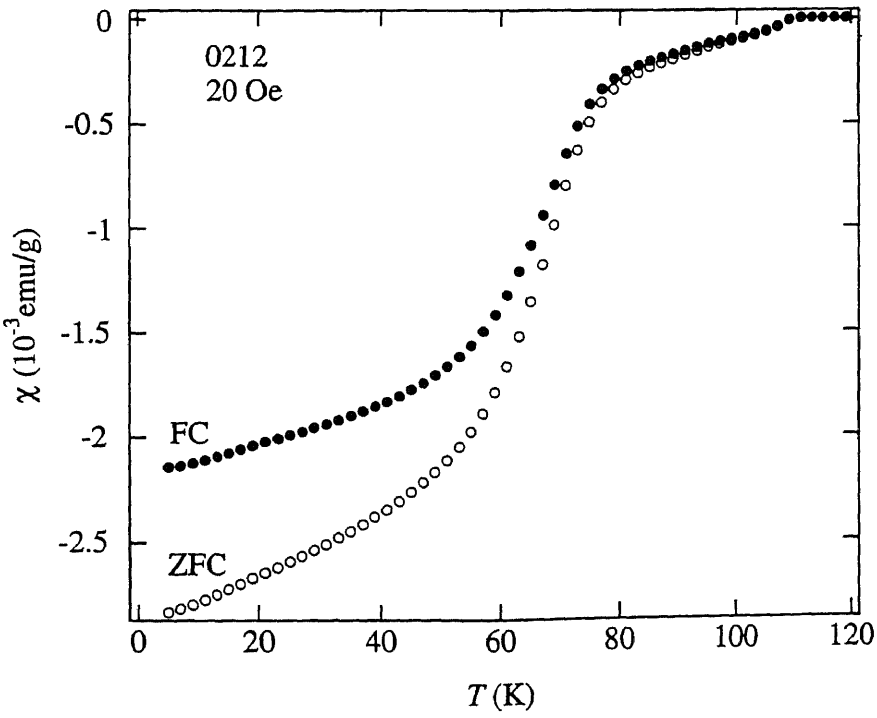

Fig. 5.6. DC magnetic susceptibility data of the 40-1-6 sample .

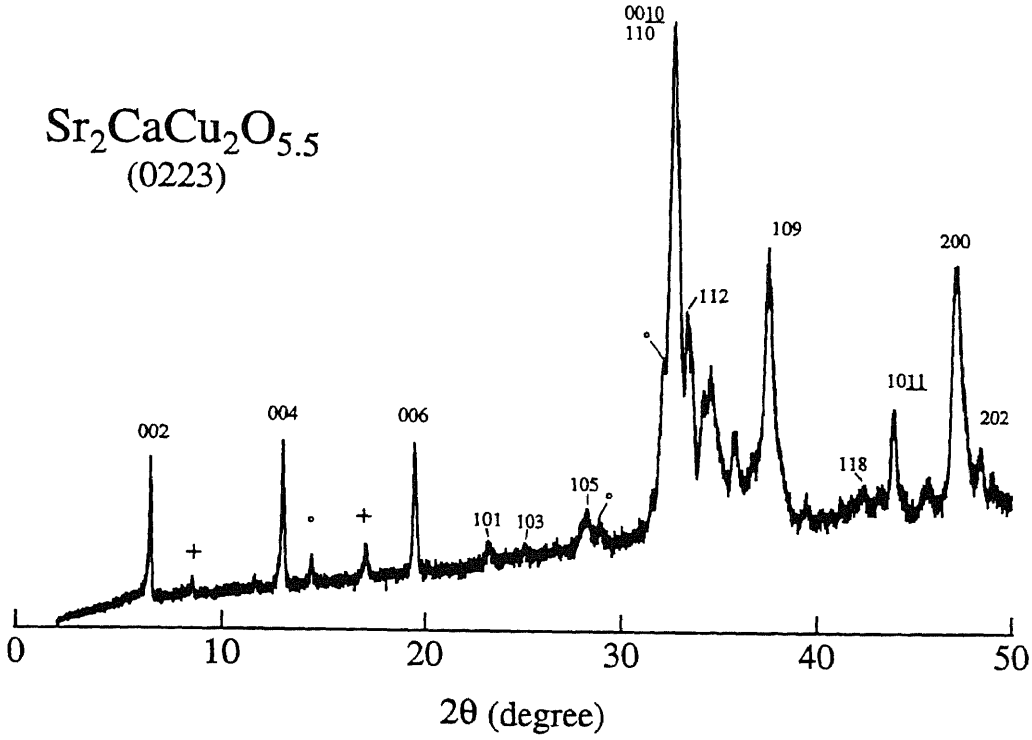

Fig. 5.7. Powder X-ray pattern of the 40-2-5 sample having the nominal compositions, "$Sr_2CaCu_2O_{5.5}$". Indexes are given based on the tetragonal cells with a=3.863(1), c=27.22(2) Å. Peaks due to 0201 and 0212 phases are denoted by "°" and "+" , respectively.

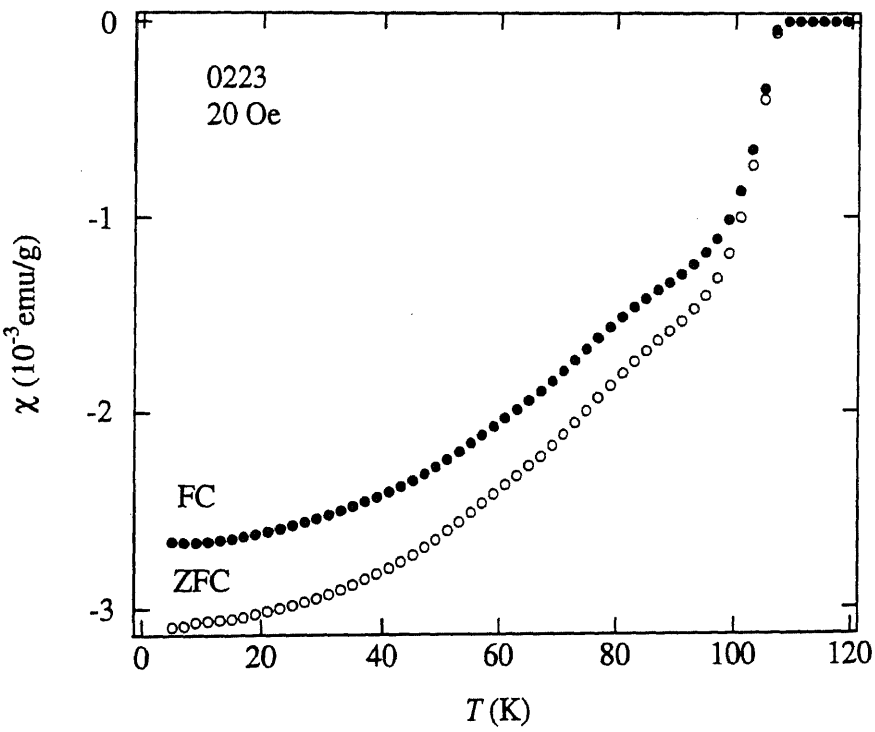

Fig. 5.8. DC magnetic susceptibility data of the 40-2-5 sample .

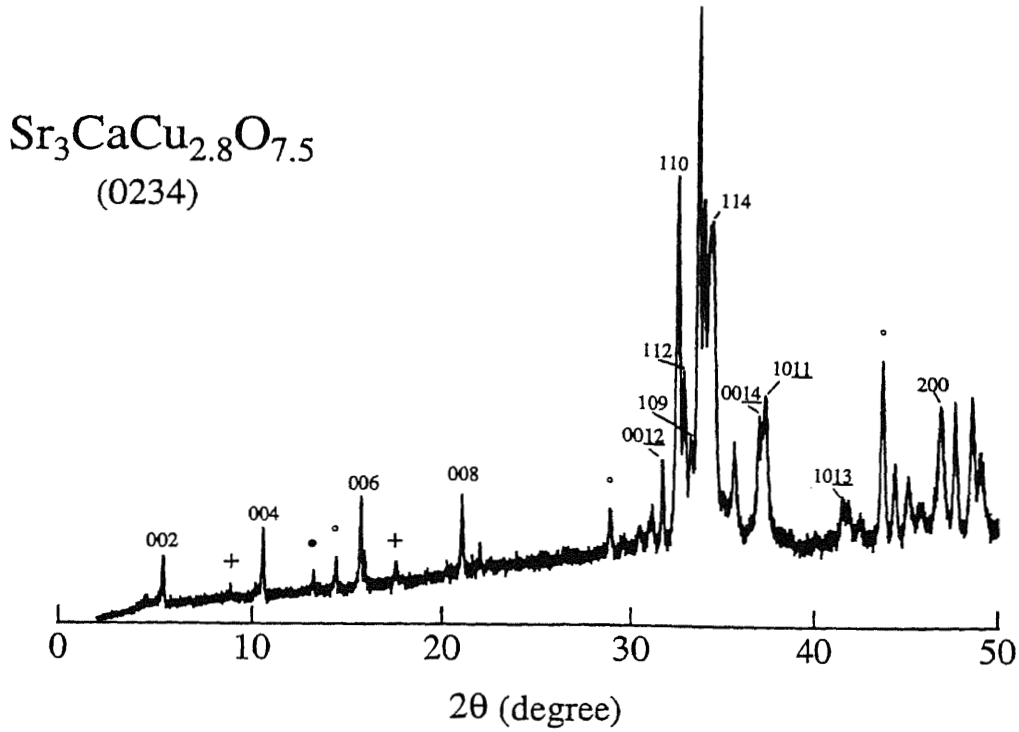

Fig. 5.9. Powder X-ray pattern of the hp-73-2 sample having the nominal compositions, "$Sr_3CaCu_{2.8}O_{7.5}$". Indexes are given based on the tetragonal cells with a=3.901(3), c=33.82(2) Å. Peaks due to 0201, 0212 and 0223 phases are denoted by "°" , "+" and "·" , respectively.

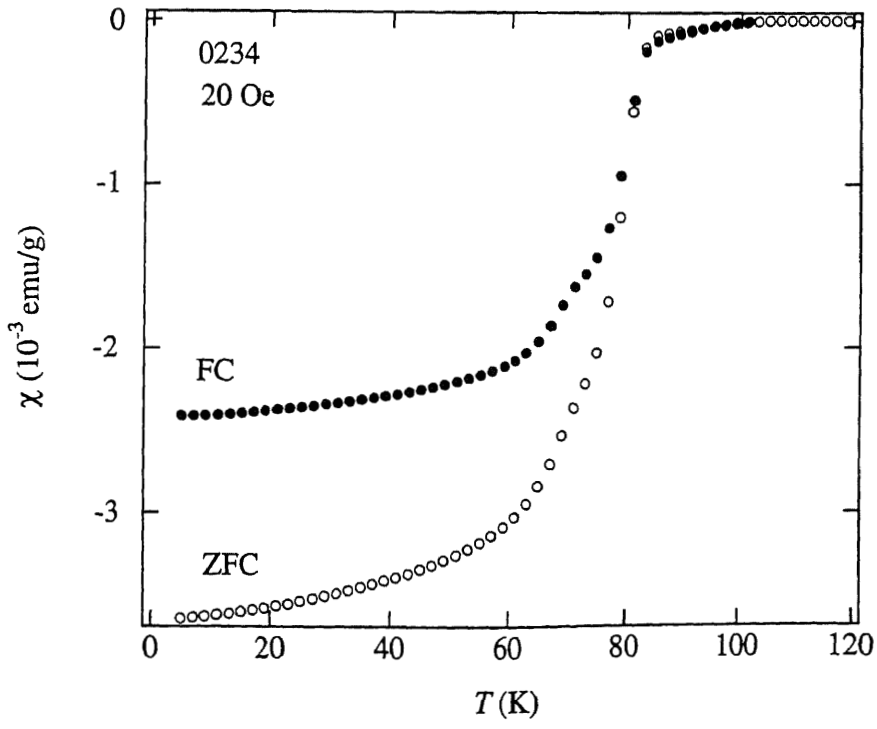

Fig. 5.10. DC magnetic susceptibility data of the hp-73-2 sample .

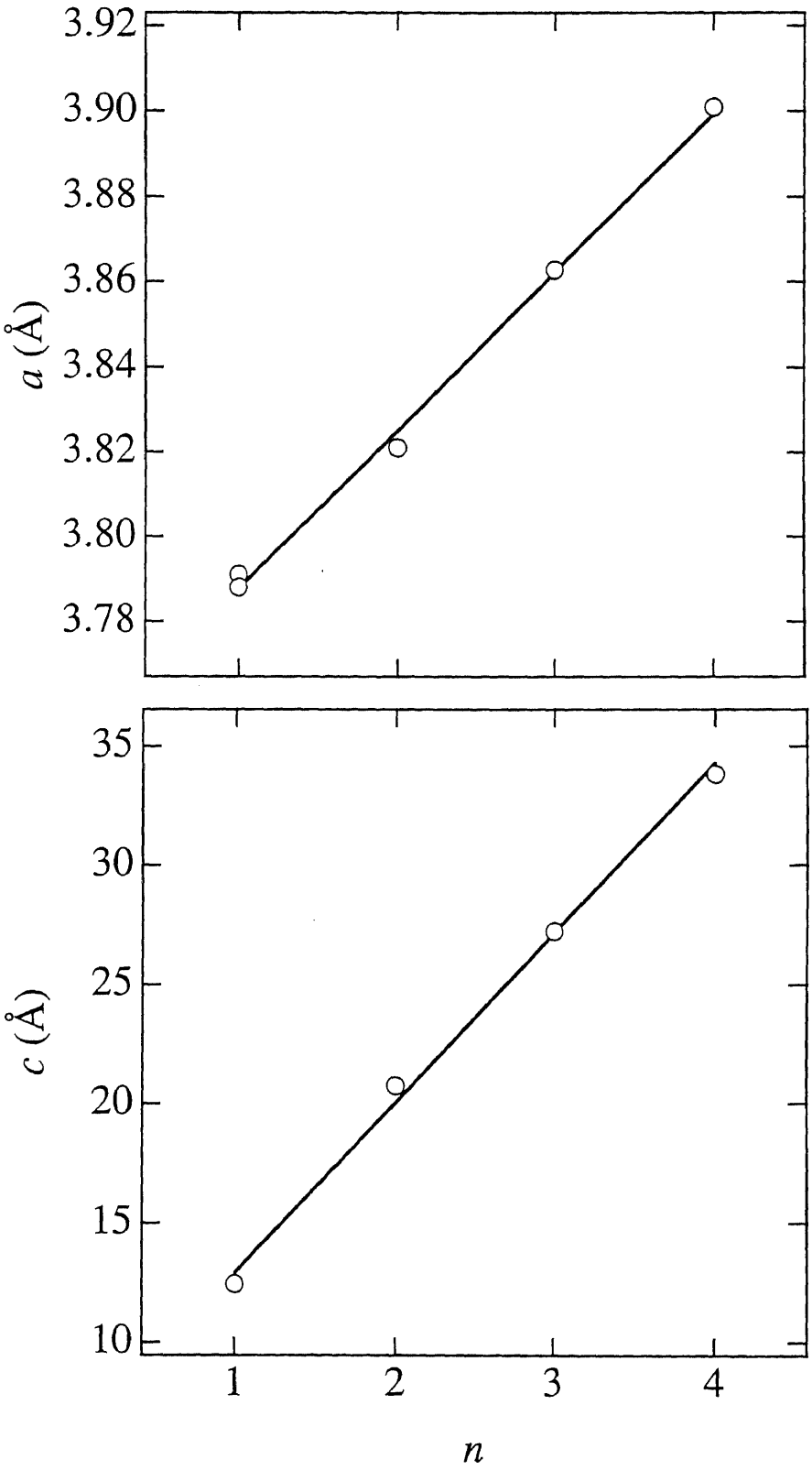

Fig. 5.11. The variation of the lattice constants of the 02(n-1)n phases as functions of *n*.

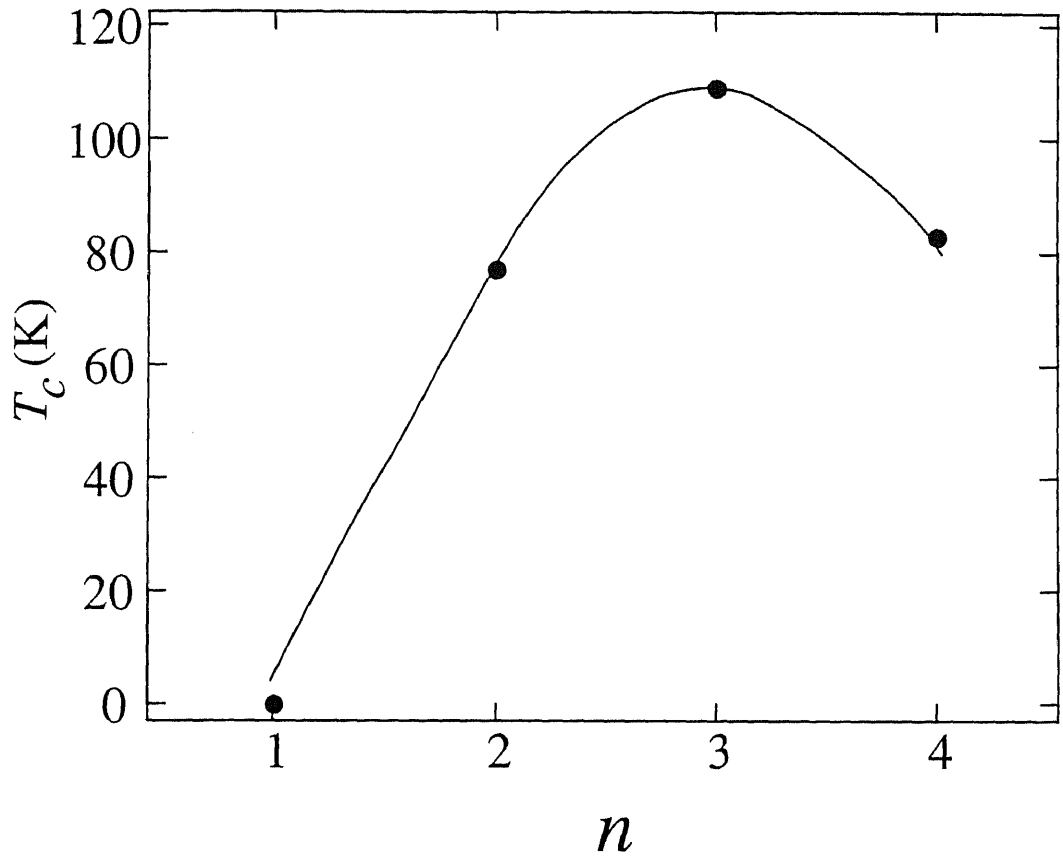

Fig. 5.12. The variation of the T_c (onset) of the 02(n-1)n phases as a function of *n*.

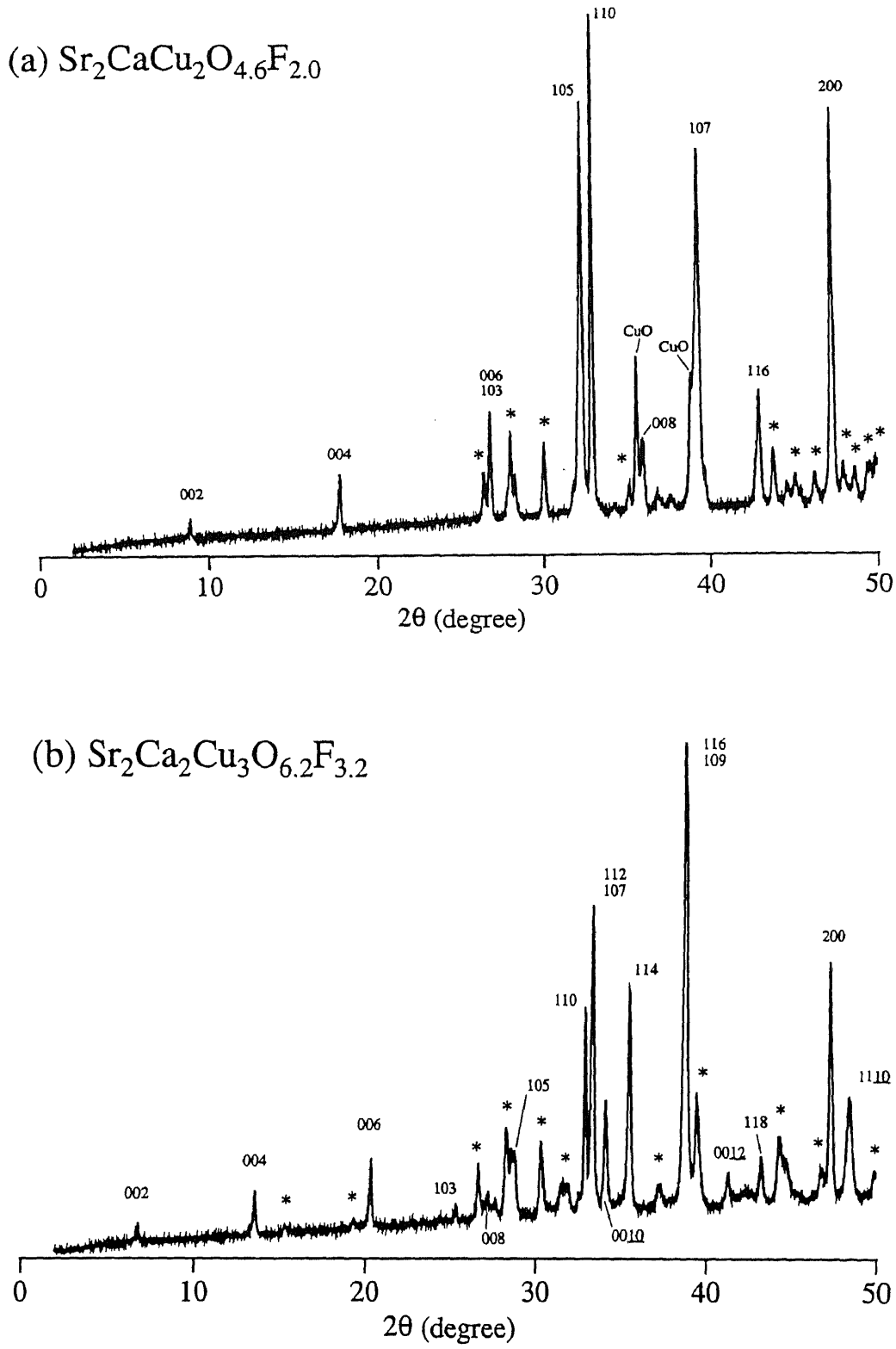

Fig. 5.13. Powder X-ray patterns of the samples having the nominal compositions, $Sr_2CaCu_2O_{4.6}F_{2.0}$ (a) and $Sr_2Ca_2Cu_3O_{6.2}F_{3.2}$ (b). Peaks due to unknown impurity phases are labeled by "*". Indexes are given based on the tetragonal cells with a=3.843(1), c=19.88(1) Å (a) anda=3.840(1), c=26.17(1) Å (b).

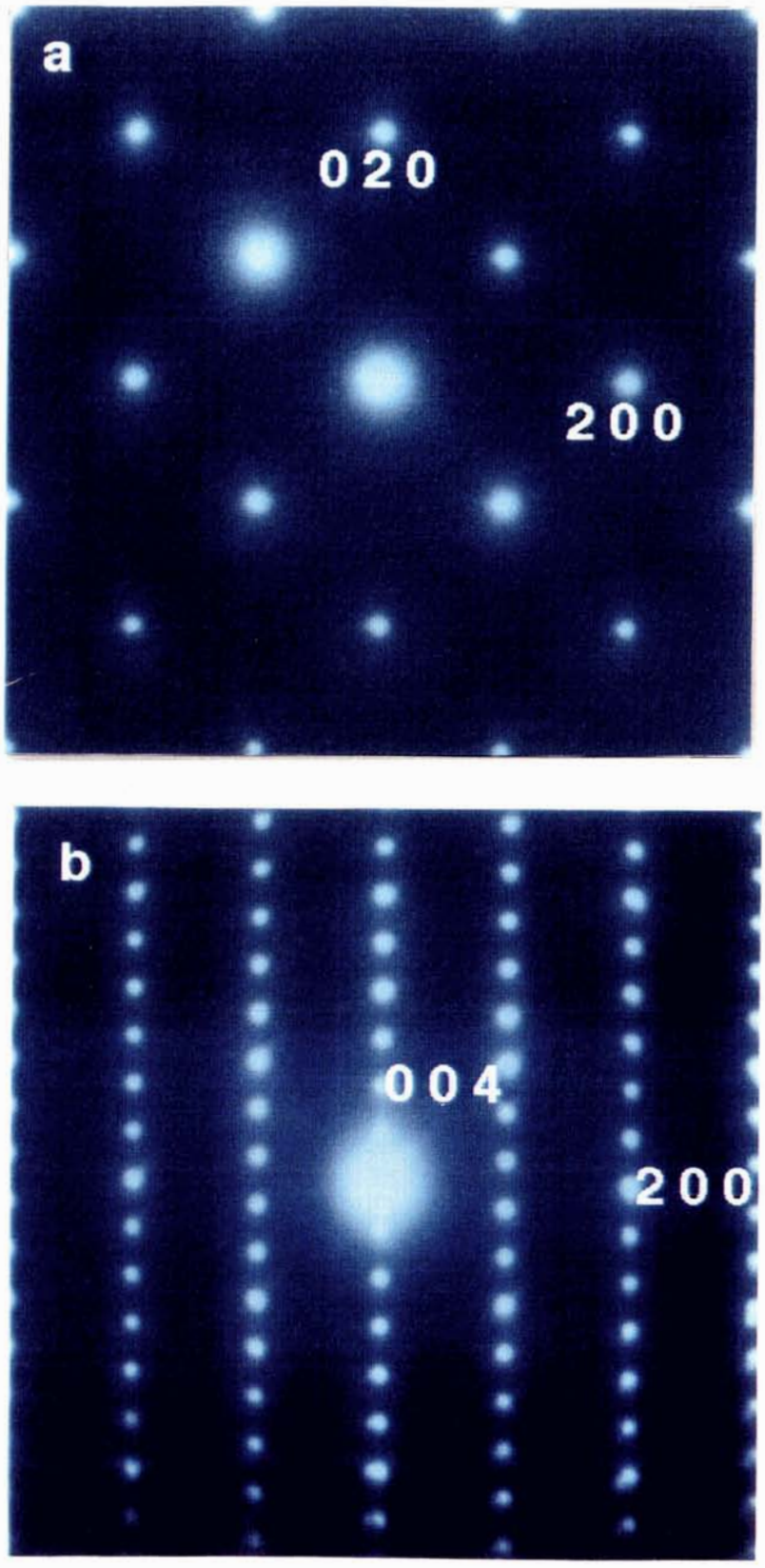

Fig. 5.14. The *hk0* (a) and *h0l* (b) electron diffraction patterns of the 0212-F phase.

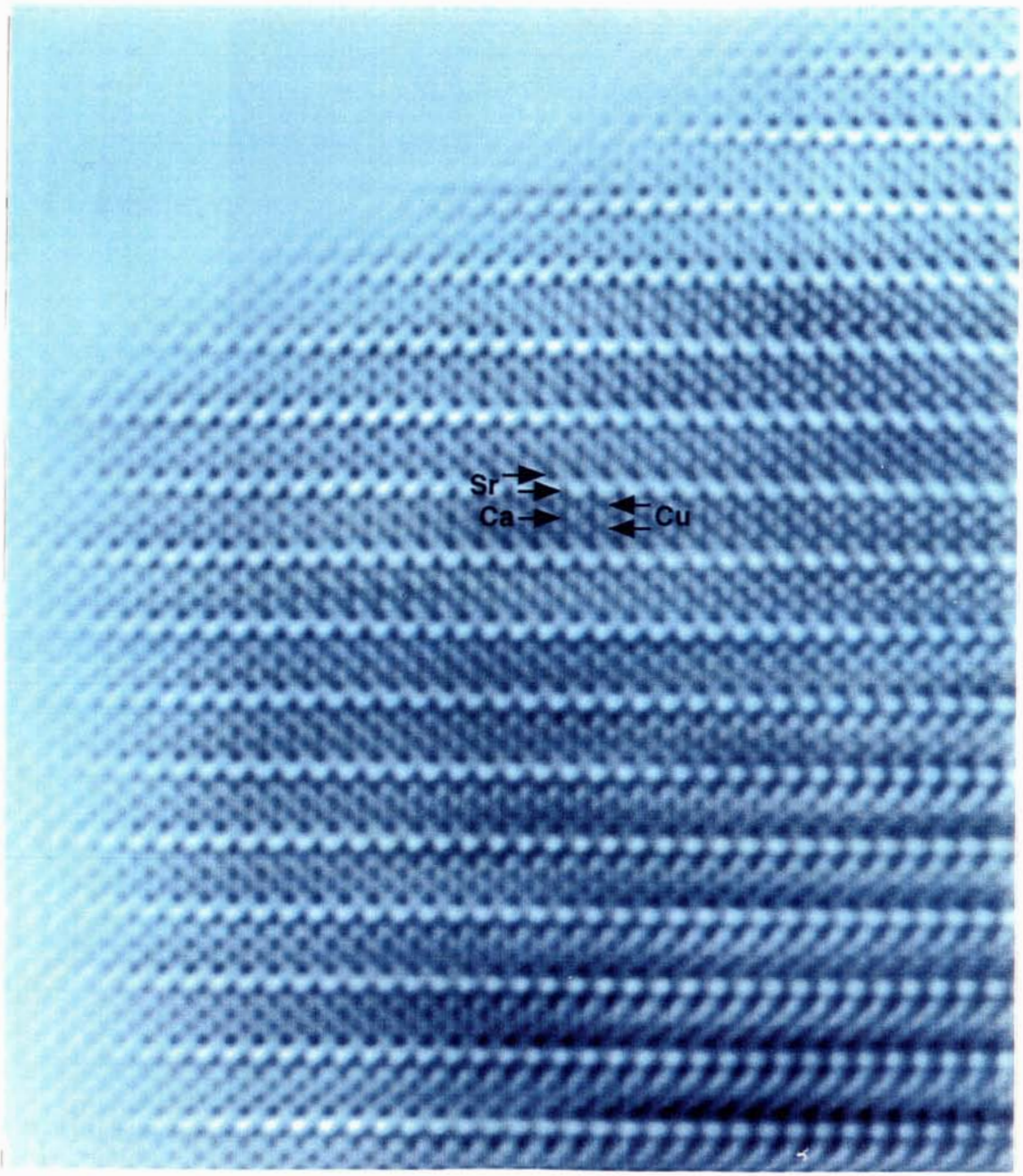

Fig. 5.15. HRTEM image of the 0212-F phase projected along [0 1 0].

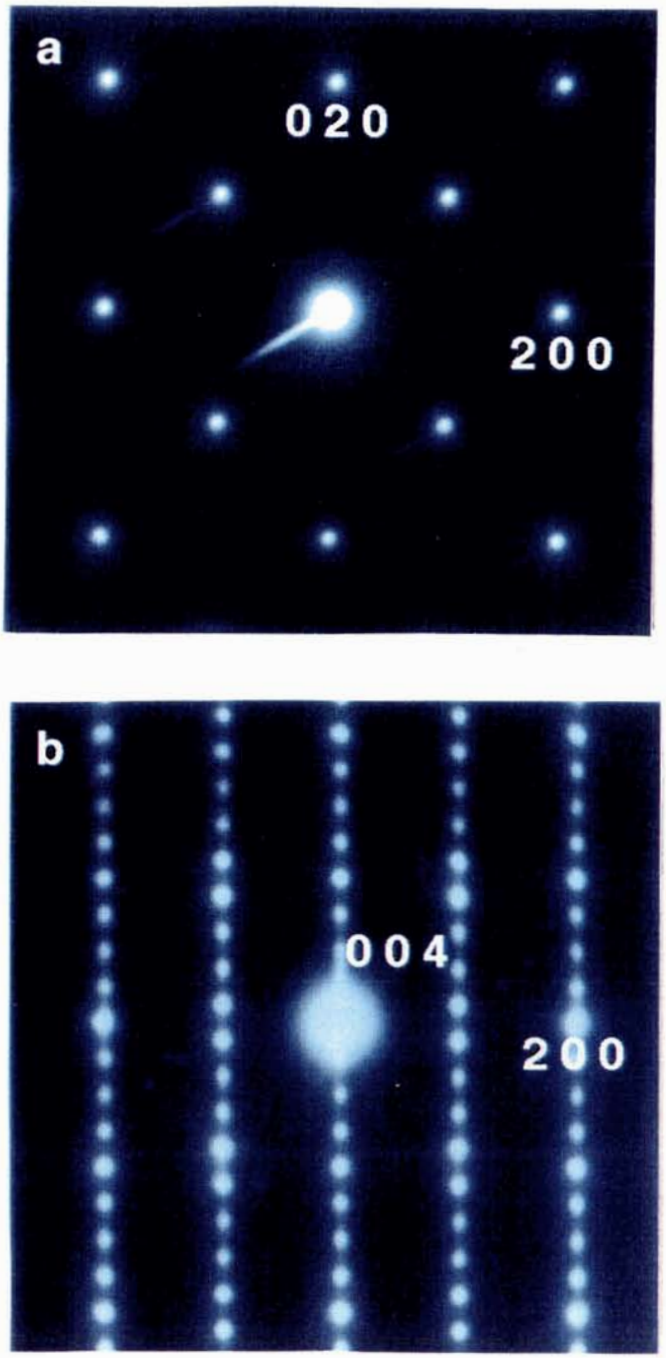

Fig. 5.16. The *hk0* (a) and *h0l* (b) electron diffraction patterns of the 0223-F phase.

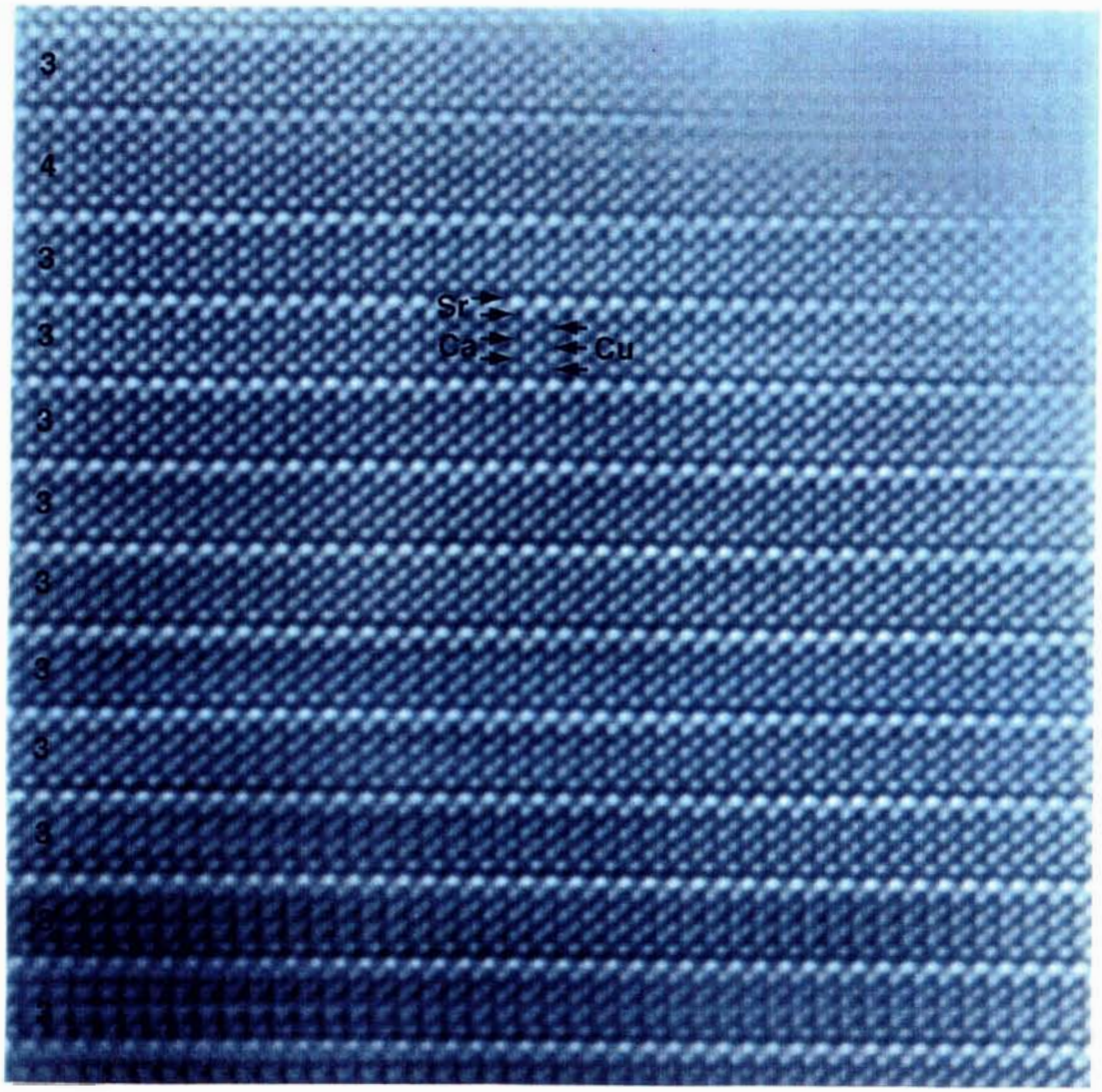

Fig. 5.17. HRTEM image of the 0223-F phase projected along [0 1 0].

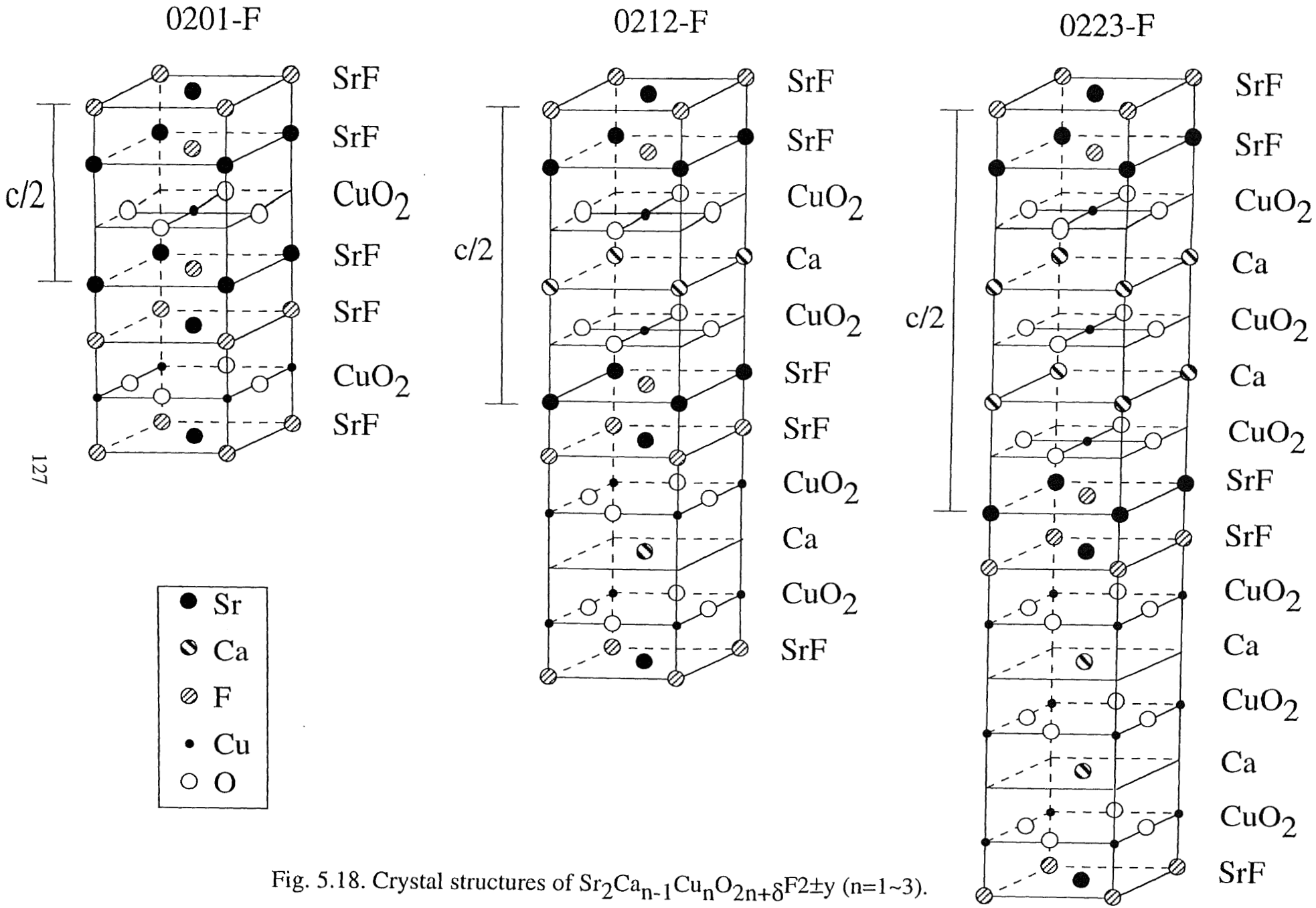

Fig. 5.18. Crystal structures of $Sr_2Ca_{n-1}Cu_nO_{2n+\delta}F_{2\pm y}$ (n=1~3).

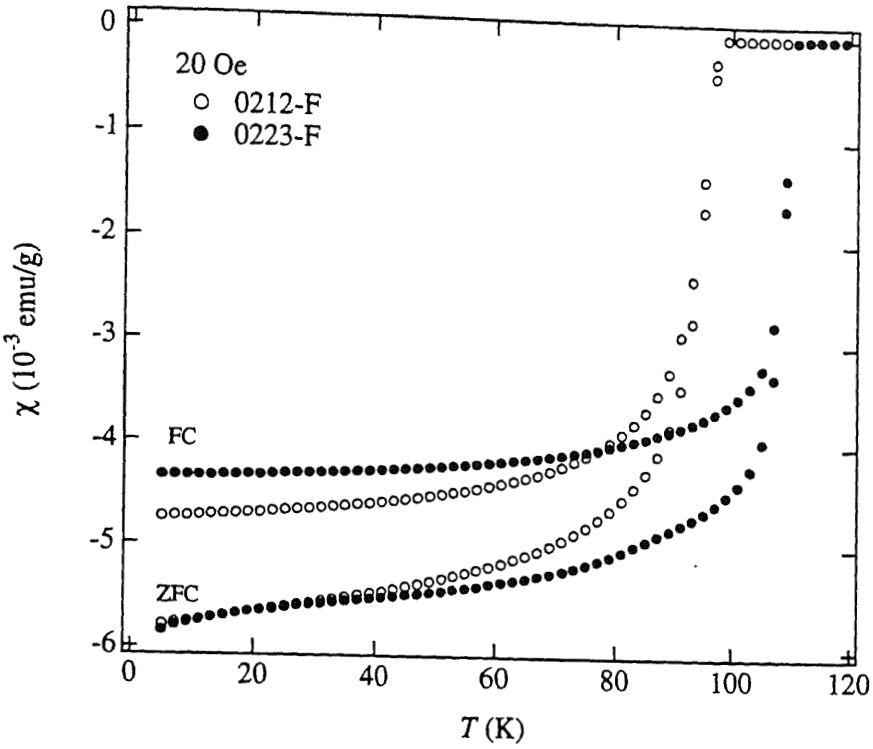

Fig. 5.19. DC magnetic susceptibility data of the samples corresponding to Fig. 5.13(a) (denoted as 0212-F) and to Fig. 5.13(b) (denoted as 0223-F).

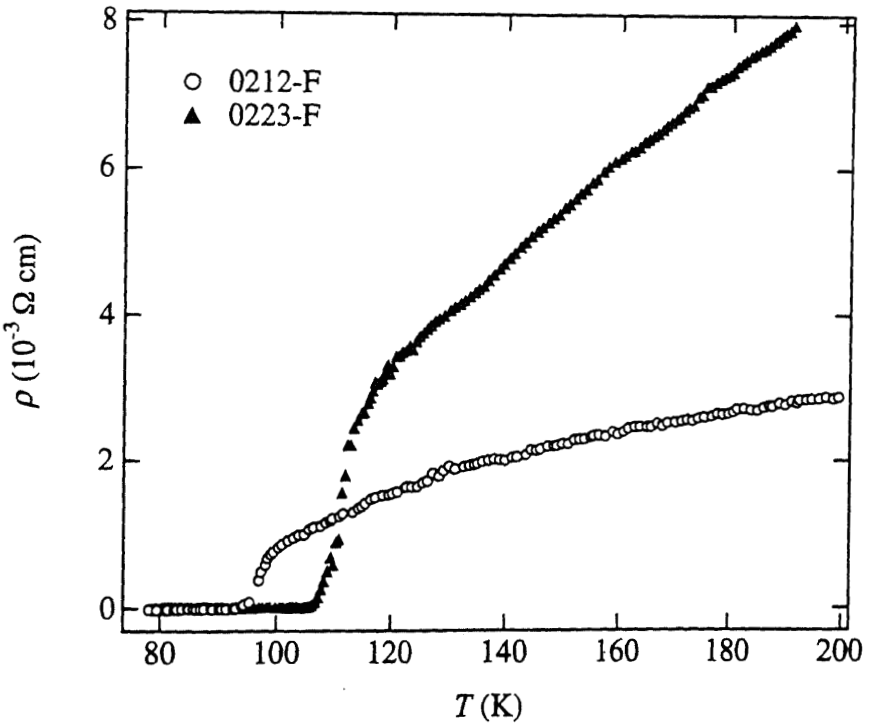

Fig. 5.20. DC electric resistivity data of the samples corresponding to Fig. 5.13(a) (denoted as 0212-F) and to Fig. 5.13(b) (denoted as 0223-F).

6. Conclusions

New oxycarbonate superconductors were prepared at 5 GPa, 1200~1250 °C. There are two series, $(Cu_{0.5}C_{0.5})Ba_2Ca_{n-1}Cu_nO_{2n+3}$ (n=3, 4) and $(Cu_{0.5}C_{0.5})_2Ba_3Ca_{n-1}Cu_nO_{2n+5}$ (n=3~5). Putting them together, they are described as $(Cu_{0.5}C_{0.5})_mBa_{m+1}Ca_{n-1}Cu_nO_{2(m+n)+1}$ ((Cu,C)-m(m+1)(n-1)n). Crystal structures of m=1 series are essentially isostructural to Tl (or Hg)-12(n-1)n, while the m=2 series have quite unique structures in which three Ba planes separated by the (Cu,C) planes form the blocking layer. In both series, the Cu and C atoms in the (Cu,C) plane are located alternately along the a-axis resulting in superlattices having a_S=2a, b_S=b, c_S=2c (for m=1; n=3,4 or m=2; n=3) or a_S=2a, b_S=b, c_S=c (for m=2; n=4,5) with respect to tetragonal subcells. All the members of the series found show superconductivity. In particular, T_c of (Cu,C)-1234, 117 K is the highest value among oxycarbonate superconductors reported hitherto.

The n=3,5 members of the oxyborate family, $BSr_2Ca_{n-1}Cu_nO_{2n+3}$ (B-12(n-1)n), were prepared for the first time. Together with the n=4 phase reported previously [41], homologous series with n=3~5 were found to exist stably under high pressure condition. Their structures are closely related to those of Hg(or Tl)-12(n-1)n. The Hg (Tl) site are occupied by B^{3+}, one of the smallest cations. The B-1234 was reported to be prepared at 1200 °C under 6 GPa and had lattice parameters of a=3.8359(1), c=17.082(2) Å and T_c of 110 K, the highest value among the series [41]. In the present study, the n=3 and n=5 phases were prepared at slightly higher synthetic temperature of 1300 °C and the same pressure of 6 GPa. They have tetragonal cells with a=3.821(1), c=13.854(6) Å for n=3 and a=3.837(1), c=20.22(1) Å for n=5 and are superconducting below 75 K and 85 K, respectively.

A series of compounds $Sr_2Ca_{n-1}Cu_nO_y$ (n=1~4) were prepared under 5~6 GPa and their superconducting properties were studied. The n=1 member of the series, $Sr_2CuO_{3+\delta}$, was believed to be a superconductor with T_c of 70 K. However, our experiments suggest strongly that it is not superconducting but the 70 K superconductivity is ascribed to the n=2 member of the series, $Sr_2CaCu_2O_y$. The n=3 and 4 members were also prepared and they were confirmed to have T_c's of 109 K and 83 K, respectively.

We prepared new oxyfluoride superconductors, $Sr_2CaCu_2O_{4+\delta}F_{2\pm y}$ and $Sr_2Ca_2Cu_3O_{6+\delta}F_{2\pm y}$, at 1250 °C under 5.5 GPa. These phases are the n=2,3 members of a homologous series, $Sr_2Ca_{n-1}Cu_nO_{2n+\delta}F_{2\pm y}$, respectively in which the n=1 phase was reported previously. X-ray and HRTEM studies indicated that they have tetragonal structures with a=3.843(1), c=19.88(1) Å for n=2 and a=3.840(1), c=26.17(1) Å for n=3. The n=2 phase showed superconducting transition at 99 K, while the n=3 one at 111 K.

In summary, we carried out phase-search experiments under high pressure, and found various new high-T_c oxide superconductors as listed below.

Superconducting phase	T_c(K)
$(Cu_{0.5}C_{0.5})Ba_2Ca_2Cu_3O_{9+\delta}$	67
$(Cu_{0.5}C_{0.5})Ba_2Ca_3Cu_4O_{11+\delta}$	117
$(Cu_{0.5}C_{0.5})_2Ba_3Ca_2Cu_3O_{11+\delta}$	91
$(Cu_{0.5}C_{0.5})_2Ba_3Ca_3Cu_4O_{13+\delta}$	113
$(Cu_{0.5}C_{0.5})_2Ba_3Ca_4Cu_5O_{15+\delta}$	(90)
$BSr_2Ca_2Cu_3O_{9+\delta}$	75
$BSr_2Ca_4Cu_5O_{13+\delta}$	85
$Sr_2CaCu_2O_{4+\delta}F_2$	99
$Sr_2Ca_2Cu_3O_{6+\delta}F_2$	111

One of the most important properties of superconductors for practical applications is superconducting transition temperature (T_C). Since 1986, many new oxide superconductors have been discovered and now the record of T_C reached 135 K. However, this record has not been renewed in the last five years. Our present study shows clearly that high-pressure condition is quite effective to stabilize the layered structures of cuprate superconductors. Indeed, including those listed above, more than two third of superconductors with T_c>100K are high pressure stable phases which were discovered in these several years. It should be, however, stressed here that most of high pressure experiments have been carried out in the pressure range P≤6 GPa and we know little about what happens under higher pressure conditions such as 8 GPa or 10 GPa. Increase of pressure will cause increase of melting point which means expansion of synthesis temperature range. Synthesis experiments in higher-pressure/higher-temperature conditions may lead to innovation in the superconductivity materials science. We believe that there still exist many unknown superconductors and that the high pressure research is full of promise.

Acknowledgments

The author expresses much gratitude to Prof. Sigeho Sueno, Institute of Geoscience, University of Tsukuba, for his careful guidance and valuable suggestion for my formalities of paper doctoral program.

I am deeply grateful to Dr. E. Takayama-Muromachi (NIRIM : National Institute for Research in Inorganic Materials) for his constant guidance and supporting of my experiments. I am also indebted to Dr. K. Kato and Dr. Y. Kanke (NIRIM) for helpful discussions and encouragements. I express their sincere thanks to Dr. M. Akaishi and Dr. S. Yamaoka for their helpful suggestions on high pressure synthesis and to Dr. Y. Matsui for his HRTEM analysis.

This work was supported by the Multi-Core Project and the COE project organized by the Science and Technology Agency, Japan.

Finally, I express their sincere thanks again to all of my co-workers in this study.

References

[1] Bednorz J.G. and Müller K.A. (1986) Possible High T_C Superconductivity in the Ba-La-Cu-O System. *Z. Phys. B*, **64**, 189-193.

[2] Uchida S., Takagi H., Kitazawa K. and Tanaka S. (1987) High T_C Superconductivity of La-Ba-Cu Oxides. *Jpn. J. Appl. Phys.*, **26**, L1-2.

[3] Kishio K., Kitazawa K., Kanbe S., Yasuda I., Sugii N., Takagi H., Uchida S., Fueki K. and Tanaka S. (1987) New high temperature superconducting oxides. $(La_{1-x}Sr_x)_2CuO_{4-\delta}$ and $(La_{1-x}Ca_x)_2CuO_{4-\delta}$. *Chem. Lett.*, 429-432.

[4] Wu M.K., Ashburn J.R., Torng C.T., Hor P.H., Meng R.L., Gao L., Huang Z.J., Wang Y.Q. and Chu C.W. (1987) Superconductivity at 93 K in a new mixed-phase Y-Ba-Cu-O compound system at ambient pressure. *Phys. Rev. Lett.*, **58**, 908-910.

[5] Siegrist T., Sunshine S., Murphy D.W., Cava R.J. and Zahurak S.M. (1987) Crystal structure of the high-T_C superconductor $Ba_2YCu_3O_{9-\delta}$. *Phys. Rev. B*, **35**, 7137-7138.

[6] Izumi F., Asano H., Ishigaki T., Ono A. and Okamura F. (1987) Crystal structure of a Ba-Y-Cu-O superconductor as revealed by rietveld analysis of x-ray powder diffraction data. *Jpn. J. Appl. Phys.*, **26**, L611-612.

[7] Maeda H., Tanaka Y., Fujitomi M. and Asano T. (1988) A new high-T_C oxide superconductor without a rare earth element. *Jpn. J. Appl. Phys.*, **27**, L209-210.

[8] Sheng Z.Z. and Hermann A.M. (1988) Bulk superconductivity at 120 K in the Tl-Ca/Ba-Cu-O system. *Nature*, **332**, 138-139.

[9] Parkin S.S.P., Lee V.Y., Nazzal A.I., Savoy R., Beyers R. and La Placa S.J. (1988) $Tl_1Ca_{n-1}Ba_2Cu_nO_{2n+3}$ (n=1,2,3): A new class of

crystal structures exhibiting volume superconductivity at up to ≈110 K. *Phys. Rev. Lett.*, **61**, 750-753.

[10] Tokura Y., Takagi H. and Uchida S. (1989) A superconducting copper oxide compound with electrons as the charge carriers. *Nature*, **337**, 345-347.

[11] Akimitsu J., Suzuki S., Watanabe M. and Sawa H. (1988) Superconductivity in the Nd-Sr-Ce-Cu-O system. *Jpn. J. Appl. Phys.*, **27**, L1859-1860.

[12] Tokiwa A., Oku T., Nagoshi M., Kikuchi M., Hiraga K. and Syono Y. (1989) Crystal structure and phase transition of $PbBaSrYCu_3O_y$ (y=7~8.4). *Physica C*, **161**, 459-467.

[13] Kinoshita K. and Yamada T. (1992) A new copper oxide superconductor containing carbon. *Nature*, **357**, 313-315.

[14] Putillin S.N., Antipov E.V., Chmaissem O. and Marezio M. (1993) Superconductivity at 94 K in $HgBa_2CuO_{4+\delta}$. *Nature*, **362**, 226-228.

[15] Schilling A., Cantoni M., Guo J.D. and Ott H.R. (1993) Superconductivity above 130 K in the Hg-Ba-Ca-Cu-O system. *Nature*, **363**, 56-58.

[16] Tokura Y. (1990) About materials and structures. *Kotai Butsuri*, **25**, 2-20.

[17] Okai B. (1990) High-pressure synthesis of superconducting $YSr_2Cu_3O_y$. *Jpn. J. Appl. Phys.*, **29**, L2180-2182.

[18] Azuma M., Hiroi Z., Takano M., Bando Y. and Takeda Y. (1992) Superconductivity at 110 K in the infinite-layer compound $(Sr_{1-x}Ca_x)_{1-y}CuO_2$. *Nature*, **356**, 775-776.

[19] Smith M.G., Manthiram A., Zhou J., Goodenough J.B. and Markert J.T. (1991) Electron-doped superconductivity at 40 K in the infinite-layer compound $Sr_{1-y}Nd_yCuO_2$. *Nature*, **351**, 549-551.

[20] Ihara H., Tokiwa K., Ozawa H., Hirabayashi M., Matuhata H., Negishi A. and Sohg Y.S. (1994) New High-T_c Superconductor $Ag_{1-x}Cu_xBa_2Ca_{n-1}Cu_nO_{2n+3-\delta}$ Family with T_c>117 K. *Jpn. J. Appl. Phys.*, **33**, L300-303.

[21] Izumi F., Kinoshita K., Matsui Y., Yanagisawa K., Ishigaki T., Kamiyama T., Yamada T. and Asano H. (1992) The crystal structure of the superconducting copper oxide carbonate $(Ba_{1-x}Sr_x)_2Cu_{1+y}O_{2n+2y+z}(CO_3)_{1-y}$. *Physica C*, **196**, 227-235.

[22] Miyazaki Y., Yamane H., Ohnishi N., Kajitani T., Hiraga K., Morii Y., Funahashi S. and Hirai T. (1992) The crystal structure of $(C_{0.4}Cu_{0.6})Sr_2(Y_{0.86}Sr_{0.14})Cu_2O_7$. *Physica C*, **198**, 7-13.

[23] Akimitsu J., Uehara M., Ogawa M., Nakata H., Tomimoto K., Miyazaki Y., Yamane H., Hirai T., Kinoshita K. and Matsui Y. (1992) Superconductivity in the new compound $(Y_{1-x}Ca_x)_{0.95}Sr_{2.05}Cu_{2.4}(CO_3)_{0.6}O_y$. *Physica C*, **201**, 320-324.

[24] Domenges B., Hervieu M. and Raveau B. (1993) Ordered substitution of "CO_3" groups for CuO_4 square groups in the "123" structure. *Physica C*, **207**, 65-78.

[25] Hervieu M., Boullay PH., Domenges B., Maignan A. and Raveau B. (1993) The Oxycarbonate $Y_{1.6}Ca_{0.4}Ba_4Cu_5CO_3O_{11}$, n=2 Member of the "123"-Type Derivatives $(Y_{1-x}Ca_x)_nBa_{2n}Cu_{3n-1}CO_3O_{7n-3}$. *J. Solid State Chem.*, **105**, 300-304.

[26] Den T., Kobayashi T. and Akimitsu J. (1993) Superconductor with T_c up to 80 K in the compound $(Ln,Ca)(Sr,Ba)_2(C,Cu)Cu_2O_{7-\delta}$. *Physica C*, **208**, 351-355.

[27] Pelloquin D., Caldes M., Maignan A., Michel C., Hervieu M. and Raveau B. (1993) The bismuth oxycarbonate $Bi_2Sr_4Cu_2CO_3O_8$. A new superconductor with a T_c onset of 30 K. *Physica C*, **208**, 121-129.

[28] Pelloquin D., Maignan A., Caldes M., Hervieu M., Michel C. and Raveau B. (1993) The bismuth oxycarbonate $Bi_2Sr_{6-x}Cu_3O_{10}(CO_3)_2$. A new 40 K superconductor, second member of the series $(Bi_2Sr_2CuO_6)_n(Sr_2CuO_2CO_3)_{n'}$. *Physica C*, **212**, 199-205.

[29] Uehara M., Nakata H., Akimitsu J., Den T., Kobayashi T. and Matsui Y. (1993) Superconductivities in the (Bi,Pb)-oxycarbonate system. *Physica C*, **213**, 51-56.

[30] Maignan A., Huve M., Michel C., Hervieu M., Martin C. and Raveau B. (1993) A 55 K superconducting copper oxycarbonate: $Tl_{1-x}Bi_xSr_4Cu_2CO_3O_7$. *Physica C*, **208**, 149-154.

[31] Huve M., Michel C., Maignan A., Hervieu M., Martin C. and Raveau B. (1992) A 70 K superconductor. The oxycarbonate $Tl_{0.5}Pb_{0.5}Sr_4Cu_2(CO_3)O_7$. *Physica C*, **205**, 219-224.

[32] Goutenoire F., Hervieu M., Maignan A., Michel C., Martin C. and Raveau B. (1993) A 62 K superconductor with an original structure: $Sr_{4-x}Ba_xTlCu_2CO_3O_7$. *Physica C*, **210**, 359-366.

[33] Matsui Y., Ogawa M., Uehara M., Nakata H. and Akimitsu J. (1993) Incommensurate and commensurate superstructures in the oxycarbonate superconductor $TlSr_{4-x}Ba_xCu_2(CO_3)O_y$ ($x\approx2$). *Physica C*, **217**, 287-293.

[34] Parkin S.S.P., Lee V.Y., Nazzal A.I., Savoy R. and Beyers R. (1988) $Tl_1Ca_{n-1}Ba_2Cu_nO_{2n+3}$ (n=1,2,3): A new Class of Crystal Structures Exhibiting Volume Superconductivity at up to ≈ 110 K. *Phys. Rev. Lett.*, **61**, 750-753.

[35] Ihara H., Sugise R., Hirabayahi M., Terada N., Jo M., Hayashi K., Negishi A., Tokumoto M., Kimura Y. and Shimomura T. (1988) A new high-T_c $TlBa_2Ca_3Cu_4O_{11}$ superconductor with T_c>120 K. *Nature*, **334**, 510-511.

[36] Zhu W.J., Yue J.J., Huang Y.Z. and Zhao Z.X. (1993) (B,Cu)$Sr_2YCu_2O_7$, a new layered copper-oxide based on the boron-oxygen group. *Physica C*, **205**, 118-122.

[37] Uehara M., Uoshima M., Ishiyama S., Nakata H., Akimitsu J., Matsui Y., Arima T., Tokura Y. and Mori N. (1994) A new homologous series of oxycarbonate superconductors $Sr_2(Ca,Sr)_{n-1}Cu_n(CO_3)_{1-x}(BO_3)_xO_y$ (n=1, 2 and 3). *Physica C*, **229**, 310-314.

[38] Takayama-Muromachi E., Matsui Y. and Ramirez-Castellanos J. (1995) New series of oxysulphate superconductors $(Cu_{0.5}S_{0.5})Sr_2Ca_{n-1}Cu_nO_y$ (n=3-7), prepared at high pressure. *Physica C*, **252**, 221-228.

[39] Isobe M., Kawashima T., Kosuda K., Matsui Y. and Takayama-Muromachi E. (1994) A new series of high-T_c superconductors $AlSr_2Ca_{n-1}Cu_nO_{2n+3}$ (n=4, T_c=110 K; n=5, T_c=83 K) prepared at high pressure. *Physica C*, **234**, 120-126.

[40] Takayama-Muromachi E. and Isobe M. (1994) New series of high T_c superconductors, $GaSr_2Ca_{n-1}Cu_nO_{2n+3}$ (n=3, T_c=70 K; n=4, T_c=107 K) prepared at high pressure. *Jpn. J. Appl. Phys.*, **33**, L1399-1402.

[41] Takayama-Muromachi E., Matsui Y. and Kosuda K. (1995) New oxyborate superconductor, $BSr_2Ca_3Cu_4O_{11}$ (T_c=110 K) prepared at high pressure. *Physica C*, **241**, 137-141.

[42] Hiroi Z., Takano M., Azuma M. and Takeda Y. (1993) A new family of copper oxide superconductors $Sr_{n+1}Cu_nO_{2n+1+\delta}$ stabilized at high pressure. *Nature*, **364**, 315-317.

[43] Adachi S., Yamauchi H., Tanaka S. and Môri N. (1993) High-pressure synthesis of superconducting Sr-Ca-Cu-O samples. *Physica C*, **208**, 226-230.

[44] Adachi S., Yamauchi H., Tanaka S. and Môri N. (1993) New superconducting cuprates in the Sr-Ca-Cu-O system. *Physica C*, **212**, 164-168.

[45] Laffez P., Wu X.J. , Adachi S., Yamauchi H. and Môri N. (1994) Synthesis of superconducting $Sr_2CuO_{3+\delta}$ using high-pressure techniques. *Physica C*, **222**, 303-309.

[46] Prouteau C., Strobel P., Capponi J.J., Chaillout C. and Tholence J.L. (1994) Optimization of superconductivity in the high-pressure Sr-Ca-Cu-O system. *Physica C*, **228**, 63-72.

[47] Han P.D., Chang L. and Payne D.A. (1994) High-pressure synthesis of the $Sr_2CuO_{3+\delta}$ superconductor. Observation of an increase in T_c from 70 K to 94 K with heat treatment. *Physica C*, **228**, 129-136.

[48] Shaked H., Shimakawa Y., Hunter B.A., Hitterman R.L., Jorgensen J.D., Han P.D. and Payne D.A. (1995) Superconductivity in the Sr-Ca-Cu-O system and the phase with infinite-layer structure. *Phys. Rev. B*, **51**, 11784-11790.

[49] Azuma M., Hiroi Z., Takano M., Bando Y. and Takeda Y. (1992) Superconductivity at 110 K in the infinite-layer compound $(Sr_{1-x}Ca_x)_{1-y}CuO_2$. *Nature*, **356**, 775-776.

[50] Shimakawa Y., Jorgensen J.D., Mitchell J.F., Hunter B.A., Shaked H., Hinks D.G., Hitterman R.L., Hiroi Z. and Takano M. (1994) Structural study of $Sr_2CuO_{3+\delta}$ by neutron powder diffraction. *Physica C*, **228**, 73-80.

[51] Howard S.A. and Preston K.D. (1989) in: Modern Powder Diffraction, Reviews in Mineralogy, Vol.20, Edited by Bish D.L. and Post J.E. (Mineralogical Society of America, Washington, DC, 1989) ch. 8.

[52] Syono Y., Kikuchi M., Nakajima S., Suzuki T., Oku T., Hiraga K., Kobayashi N., Iwasaki H. and Muto Y. (1989) Structure, composition and superconductivity of high Tc Tl-Ba-Ca-Cu-O system. *Mat. Res. Soc. Simpo. Proc.*, **156**, 229-238.